

STATUS OF THESIS

Title of thesis

NUMERICAL AND EXPERIMENTAL STUDIES ON THE
SLOW DRIFT MOTIONS AND THE MOORING LINE
RESPONSES OF TRUSS SPAR PLATFORMS

I

MONTASIR OSMAN AHMED ALI

hereby allow my thesis to be placed at the information Resource Center (IRC) of
Universiti Teknologi PETRONAS (UTP) with the following conditions:

1. The thesis becomes the property of UTP
2. The IRC of UTP may make copies of the thesis for academic purposes only.
3. This thesis is classified as

Confidential

Non-confidential

If the thesis is confidential, please state the reason:

The contents of the thesis will remain confidential for _____ years.

Remarks on disclosure:

Endorsed by

Signature of Author

Permanent Address:

Department of Civil Engineering

Faculty of Engineering & Technology

University of Gezira

P.O. Box. 20, Wad Medani, SUDAN

Signature of Supervisor

Prof. Dr. Kurian V. John

Date: _____

Date: _____

UNIVERSITI TEKNOLOGI PETRONAS
NUMERICAL AND EXPERIMENTAL STUDIES ON THE SLOW DRIFT
MOTIONS AND THE MOORING LINE RESPONSES OF TRUSS SPAR
PLATFORMS

By

MONTASIR OSMAN AHMED ALI

The undersigned certify that they have read, and recommend to the Postgraduate Studies Programme for acceptance this thesis for the fulfillment of the requirements for the degree stated.

Signature:

Main Supervisor:

Prof. Dr. Kurian V. John

Signature:

Co-Supervisor:

Assoc. Prof. Ir. Dr. Mohd Shahir Liew

Signature:

Head of Department:

Assoc. Prof. Ir. Dr. Mohd Shahir Liew

Date:

NUMERICAL AND EXPERIMENTAL STUDIES ON THE SLOW DRIFT
MOTIONS AND THE MOORING LINE RESPONSES OF TRUSS SPAR
PLATFORMS

By

MONTASIR OSMAN AHMED ALI

A Thesis

Submitted to the Postgraduate Studies Programme
as a Requirement for the Degree of

DOCTOR OF PHILOSOPHY
CIVIL ENGINEERING DEPARTMENT
UNIVERSITI TEKNOLOGI PETRONAS
BANDAR SRI ISKANDAR
PERAK

FEBRUARY 2012

DECLARATION OF THESIS

Title of thesis

NUMERICAL AND EXPERIMENTAL STUDIES ON THE
SLOW DRIFT MOTIONS AND THE MOORING LINE
RESPONSES OF TRUSS SPAR PLATFORMS

I MONTASIR OSMAN AHMED ALI

hereby declare that the thesis is based on my original work except for quotations and citations which have been duly acknowledged. I also declare that it has not been previously or concurrently submitted for any other degree at UTP or other institutions.

Witnessed by

Signature of Author

Permanent Address:

Department of Civil Engineering
Faculty of Engineering & Technology
University of Gezira
P.O. Box. 20, Wad Medani, SUDAN

Date: _____

Signature of Supervisor

Prof. Dr. Kurian V. John

Date: _____

ACKNOWLEDGEMENTS

First and foremost, I thank ALLAH for the strength that keeps me standing and for the hope that keeps me believing that this affiliation would be possible and divine. There are many who have contributed in small and large ways to the completion of this thesis and to whom I give special thanks for what they have given and for what I have learned from them.

I would like to express my genuine appreciation to my supervisor, Prof. Dr Kurian V. John, for his excellent guidance, motivation and support throughout the course of my study at Universiti Tecknologi PETRONAS. I appreciate his patience, insightful comments and for giving me the opportunity to think and learn independently and for giving me the freedom in performing the research. I am very fortunate to have a wonderful mentor and advisor guiding and assisting me. Special thanks are due to AP. Ir. Dr Mohd Shahir Liew, my co-supervisor, for giving valuable suggestions.

I would like to thank Universiti Teknologi PETRONAS for the facilities provided in this work. I am indebted for University of Gezira and Ministry of Higher Education (SUDAN) for my sponsorship.

I express my warmest gratitude to my wife, Nuha, for her dedication, encouragement, and love during my hectic time in research. Heartfelt thanks are also due to my family, especially to my dear father and mother, my brother and sisters, for their love, prayers, sincerity and unconditional support at every stage of my life.

I extend my thanks and gratitude to all my friends, near and far, who gave me friendship, prayers, and support and who share a great and memorable time during the tenure of my research and thesis work.

DEDICATION

To my father, Prof. Osman, and my mother, Agba

To my wife, Huha

To my daughter, Lina, and my son,

Ahmed,

To my brother and sisters

To my family members

To my friends and colleagues

ABSTRACT

An efficient methodology has been developed for the dynamic analysis of offshore floating structures. In this methodology, special attention was given to the second order difference frequency forces and responses. According to this numerical scheme, a MATLAB program named TRSPAR was developed to predict the dynamic responses of truss spar platform in time domain. In this program, the truss spar platform was modeled as a rigid body with three degrees of freedom. Hydrodynamics of the structure, which include the linear and second order wave forces, mean drift forces, added mass, radiation damping, wave drift damping and system stiffness were included in the program. Current and wind forces were also considered showing their effects on the slow drift responses. The wave forces, including inertia and drag forces, were calculated using Morison equation assuming the wave field as undisturbed. An efficient time domain integration scheme was adopted based on Newmark Beta method.

Comprehensive experimental studies were conducted and the numerical predictions were systematically compared with model test results. These comparisons consisted of structure's dynamic responses in different environmental conditions and two structural situations. The first situation was the structure with intact mooring lines and the other one was the structure under mooring line failure. The responses of the platform with mooring line system damage were investigated with the emphasis on finding the critical effects of line failure on the resonant responses.

The effects of the second order difference frequency wave forces on the truss spar motion characteristics were examined numerically. Published numerical results were used to verify the developed numerical model in predicting the truss spar dynamic responses when subjected to combined wave, current and wind forces. The effects of

strengthening mooring line system on the motion characteristics of the structure were examined numerically. For the assessment of the fluid to mooring nonlinear interactions, a deterministic approach based on lumped mass method with equations of dynamic equilibrium and continuity was adopted. Finally, parametric studies on deepwater mooring line analysis have been conducted for investigating the contributions of the various design parameters on mooring line tension.

The experimental results verified the validity of the developed numerical scheme for prediction of the wave frequency and low frequency motions of the truss spar platform with its intact mooring and in the case of mooring line damage condition. RMSD values for the numerical and the experimental results show that the simulated wave frequency responses (WFR) trend was relatively agreed well with the experiments compared to the low frequency responses (LFR). For the intact mooring line condition, RMSD values for the WFR ranged from 109.9 to 182.4 while for LFR were ranged from 499.6 to 550.2. The same has been noticed in the mooring line damage condition in which RMSD values ranged from 107.4 to 323.6 and 209.1 to 1074 for WFR and LFR respectively. With regard to the peak responses, good accuracy has been achieved between the predictions and the measurements. The percentage errors for the peak responses in the intact mooring and the mooring line damage conditions were ranged from 9.5% to 17.3%.

ABSTRAK

Satu kaedah cepak telah diusahakan untuk analisa dinamik struktur terapung luar pantai. Dalam kaedah ini, perhatian khusus telah diberikan kepada pembezaan peringkat kedua daya frekuensi dan tindakbalas struktur. Menurut skim berangka ini, satu program MATLAB bernama TRSPAR telah diusahakan untuk meramal tindakbalas dinamik sesebuah pelantar kekuda SPAR dalam domain masa. Dalam program ini, pelantar kekuda SPAR tersebut telah dimodel sebagai sebuah badan kukuh dengan tiga darjah kebebasan. Hidrodinamik struktur tersebut meliputi faktor-faktor seperti daya ombak yang linear dan yang berperingkat kedua, menggunakan jisim tambahan, penyusutan radiasi, penyusutan hanyutan ombak, daya hanyutan ombak, dan kukuhan sistem; telah dimasukkan dalam program ini. Daya arus dan angin juga telah diambilkira; dengan menonjolkan kesan ke atas tindakbalas linear dan hanyutan berubah lemah. Daya ombak, meliputi daya heretan dan inertia, telah diambilkira menggunakan Persamaan Morison, dengan anggapan lapangan ombak sebagai yang tidak terganggu. Suatu skim bersepadu domain masa yang cepak telah digunapakai menurut kaedah Newmark Beta.

Kajian eksperimen yang menyeluruh dijalankan dan ramalan berangka telah dibandingkan secara sistematik dengan keputusan ujian model. Perbandingan dibuat meliputi tindakbalas dinamik struktur di dalam kaedah persekitaran yang berbeza dan dalam dua situasi struktur yang berbeza. Situasi pertama adalah bagi struktur dengan dawai tambatan yang sempurna, manakala situasi kedua adalah bagi struktur dengan dawai tambatan yang gagal/tidak berfungsi. Tindakbalas pelantar bagi situasi kedua telah dikaji dengan tumpuan diberikan kepada pencarian kesan ketara/kritikal bagi dawai tambatan yang gagal; ke atas tindakbalas resonan di dalam keadaan bebanan yang berbeza.

Kesan daya hanyutan berubah lemah ke atas tingkah laku pergerakan kekuda SPAR telah dikaji menggunakan kaedah berangka. Nilai-nilai dari pada terbitan sebelum ini telah digunakan untuk tujuan pengesahan model berangka yang diusahakan; dalam meramalkan tindakbalas dinamik kekuda SPAR apabila dikenakan gabungan daya ombak, arus dan angin. Kesan pengukuhan sistem dawai tambatan ke atas sifat pergerakan struktur dikaji secara kaedah berangka. Bagi penilaian interaksi tidak linear bendalir ke atas dawai tambatan, suatu pendekatan ketentuan berdasarkan kaedah jisim terkumpul dengan persamaan keseimbangan dinamik dan kesinambungan telah diguna pakai. Akhirnya, kajian parametrik ke atas analisa dawai tambatan laut dalam telah dijalankan untuk mengkaji sumbangan daripada kepelbagaian parameter reka bentuk ke atas daya tegangan dawai tambatan.

Keputusan ujikaji mengesahkan bahawa skim angkaan untuk meramal frekuensi gelombang dan gerakan frekuensi rendah untuk Truss Spar dengan tambatan kukuh dan tambatan rosak. Nilai RMSD untuk keputusan angkaan dan ujikaji menunjukkan bahawa trend simulasi Wave Frequency Responses (WFR) setuju dengan ujikaji berbanding dengan Low Frequency Responses (LFR). Untuk tambatan kukuh, nilai RMSD untuk WFR melingkung dari 109.9 hingga 182.4, manakala LFR melingkung dari 499.6 hingga 550.2. Keadaan serupa diperhatikan untuk tambatan rosak, di mana nilai RMSD didapati di lingkungan 107.4 hingga 323.6 dan 209.1 hingga 1074 untuk WFR dan LFR. Dengan mengambilkira respons kemuncak, ketepatan yang memuaskan diperhatikan untuk anggaran dan ukuran. Peratusan kesilapan untuk response kemuncak untuk tambatan kukuh dan tambatan rosak melingkung dari 9.5% hingga 17.3%.

In compliance with the terms of the Copyright Act 1987 and the IP Policy of the university, the copyright of this thesis has been reassigned by the author to the legal entity of the university,

Institute of Technology PETRONAS Sdn Bhd.

Due acknowledgement shall always be made of the use of any material contained in, or derived from, this thesis.

© MONTASIR OSMAN AHMED ALI, 2011
Institute of Technology PETRONAS Sdn Bhd
All rights reserve

TABLE OF CONTENTS

ACKNOWLEDGEMENTS.....	V
DEDICATION.....	VI
ABSTRACT.....	VII
ABSTRAK.....	IX
LIST OF FIGURES.....	XVI
LIST OF TABLES.....	XX
LIST OF ABBREVIATIONS.....	XXI
NOMENCLATURE.....	XXIII
Chapter 1.....	1
INTRODUCTION.....	1
1.1 BACKGROUND.....	1
1.2 PROBLEM STATEMENT.....	3
1.3 OBJECTIVES OF THE STUDY.....	6
1.4 SCOPE OF THE STUDY.....	7
1.5 THESIS ORGANIZATION.....	8
Chapter 2.....	11
LITERATURE REVIEW.....	11
2.1 CHAPTER OVERVIEW.....	11
2.2 REPORTED STUDIES.....	11
2.3 HISTORY OF SPAR PLATFORM.....	11
2.4 RESEARCH DIRECTIONS.....	12
2.4.1 Second order slow drift responses.....	12
2.4.2 Damping and added mass.....	17
2.4.3 Mooring lines.....	22
2.4.4 Spar platform generations development.....	26
2.5 CRITICAL LITERATURE REVIEW.....	29
Chapter 3.....	33
SECOND ORDER SLOWLY VARYING DRIFT FORCES.....	33
3.1 INTRODUCTION.....	33

3.2 WAVE THEORIES	33
3.2.1 Governing equation and boundary conditions	33
3.2.2 Wave theories kinematics	36
3.3 DESIGN WAVE ENVIRONMENT	39
3.3.1 Single wave method	39
3.3.2 Wave spectrum.....	39
3.3.2.1 JONSWAP spectrum.....	39
3.4 MEAN DRIFT FORCES	41
3.5 SECOND ORDER DIFFERENCE FREQUENCY WAVE FORCES	42
3.5.1 Inertia force	47
3.5.1.1 Structural displacement	47
3.5.1.2 Axial divergence	48
3.5.1.3 Free surface fluctuation	51
3.5.1.4 Convective acceleration	51
3.5.1.5 Temporal acceleration	52
3.5.2 Drag force	53
3.5.2.1 Structural displacement	54
3.5.2.2 Free surface fluctuation.....	55
3.5.2.3 Mean drag force	55
3.6 QUALITATIVE COMPARISON BETWEEN SECOND ORDER INERTIA AND DRAG FORCES	56
3.7 CHAPTER SUMMARY	56
Chapter 4.....	59
TIME DOMAIN FORMULATIONS	59
4.1 INTRODUCTION.....	59
4.2 NUMERICAL SOLUTION OF THE EQUATION OF MOTION	60
4.2.1 Equation of motion	60
4.2.2 Numerical integration approach.....	64
4.3 QUASI-STATIC MOORING LINE ANALYSIS.....	67
4.4 DYNAMICS OF MOORING LINES.....	71
4.5 EFFECT OF CURRENT	75
4.6 EFFECT OF WIND.....	77
4.7 CHAPTER SUMMARY	78

Chapter 5.....	79
EXPERIMENTAL STUDIES.....	79
5.1 INTRODUCTION.....	79
5.2 EXPERIMENTAL STUDIES AT UTM (PHASE 1).....	79
5.2.1 Test facilities and instrumentations	80
5.2.2 Model description	82
5.2.3 Experimental programs.....	84
5.3 EXPERIMENTAL STUDIES AT UTP (PHASE 2).....	85
5.3.1 Test facilities and instrumentations	87
5.3.2 Choice of the scale and physical modeling law	89
5.3.3 Model description	92
5.3.4 Mooring line system	94
5.3.5 Experimental programs.....	95
5.3.5.1 Quasi-static and free decay tests	95
5.3.5.2 Sea-keeping tests.....	95
5.4 CHAPTER SUMMARY.....	96
Chapter 6.....	97
RESULTS AND DISSCUSIONS.....	97
6.1 INTRODUCTION.....	97
6.2 EXPERIMENTAL STUDIES AT UTM	97
6.3 EXPERIMENTAL STUDIES AT UTP	100
6.3.1 Intact mooring lines condition	101
6.3.1.1 Static-offset test and free-decay results.....	101
6.3.1.2 Wave frequency responses	103
6.3.1.3 Low frequency responses	105
6.3.2 Mooring lines damage condition	107
6.3.2.1 Static-offset test and free-decay results.....	108
6.3.2.2 Wave frequency responses	110
6.3.2.3 Low frequency responses	112
6.3.2.4 Mooring line failure mechanism for regular wave.....	115
6.4 NUMERICAL AND EXPERIMENTAL STUDIES ON MARLIN TRUSS SPAR PLATFORM ...	117
6.4.1 Static offset test.....	120
6.4.2 Slow varying drift forces	120

6.4.3 Effect of current and wind	126
6.4.4 Numerical studies on strengthening of the station keeping systems.....	130
6.4.5 Mooring line dynamic analysis in regular waves	133
6.5 PARAMETRIC STUDIES ON DEEPWATER MOORING LINE.....	137
6.6 CHAPTER SUMMARY.....	139
Chapter 7.....	141
CONCLUSIONS AND RECOMMENDATIONS.....	141
7.1 SUMMARY	141
7.2 CONCLUSIONS	142
7.2.1 Comparison with laboratory test results	142
7.2.2 Second order difference frequency forces	143
7.2.3 Current and wind forces.....	144
7.2.4 Strengthening of mooring line system	145
7.2.5 Quasi-static and dynamic mooring line analysis	145
7.2.6 Investigations on the taut deepwater mooring line design parameters	145
7.3 FUTURE STUDIES	146
REFERENCES	147
PUBLICATIONS LIST.....	162

LIST OF FIGURES

Figure 1.1: Platform cost comparison, Gulf of Mexico [4]	2
Figure 1.2: Spar platform generations	2
Figure 1.3: Six degrees of freedom for truss spar platform	4
Figure 1.4: Definition sketch for a progressive wave train.....	5
Figure 3.1: JONSWAP energy density spectrum for a given $H_s = 12.7$ m and $\omega_0 = 0.45$ rad/s.....	40
Figure 3.2: Wave kinematics components on a segment on inclined cylinder	44
Figure 3.3: Global and local coordinates used for dynamic analysis	45
Figure 4.1: Flow chart of the Newmark Beta integration method	66
Figure 4.2: Multi-component taut mooring line: (a) Mooring line configuration; (b) Free body diagram of mooring line segment.	68
Figure 4.3: Flow chart of the quasi-static analysis of a mooring line.....	70
Figure 4.4: Discretization of mooring line by a lumped mass method.....	72
Figure 4.5: Lumped mass method flow chart	75
Figure 5.1: Schematic diagram for the Marine Technology Laboratory towing tank (<i>Source: Marine Technology laboratory report No. MTL 056/2008</i>)	81
Figure 5.2: Model test arrangement in the wave basin (top view- Phase 1).....	82
Figure 5.3: Truss spar model (Phase 1)	83
Figure 5.4: Truss spar model in the wave basin (Side view - Phase 1)	83
Figure 5.5: Sea keeping tests setup (side view - Phase 2)	86
Figure 5.6: Model mooring line arrangement (Phase 2).....	86
Figure 5.7: UTP wave basin.....	87
Figure 5.8: UTP basin wave maker system	88
Figure 5.9: Truss spar model configuration (All dimensions are in mm - Phase 2)....	93
Figure 5.10: The truss spar model during tests (Phase 2).....	93
Figure 6.1: Static offset test results: Multi-segment force-displacement relationship.	98
Figure 6.2: Comparison of surge motion RAO.....	99
Figure 6.3: Comparison of heave motion RAO	100

Figure 6.4: Comparison of pitch motion RAO	100
Figure 6.5: Static offset test results	101
Figure 6.6: Surge free-decay results	102
Figure 6.7: Heave free-decay results	102
Figure 6.8: Pitch free decay results.....	103
Figure 6.9: Surge RAOs.....	104
Figure 6.10: Heave RAOs.....	104
Figure 6.11: Pitch RAOs.....	105
Figure 6.12: Surge spectra.....	106
Figure 6.13: Heave spectra	106
Figure 6.14: Pitch spectra	107
Figure 6.15: Static offset test results.....	108
Figure 6.16: Surge free decay results.....	109
Figure 6.17: Heave free decay results.....	109
Figure 6.18: Pitch free decay results.....	110
Figure 6.19: Surge RAOs.....	111
Figure 6.20: Heave RAOs.....	111
Figure 6.21: Pitch RAOs.....	112
Figure 6.22: Surge spectra	113
Figure 6.23: Heave spectra	114
Figure 6.24: Pitch spectra\	114
Figure 6.25: Surge time series for Case1 (experiment measurements)	116
Figure 6.26: Surge time series for Case 2 (experiment measurements)	116
Figure 6.27: Surge time series for failure condition (numerical predictions).....	117
Figure 6.28: Overall configuration	118
Figure 6.29: Truss spar mooring arrangement.....	118
Figure 6.30: Static offset results comparisons (experiment vs. numerical).....	120
Figure 6.31: Surge: linear solution (LS)	122
Figure 6.32: Surge: LS+ surge effect (SD1).....	122
Figure 6.33: Surge: LS + SD1 + pitch effect (SD2)	122
Figure 6.34: Surge: LS + SD1 + SD2 + Drag force without damping (DF1).....	122
Figure 6.35: Surge: LS + SD1 + SD2 + DF1 + Drag damping effect (DF2).....	123

Figure 6.36: Surge: LS + SD1 + SD2 + DF1 + DF2 + Axial divergence (AD)	123
Figure 6.37: Surge: LS + SD1 + SD2 + DF1 + DF2 + AD+ Free surface (FS)	123
Figure 6.38: Surge: LS + SD1 + SD2 + DF1 + DF2 + AD + FS + Convective acceleration(CA).....	123
Figure 6.39: Surge: LS + SD1 + SD2 + DF1 + DF2 + AD + FS + CA + Temporal acceleration (TA).....	123
Figure 6.40: Pitch: LS	124
Figure 6.41: Pitch: LS+ SD1.....	124
Figure 6.42: Pitch: LS + SD1 + SD2	125
Figure 6.43: Pitch: LS + SD1 + SD2 + DF1	125
Figure 6.44: Pitch: LS + SD1 + SD2 + DF1 + DF2	125
Figure 6.45: Pitch: LS + SD1 + SD2 + DF1 + DF2 + AD	125
Figure 6.46: Pitch: LS + SD1 + SD2 + DF1 + DF2 + AD+ FS.....	125
Figure 6.47: Pitch: LS + SD1 + SD2 + DF1 + DF2 + AD+FS+ CA.....	125
Figure 6.48: Pitch: LS + SD1 + SD2 + DF1 + DF2 + AD+FS+ CA + TA	125
Figure 6.49: Surge spectrum due to combined random waves and current.....	126
Figure 6.50: Pitch spectrum due to combined random waves and current	127
Figure 6.51: Surge time series due to random waves	127
Figure 6.52: Surge time series due to random waves and current	128
Figure 6.53: Surge spectra comparisons	129
Figure 6.54: Pitch spectra comparisons	129
Figure 6.55: Surge time series due to random waves, current and wind	130
Figure 6.56: Marlin truss spar side view with additional mooring lines	131
Figure 6.57: Marlin truss spar top view with additional mooring lines.....	131
Figure 6.58: Additional mooring lines restoring force vs. horizontal excursion.....	132
Figure 6.59: Surge spectrum.....	132
Figure 6.60: Pitch spectrum	133
Figure 6.61: Mooring line No. 5 attached to the structure.....	134
Figure 6.62: Mooring line No. 5 dynamic tension due to Reg1	135
Figure 6.63: Mooring line No. 5 dynamic configuration due to Reg1	135
Figure 6.64: Mooring line No. 5 dynamic tension due to Reg2	136
Figure 6.65: Mooring line No. 5 dynamic configuration due to Reg2	136

Figure 6.66: Effect of pretentions on the fairlead horizontal tension	137
Figure 6.67: Effect of cable elongation on the fairlead horizontal tension.....	138
Figure 6.68: Effect of cable components unit weight on the fairlead horizontal tension.....	139

LIST OF TABLES

Table 5.1: Wave height and period of regular waves used for testing.....	85
Table 5.2: Model to prototype multipliers for the variables under Froude scaling	92
Table 5.3: The truss spar data (full scale)	94
Table 5.4: Regular waves.....	96
Table 6.1: Natural periods of vibrations of the model	98
Table 6.2: Comparison of natural periods and damping ratios	103
Table 6.3: RMSD for dynamic motions due to regular waves	105
Table 6.4: RMSD for dynamic motions due to random waves.....	107
Table 6.5: Comparison of natural periods and damping ratios	110
Table 6.6: RMSD for dynamic motions due to regular waves	112
Table 6.7: RMSD for dynamic motions due to regular waves	114
Table 6.8: Physical characteristics of the truss spar	119
Table 6.9: Characteristics of truss spar mooring lines	119
Table 6.10: Regular waves used in the experiment and simulation.....	133
Table 6.11: Comparison between numerical and experimental results [86].....	136

LIST OF ABBREVIATIONS

ALP	Articulated Leg Platform
AD	Axial divergence force
BVP	Boundary value problem
CA	Convective acceleration
CB	Center of buoyancy
CG	Center of gravity
DF1	Drag force without viscous damping
DF2	Drag force with viscous damping
DHWM	Directional Hybrid Wave Model
DNV	Det Norske Veritas
DOF	Degree of freedom
EOM	Equation of motion
FE	Finite Element
FFT	Fast Fourier Technique
FLIP	Floating Instrument Platform
FS	Free surface fluctuation force
GOM	Gulf of Mexico
HOBEM	Higher order boundary element method
HWM	Hybrid Wave Model
ISSC	International Towing Tank Conference
JIP	Joint Industry Project
JONSWAP	Joint North Sea Wave Project
KC	Keulegan-Carpenter
KN	Kilonewton
LAT	Linear Airy Theory
LFR	Low frequency responses
LS	Linear response

LMM	Lumped mass method
MATLAB	Matrix laboratory
MWL	Mean water level
OTRC	Offshore Technology Research Center
PM	Pierson-Moskowitz spectrum
RAO	Response amplitude operator
RMSD	Root Mean Square Deviation
SBF	SPAR buoy flare
SD1	Structure displacement with respect to surge
SD2	Structure displacement with respect to pitch
SJTU	Shanghai Jiaotong University
SKLOE	State Key Laboratory of Ocean Engineering
TA	Temporal acceleration force
TBT	Tethered Buoy Tower
TDSIM	Time Domain Simulation
TLP	Tension Leg Platform
TML	Transducer Markup Language
TRSPAR	Truss Spar simulation code
UHWM	Unidirectional Hybrid Wave Model
UTM	Universiti Teknologi Malaysia
UTP	Universiti Teknologi PETRONAS
WFR	Wave frequency responses

NOMENCLATURE

A	Cross-sectional area
a	Wave amplitude
a_{nj}, a_{tj}	Normal and tangential added mass
B	Bottom surface of the structure
$B_{11_{wd}}$	Wave drift damping
$\{C\}$	Damping matrix
C_D	Drag coefficient
C_M	Inertia coefficient
C_m	Added mass coefficient
C_y	Cauchy Number
C_x, C_z	x and z components of the unit vector C which is acting along the cylinder axis directed up or down
D	Structure diameter
d	Water depth
EA	Modulus of elasticity
Eu	Euler Number
$[F(t)]$	Force vector
F_{Ext}	Tangential wave component
F_e	Gravity force
F_G	Elastic force
F_I	Inertia force
F_P	Pitch mean drift forces
F_V	Viscous force
F_r	Froude Number
F_s	Surge mean drift forces
$F_w(t)$	Wind force

f	Wave frequency in Hz
f_D	Drag force for unit length
g	Gravity acceleration
H	Wave height
H_s	Significant wave height
h_1	Distance from CG to CB
h_2	Distance from CG to fairlead
I	Mass moment of inertia
I_v	Iverson Modules
$\{K\}$	Stiffness matrix
k	Wave number
k_x	Horizontal spring stiffness
L	Wave length
$\{M\}$	Mass matrix
$[m]$	Added mass matrix
p	Dynamic pressure
R	Cylinder radius
Re	Reynolds Number
$S(w)$	Wave energy spectral density
s	Effective water depth
T	Wave period
T_i	Average segment tension
T^k	Tentative segment tension vector
t	Time
U_c	Current velocity
u	Water- particle velocities in the x direction
u_{re}	Relative velocity
V	Velocity gradient
v	Water- particle velocities in the z direction
w_r	Relative normal velocity
$[x_G]$	Structure displacements vector
x_{Gm}	Surge amplitude

xoz	Global axis
Z_{Gm}	Heave amplitude
z_G	z -coordinate of the centre of gravity
$\left[\frac{\partial x_G}{\partial t} \right]$	Structure velocity
$\left[\frac{\partial^2 x_G}{\partial t^2} \right]$	Structure acceleration
η	Wave elevation
$\phi^{(1)}, \phi^{(2)}$	First and second order velocity potential
ε	Nondimensional perturbation parameter
ω	Wave frequency in rad/s
ω_0	Frequency at spectral peak
ω_n	Natural frequency
ω_a	Apparent frequency
β	Initial phase angle
ξ	Damping ratio
ζGn	Local axis
σ	Shape parameter
σ_{wr}	Variance of the relative normal wave particle velocity
γ	Peakedness parameter
γ_m	Pitch amplitude
α	Phillip's constant
\mathcal{G}	Pitch angle
ρ	Mass density of water
ρ_d	Wind dynamic pressure
ρ_w	Wind density
λ	A parameter measuring the strength of the current
ψ	Segment length error vector
$\mu_{u_{re}}$	Mean value of u_{re}
$\Delta\psi$	Length error derivative matrix
$[\Lambda_n j], [\Lambda_t j], [\Omega_j]$	Directional matrices

π Mathematical constant, which is approximately equal to 3.14
 τ Unit vector along the n -axis

CHAPTER 1

INTRODUCTION

1.1 Background

In the global oil and gas industry, demand for hydrocarbons is increasing rapidly with declining resources available onshore and at shallow water depths. This fact makes exploring new reservoirs in aggressive environments such as deepwater regions essential for future energy supplies. In view of the challenges related to deepwater exploration, the offshore oil and gas industry is rapidly developing technology for extracting hydrocarbons from ultra deepwater.

The challenging deepwater environment makes the traditional fixed based offshore structures unsuitable. This is primarily due to the cost of fabrication, technical and installation constraints. A comparison of the relative cost trends for different types of offshore structures for the Gulf of Mexico is shown in Figure 1.1. For deepwater, the alternative innovative platforms have been developed, such as Tethered Buoy Tower (TBT), Articulated Leg Platform (ALP), Tension Leg Platform (TLP) etc.

The Spar is the latest among this new generation of compliant offshore structures, and it has been used for drilling, production and storage of oil in deepwater [1-3]. As shown in Figure 1.2, the development of spar concept can be categorized into three generations known as classic spar, truss spar and cell spar.

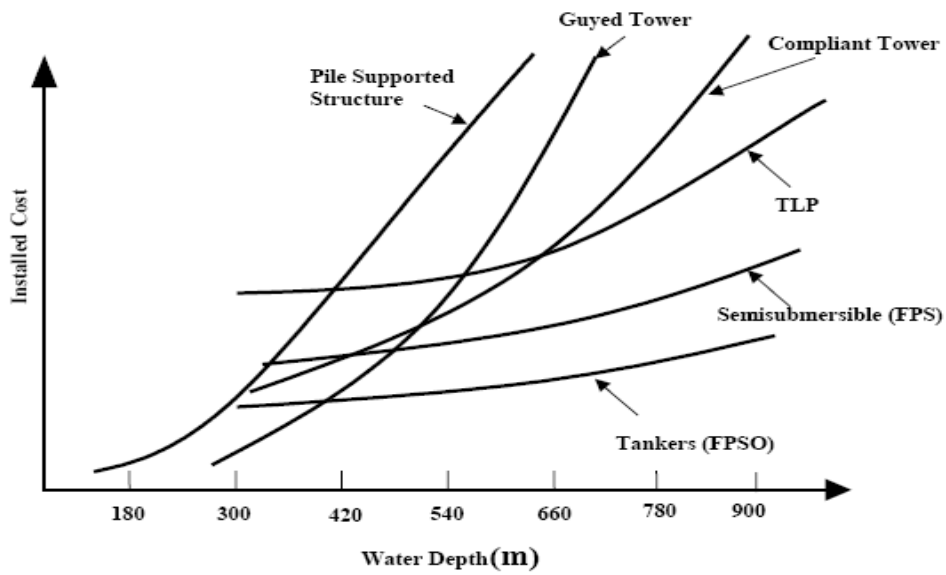


Figure 1.1: Platform cost comparison, Gulf of Mexico [4]

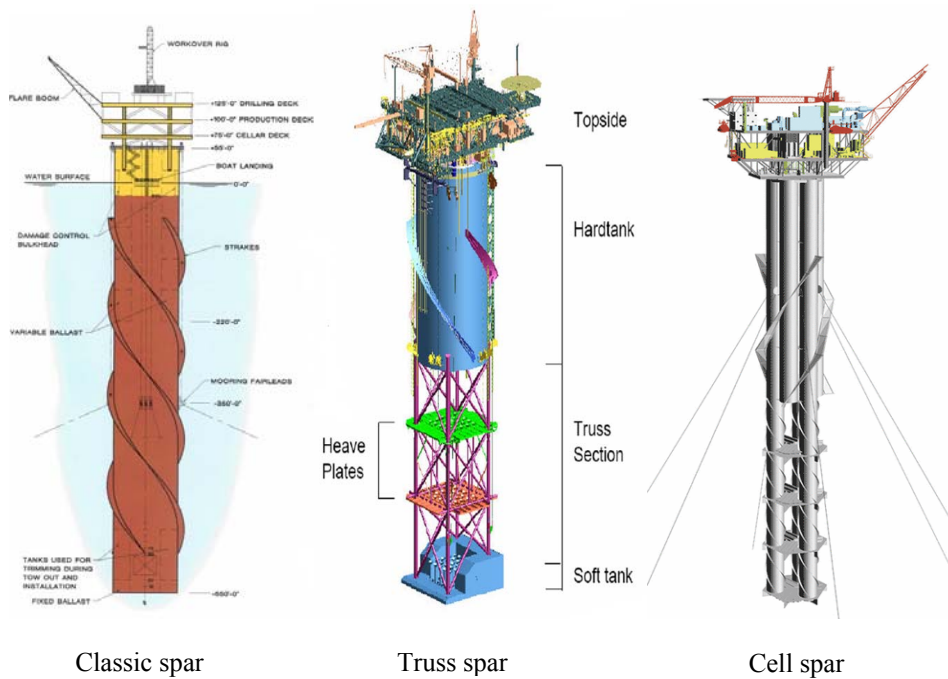


Figure 1.2: Spar platform generations

The classic spar comprises of a large uniform circular cylinder with a long draft. This configuration allows the installation of rigid risers with dry trees, as the heave and pitch responses are small. Truss spar consists of a large volume of hard tank in the upper part and a lower soft tank. These tanks are separated by a truss portion,

which reduces the hull construction costs by 20% to 40% [5]. Moreover, truss section is relatively transparent to the ambient current, resulting in significantly less surge offset and mooring requirements. The soft tank provides stability, whereas the hard tank, which has a circular cylinder cross-section, provides buoyancy. The truss section comprises of heave plates supported by slender members. The heave plates contribute to the heave added mass and viscous damping, thereby minimizing the heave motion regardless of the increase of vertical exciting wave force due to the shallower hard tank. Cell spars excel compared to the first two generations by saving the construction period, attained by parallel fabrication of the cylinder shell components. Experimental studies on deep draft columns show that multiple cells forming a column can be less subjected to vortices since the spacing between them allows interstitial flow of water through their spaces [6-8].

The research interest on spars has developed recently and within a short time, quite a number of studies have been conducted on the dynamic responses of spars numerically as well as experimentally. Most of the previous studies were applied to the first generation spar, namely classic spar. For the study reported in this thesis, numerical and experimental methods were applied to truss spar platform focused on its motion characteristics in different environmental conditions.

1.2 Problem statement

Spar platform has six degrees of freedom translational and rotational, and are connected to the seabed by using mooring line system as shown in Figure 1.3. However, the dominant motions for spar are only three; i.e., surge, heave and pitch. Therefore, it is often modeled as a two dimensional structure with three degrees of freedom. The spar has natural frequencies of motions far below the dominant ocean exciting wave forces frequencies; this is due to its large mass and relatively small restoring stiffness. Therefore, the dynamic responses of spar due to the linear ocean wave forces are insignificant. Nonlinear wave structure interactions may result in second order difference frequency forces, which have frequencies close to the natural frequencies of the spar. Consequently, these forces should be taken into consideration

in the design because of its substantial contribution to the motions and mooring line tensions. Accordingly, a reliable scheme should be used for analyzing spar platform.

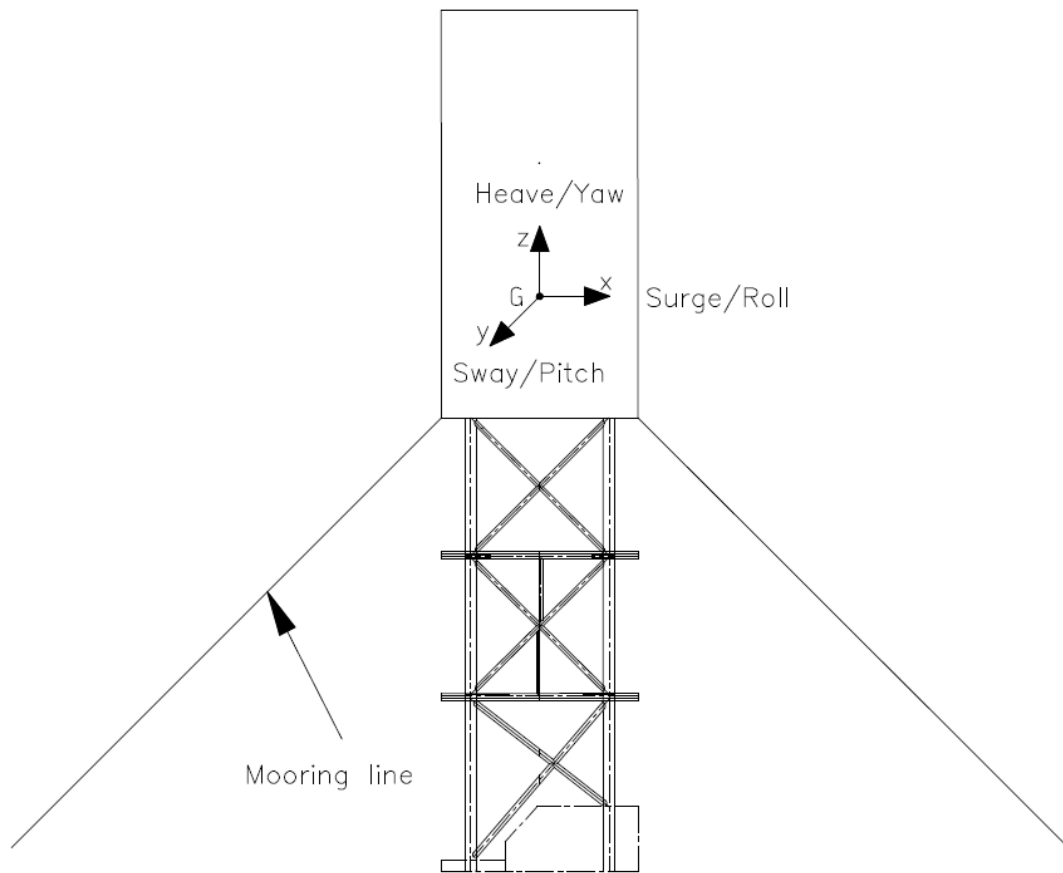


Figure 1.3: Six degrees of freedom for truss spar platform

There are two main approaches, which can be used to evaluate the dynamic responses of any floating offshore structure. An approximate approach is to carry out the analysis in the frequency domain, which gives the steady state responses. Therefore, this approach is adopted only in the preliminary design. An accurate approach is to analyze the structure in the time domain when the structure responses can be evaluated numerically at each time step.

Several theories can be adopted to predict the wave kinematics which is essential for wave force calculations. One of the most useful theories in calculating the kinematics of a progressive wave (Figure 1.4) is the Linear Airy Theory (LAT) which is based on the assumption that the wave height (H) is small compared to the wave

length (L) or water depth (d). This assumption allows the free surface boundary conditions to be linearized by dropping wave height terms, which are beyond the first order and also to be satisfied at the mean water level (MWL), rather than at the oscillating free surface. A number of modifications have been made to LAT to extend the wave kinematics to the free surface. These modifications are different extrapolations (hyperbolic, linear and uniform) and stretching formula [9-10].

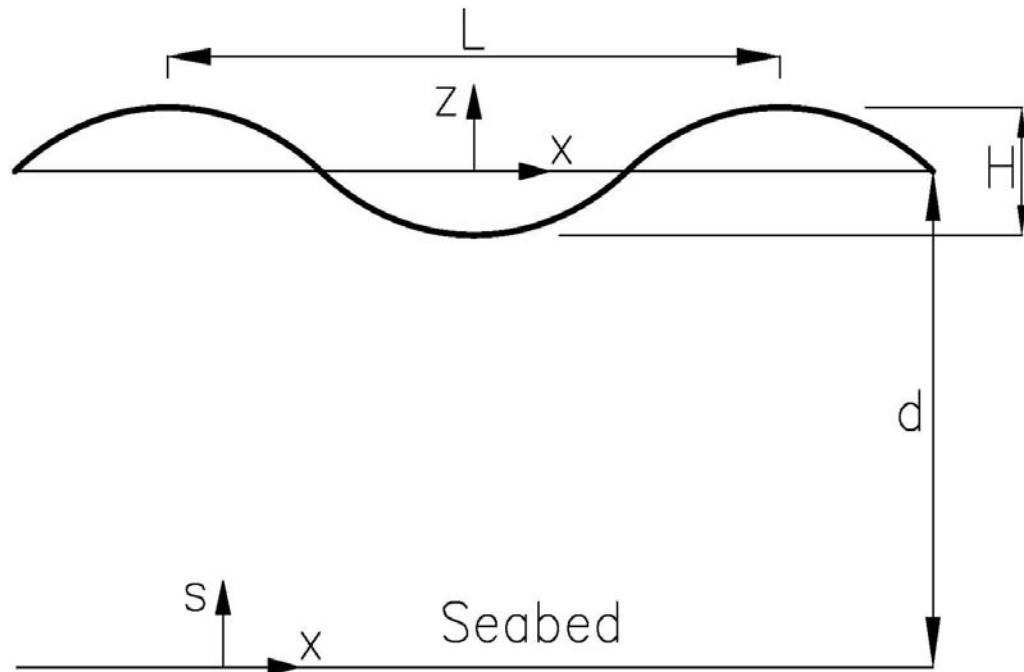


Figure 1.4: Definition sketch for a progressive wave train

Exciting wave forces can be predicted by the Morison equation, which assumes the force to be composed of inertia and drag forces linearly added together. These components involve inertia and drag coefficients, which can be determined experimentally. Morison equation is applicable when the structure is small in dimension compared to the wave length $\left(\frac{\text{Structure Diameter}}{\text{Wave Length}} \leq 0.2\right)$. When the size of the structure is comparable to the wave length, the presence of the structure is expected to change the wave field in the vicinity of the structure. In this case, diffraction of the waves from the surface of the structure should be taken into account in the evaluation of the wave forces. It is generally known as diffraction theory.

Second order difference frequency forces should be considered in the calculation of the wave forces. These forces are due to second order potential velocity, free surface fluctuation, convective acceleration, axial divergence, and calculation of the wave forces in the displaced position. In addition to the aforementioned forces, there are mean drift forces, which cannot be predicted by Morison equation. Due to these forces, the structure is initially displaced at its mean position. Weggel [11] developed equations to predict these forces which represent curve fitting of results obtained from second order diffraction theory.

Mooring lines, which are essential components of spar, are used to anchor the spar to the seabed. In common offshore engineering practice, mooring lines are modeled as linear or nonlinear springs to predict their contribution to the restoring force of the system. This is known as quasi-static analysis, which addresses the dynamics of the mooring lines in static manner, whereby a static equilibrium state is assumed at each time step of the simulation. This sort of analysis neglects the inertia of the mooring line as well as the additional drag forces that may increase the damping of the moored offshore structure. Therefore, a fully coupled dynamic analysis may be adopted to analyze the structure and mooring lines as a coupled system. However, such analysis may become quite expensive.

Based on the above, many aspects should be considered in the dynamic analysis of the spar platform. Therefore, a reliable approach, which suitably considers all the important factors affecting the motion characteristics for truss spar platforms, is developed in this study.

1.3 Objectives of the study

Despite the considerable amount of analytical and experimental studies conducted on the spar platform, there is still a need to explore new approaches that can accurately predict the dynamic responses of the structure and mooring line tension. Quite a number of studies have been conducted on classic spar platforms and large information is available from literature. Nevertheless, only limited research studies on

truss spar platforms have been published. Since these two types of spars are quite different in shape, their motion characteristics are also different.

The objectives of this study are listed below:

1. To develop an efficient methodology for determining the dynamic responses of slender floating offshore structures such as truss spar platforms. This includes the derivation of the horizontal and vertical wave particle kinematics up to the second order using hyperbolic extrapolation method. These wave kinematics were used for predicting the second order difference frequency forces using the principles of the extended Morison equation for an inclined cylinder to account for the inclination of the structure during the analysis.
2. To produce well documented model test results functioning as benchmark data for numerical model's validation. This is to prove the validity of the numerical models for predicting of wave frequency and resonant responses in different environmental conditions as well as the responses due to mooring failure.
3. To examine the effect of current and wind forces on the truss spar dynamic motions.
4. To develop MATLAB codes for quasi-static and dynamic mooring analysis. The first one was used to provide the force-excursion relationship needed for the analysis, while the other was used to accurately predict the mooring line tension.
5. To investigate the effect of mooring line failure and the effect of strengthening the mooring line system on the truss spar motions.
6. To investigate the contributions of mooring line pretension, cable elongation and cable unit weight on the mooring line restoring forces.

1.4 Scope of the study

The scope of the research is confined within the following constrains:

1. The environment is limited to unidirectional waves and steady currents and winds.
2. Truss spar dynamic responses are limited to surge, heave and pitch.
3. The dynamic analysis in this study is conducted only in time domain.
4. The contributions of risers and strakes are not considered in the numerical or experimental modeling.

5. Station keeping systems are limited to taut mooring lines.
6. For the model tests, linear springs are used to represent the restoring force for the prototype mooring system.

1.5 Thesis organization

In this section, the organization of the thesis presented herein.

Chapter 2 presents a general summary of the literature pertaining to the objectives of the study. The reported researches are classified into four categories and a general description of each category is given.

In Chapter 3, different wave theories are discussed in the calculation of the wave kinematics. This includes the governing equation and the boundary conditions. For the purpose of wave force calculations, the design wave environments are explained. Mean drift forces and wave drift damping is explored to account for the structure initial offset and damping respectively. At the end of this chapter, the second order difference frequency forces are derived and presented.

Chapter 4 discusses the theoretical formulations of the problem in time domain. This includes the governing equations of motion and the numerical formulation. In the analysis, the stiffness, mass and damping matrices are formed in time domain. Quasi-static analysis is discussed in the calculation of the mooring line restoring force. Dynamic analysis of the mooring system is explored by using lumped mass numerical algorithm. Finally, the effects of current and wind on the structure's damping and exciting force are discussed.

Chapter 5 concerns with the methodology for the physical modeling of the structure and environments. Model specifications and construction, physical modeling law, tests setup and facilities are described. The laboratory tests are described with special focus on sea keeping tests.

To verify the accuracy of the numerical program, a comprehensive detailed experimental studies and comparisons with the numerical results are presented in

Chapter 6. The comparisons are made for the structure with intact mooring and mooring lines failure conditions. Moreover, comprehensive numerical and experimental studies are presented for a typical truss spar platform. This begins with predicting the mooring system restoring forces by using quasi-static analysis and comparing the numerical results with the corresponding literature measurements. Then the effects of adding different nonlinear effects on the spar responses are observed. Also, the effect of current and wind loads on the structure motions are presented and the numerical results are compared to the corresponding literature predictions. Strengthening of the mooring system effects are also studied numerically in this chapter by showing its effects on the dynamic responses of the truss spar platform. Moreover, mooring lines dynamic analysis is presented and the numerical results are compared to published experimental measurements. Finally, parametric studies on the mooring line restoring force are presented.

Chapter 7 summarizes the findings of this study. The conclusions addressing each objective are mentioned. Finally, recommendations for further improvements and research are proposed.

CHAPTER 2

LITERATURE REVIEW

2.1 Chapter overview

In this chapter, the related research on the aspects of the dynamic analysis of floating offshore structures particularly spar platform, are discussed. These studies are categorized into four general research directions. The critical review on the research topics related to the study is presented.

2.2 Reported studies

The pioneer studies which led to the spar concept are included in this chapter. First, the studies related to the calculations of the wave forces particularly the second order difference frequency wave forces, are presented. Second, the studies which investigate the added mass and damping sources of the system are discussed. Some of these studies investigate the contribution of the heave plates to the structures damping. As a third part, quite a number of researches dealing with the station keeping systems for the offshore floating structures, are presented and discussed. Finally in this chapter, the researches about the new generation spars are presented.

2.3 History of spar platform

The oil industry's first large spar was Shell's Brent spar, installed in the North Sea for oil storage and offloading in the 1970's [1, 12]. Although further research was conducted by some oil companies on the spar concept no other spar platforms were

constructed until 1997 when Neptune was anchored in 590 m water depth in the Gulf of Mexico. Hunter et al. [13] describe a turn-key drilling and production spar developed for the Gulf of Mexico.

The design, analysis and behavior of spars have been outlined in several papers [1, 3, 14]. Among these studies, Glanville et al. [2] gave the details of the concept, construction and installation of a spar platform. He concluded that a spar platform allows flexibility in the selection of well systems and drilling strategies, including early production or pre-drilling programs. Halkyard [14] reviewed the status of several spar concepts emphasizing on the design aspect of these platforms. General design and analysis procedures for buoys (surface and subsurface) and spar buoys is presented in a text by Berteaux [15]. It should be noted that spar concepts have not been limited to production and/or drilling and production systems or to deepwater applications exclusively. FLIP [16] and the French Bouee Laboratoire I [15] are mobile spar-type measurement laboratories that can be deployed at any water depth. However, this is limited by their drafts when they are in their upright positions. Because of their deep drafts (91.5 m and 50 m) when ballasted upright like a spar, these vessels provide heave and pitch (roll) stability in the most common sea states thus allowing sensitive measurements to be conducted. Korloo [17] outlines the design of a cost-effective spar buoy flare (SBF) system that remotely flare large quantities of gas from a fixed offshore production platform 150 m away. The SBF was designed, fabricated and installed in 65 m of water in less than one year; its draft, upper diameter and lower diameter were 52 m, 1.6 m and 2.25 m respectively.

2.4 Research directions

2.4.1 Second order slow drift responses

The research on spar platforms began during the 1990's. Since that time, many numerical and experimental studies have been conducted to investigate the dynamic characteristics of spar platform. Most of the early numerical studies were applied to

the first generation spar, namely classic spar. These studies were validated by an extensive experimental work conducted on the Joint Industry Project (JIP) Spar under Johnson [18] at the Offshore Technology Research Center (OTRC). The responses of the spar buoy at the wave frequency, even near the spectrum peak frequency were small, but relatively large near its natural frequencies, although elevation measurements showed that the incident waves had insignificant energy at these low frequencies. It was shown that the large-amplitude slow drift motions are induced by second order difference frequency wave loading due to nonlinear wave-wave and wave-body interactions [19-20].

Second order wave loading has mostly been computed using the second order diffraction theory [21-22]. As an example, the JIP Spar motions were calculated by Ran et al. [23] using higher order boundary element method (HOBEM) [24]. Several nonlinearities such as computations in the instantaneous displaced position, nonlinear drag damping, and wave drift damping were considered. It was found that the linear wave-body interaction theory alone was not adequate, and the second order wave-body interaction theory had to be used for the reliable motion prediction of a spar. The resulting numerical results agreed well with the measurements data. But the method is often computationally intensive and thus may not be suitable for parametric studies in the preliminary designs.

A simplified alternative approach is to compute the second order wave loading based on the slender body approximation [25], that is, without explicitly considering the diffraction and radiation effects due to the presence of the structure. It can be applied when inertia effects are important and the structure dimension is small compared to the characteristic design wave length. In this method, the second order difference frequency inertia force was obtained from the complete description of the second order acceleration field which includes both temporal and convective terms. Additional second order contributions due to the axial divergence and fluctuation of the free surface were also included. The slender body analysis was applied to the computation of the slow varying pitch moments on an articulated loading platform (ALP) and the results agree well with the second order diffraction computation. This

method was found to be several order faster compared to the second order diffraction theory.

For a typical deepwater offshore structure such as the spar, the ratio of the structure dimension to the characteristic design wave length is usually small (less than 0.2). Hence it may be assumed that the wave field is virtually undisturbed by the structure and that the modified Morison equation [26] is adequate to calculate the first and second order wave exciting forces. Based on this assumption, a new methodology [27] was developed to predict slow drift responses of slender compliant offshore structures due to ocean waves. Hybrid wave model [28] and Morison equation were used to predict the wave kinematics and wave forces respectively for irregular waves. The results of the numerical method achieved good agreement with experimental measurements for classic spar and floating jacket platforms.

Based on the slender body approximation method, several studies demonstrated the importance of the second order low frequency forces. Mekha et al. [29-30] and Johnson et al. [31] studied the behavior of spar in deep water. In their work, they used Morison equation to calculate the wave forces in time domain considering several second order effects and wave kinematics. They also investigated the effect of neglecting the hydrodynamic forces acting on the mooring lines by modeling them as nonlinear springs. In their studies, they used regular, bichromatic and random waves to predict the responses which are compared with the experimental results showing the effect of each individual second order effect on the spar responses. However, in their studies they neglected the second order temporal acceleration in the analysis. An interesting result [32] was that some of these effects acted in opposite direction, therefore inclusion/exclusion of any of them gave entirely different numerical predictions. Weggel and Roesset [33-34] did similar work using second order diffraction theory implementing WAMIT [35], TFPOP [36] as well as an approximation suggested by Donley and Spanos [37].

Slender body approximation method proves to be an attractive analysis tool for spar which is subjected to various environmental conditions. This was shown by a study [38] concerned with the nonlinear response of a spar platform under different

environmental conditions, i.e., regular wave, bichromatic, random waves and current using a time domain simulation model. The model could consider several nonlinear effects. Hydrodynamic forces and moments were computed using the Morison equation. It was concluded that Morison equation combined with accurate prediction of wave particle kinematics and force calculations in the displaced position of the platform gave a reliable prediction of platform response both in wave frequency and low frequency range.

A study [39] on the motions of a truss spar based on the full slender body formulation incorporating all nonlinear terms were conducted. For this purpose, a code written in MATLAB was developed by extending the code for classic spar. Satisfactory agreement was achieved between the predicted results and limited experiment results. In addition, different simplified methods for estimating the forces on the truss section and the hard tank were studied. It was found that only the full slender body formulation could lead to reasonable results.

At the same time, wave kinematics methods were subjected to intensive investigations. A methodology has been developed [40] to establish second order corrections to the engineering methods, which are used to calculate the wave kinematics. The purpose was to find a description of the wave kinematics which predicts measured behavior with good degree of accuracy. The methodology has been applied to the engineering methods proposed by Wheeler [9] and Chakrabarti [10]. The second order Chakrabarti approximation demonstrates good agreement with measured wave kinematics.

A new hybrid wave model (HWM) for the prediction of the wave kinematics of the unidirectional irregular wave train was introduced by Zhang et al. [28]. HWM is different from the other approaches by decomposition of the observed wave elevation into 'free' waves up to second order accuracy while the conventional methods consider the wave elevations to be only linear combinations of individual sinusoids. The numerical model was extensively examined using various wave spectra and was found to be convergent and accurate. The application of the HWM were demonstrated by comparison with two sets of laboratory measurements and with the linear random wave theory and its stretching and extrapolation modification by Spell [41]. It was

concluded that the HWM is more accurate and reliable than the linear random wave theory especially near steep wave crest.

The differences between various approximate methods to compute the wave kinematics and forces acting on a spar platform up to the instantaneous free water surface was investigated [42]. Three types of procedures were considered; i.e., extrapolation, stretching and the hybrid wave model. Of particular interest for the dynamic response of a spar are the nonlinear low frequency forces. The effects of the different procedures were compared analytically and numerically for the inertia forces using Morison equation [26] as reported in 1950, but the conclusions can be extended to diffraction theory formulations.

A method for resolving incident free-wave components from wave elevations measured around a spar offshore platform [43] was discussed. The importance of this method was proven by comparison between full scale measurements of motions for the Moomvang Truss Spar and the analytical predictions. Particular attention was given to the wave frequency responses. Results revealed an excellent match between the measured and analytically predicted spar responses when the measured waves were adequately decomposed into incident free-wave components and inserted into the numerical model.

The spar motion characteristics in directional wave environment were studied [44] using the unidirectional hybrid wave model (UHWM) and directional hybrid wave model (DHWM). Comparisons between numerical results from these two different wave models indicated that the slow drifting surge and pitch motions based on DHWM are slightly smaller than those based on UHWM. The slow drifting heave motions from the two wave models were almost the same because the heave motion was mainly excited by the pressure applied on the structure bottom and the predicted bottom pressure from the two methods had almost no differences.

A study by Chitrapu et al. [45] discussed the motion response of a large diameter spar platform in long crested and random directional waves and current using a time domain simulation model. Several nonlinearities such as the free surface force calculation, displaced position force computation, nonlinearities in the equation of

motion and the effect of wave current interaction were considered for determining the motion response. The effect of wave directionality on the predicted surge and pitch response of the spar platform was studied. It was seen that both wave-current interaction and directional spread of wave energy had a significant effect on the predicted response.

Results from a study [46] on the dynamic response analysis of spar platform subjected to wave and wind forces were presented. The motions considered were surge and pitch. The wind gust was modeled with the Harris [47] and Ochi and Shin [48] wind gust spectra. The effect of the wave age on the wind gust spectrum was included by adopting the Volkov wave age dependent sea surface roughness parameter. The wave age independent Charnock roughness parameter was also used. The results demonstrated clear effects of wave age on the dynamic response. Moreover, for high mean wind speeds the total wind response was much smaller than the wave response but for low speeds the wind appeared to be more important.

With respect to the method of analysis, Halkyard [14] stated that the time domain analysis is most appropriate for response predictions in survival conditions while frequency domain analysis is more appropriate for operational conditions. Iftekhhar [49] studied the differences between time domain and frequency domain analysis in predicting the slow drift responses of the spar by using Morison equation. The limitation of the frequency domain in modeling the nonlinearities in the exciting forces and the structural properties was shown.

2.4.2 Damping and added mass

Spar platforms have low natural frequencies, particularly in surge and pitch. Due to the nonlinear low frequency wave forces, the structure experiences large low frequency motions. Near the resonant frequency, damping is essential for the slow drift motions. Radiation damping causing from the radiation of the waves due to the body motions is negligible in low frequency range. Viscous damping, wave drift damping and mooring line damping are the three main components of slow drift damping [50]. The sources of these damping are different. Viscous damping results

from pressure drag and friction drag on the structure. Wave drift damping is due to the dependence of wave drift forces on slow drift motion of the moored structure [51-53]. The mooring damping is from drag forces on mooring lines and the friction between mooring lines and the seabed. Many studies revealed that the damping induced by the mooring system could substantially reduce the slow drift surge motions of a moored semi submersible or ship [54-57]. In addition to added mass, the subsequent discussion in this category will focus on the studies related to viscous damping and wave drift damping only.

The drag force on the platform, commonly predicted using Morison equation [58], is considered as the major damping source in the system. This damping is difficult to quantify due to its nonlinear nature (force is proportional to the square of the fluid velocity). Many studies were carried out to simplify the drag damping [59-60] for frequency domain analysis.

Several research projects have been conducted to study the hydrodynamic behavior of axial oscillating cylinders. Huse [61] tested a cylinder with Keulegan-Carpenter (KC) ranging from 0.0005 to 0.01 and frequency parameter (β) approximately 5×10^6 . His results showed that the drag force varied linearly with velocity. Chakrabarti and Hanna [62] reached a similar conclusion from their tests with $KC = 0.126$ and β ranging from 0.25×10^6 to 1×10^6 . Huse and Utnes [63] placed a TLP column in a current and the results showed that the current increased the damping over the range of KC being tested.

Thiagarajan and Troesch [64] reported a nonlinear trend between the drag force and velocity for axial oscillating cylinders conflicting with the previous results [61]. The tested KC numbers ranged from 0.1 to 1 and $\beta = 0.89 \times 10^5$. In their studies they decomposed the drag force into its friction and form (pressure) drag components. The friction drag is due to the viscous tangential stress acting along the walls of the cylinder. The form drag is mainly due to the separation at cylinder edges. At very low KC , the drag is due primarily to the effect of the surface area of the cylinder wall. The friction drag varies linearly with velocity, while the form drag is nonlinear with velocity. Alternatively, in relation to KC , the friction drag is KC -independent, while the form drag is linear with KC . The former experiments [61-62] were conducted at

KC s from 0.0005 to 0.126, where friction drag is dominant. The latter study [64] covered KC from 0.1 to 1, where form drag becomes dominant.

Although the previous studies [61-64] focus on Tension Leg Platforms, the results of the axial oscillating cylinder research are also applicable to spar platforms. The underwater part of a spar platform is comprised of a long cylinder hull, which can also be modeled as an axially oscillating cylinder.

In addition to the previous studies which deal with viscous damping, number of researchers studied the damping-augmenting devices designed to substantially reduce the heave motion. Different form of devices, such as tubes, appendages and plates have been proposed and researched. Srinivasan et al. [65] showed through experiments that an array of small diameter diamond-shaped tubes increased the inline drag coefficient for a cylinder by as much as five times at low KC numbers, whereas the inertial coefficients were found to be insensitive to the device.

Thiagarajan and Troesch [66] examined the effect of adding an appendage in the form of a disk to TLP columns. The model test conducted in heave on a cylinder disk configuration showed that the heave damping induced by the disk is linear with the amplitude of oscillation. The disk was found to increase the form drag coefficient by double. The effects of a small uniform current were also examined during the model tests. In the presence of a disk, the damping induced by the current was doubled as well. The tests were conducted at $\beta = 0.89 \times 10^5$ and KC range of 0.1 – 1.

Lake et al. [67] investigated three possible configurations of TLP/spar platforms and the results showed that the addition of a disk to the base of the column can enhance the damping but does little to increase the added mass. Separating the disk and cylinder, nearly doubles the added mass and increases the damping ratio by 58 percent over the attached cylinder disk platform and an impressive 344 percent over the single column.

Prislin et al. [68] experimentally studied the variation of added mass and damping of both the single plate and multi plate arrangement for a spar platform. He did not include the effect of the vertical column. The tested Reynolds number ranged from 4.5×10^3 to 1.8×10^5 and the KC number ranged from 0.1 to 1. His results showed

that the drag coefficient of an oscillating plate is dependent on both Reynolds number and KC number for Reynolds number less than 1×10^5 . At higher Reynolds number, the drag coefficient does not vary significantly with the Reynolds number and it is significantly lower than the drag coefficient measured at low Reynolds number.

Magee et al. [5] discussed the application of squared plate to truss spar. His experimental results and numerical predictions showed that square plates significantly help to reduce the heave response of truss spar. He also observed that the loads on the square plates can be predicted accurately by using Morison equation.

Heave damping augmentation effect on the heave behavior of a classic spar was studied experimentally [69]. The importance of heave damping augmentation for spars and the possibility of achieving this augmentation via the use of circular plate sections protruding from the spar hull, were studied. The tests had two main goals, one to determine whether more than one plate could be added with effect and the other to find the optimum spacing between plates for more than one plate. The results showed that, with a number of damping plates, each additional plate did increase the total damping; however, the largest increase was achieved with the first plate added to the cylinder. With respect to the optimum spacing between two plates, the results showed that the optimum spacing was approximately one cylinder diameter; further increase in spacing does not significantly increase the damping.

The effect of different types of heave plates on the dynamic responses of a truss spar platform was studied experimentally [70]. Four types of plate were used in the experiment. Two of them were perforated (large and small) and two were solid (large and small). It was found that, over most of the range considered, the heave responses were larger for the spars with the smaller plates and the perforated plates than for those with the larger and solid ones. This was because of the large added masses of the large and solid plates compared to the small and perforated ones, which led to lower natural frequencies further away from the peak wave energy and resonant behavior.

An alternative solution to increase the viscous damping of classic spar in the vertical direction is to change the hull shape. The study [71] investigated different

alternative hull shapes proposed by Haslum and Faltinsen [72] in reducing the heave resonant response. The wave forces, added mass and radiation damping were calculated from the well-known hydrodynamic software package called SESAM [73] based on potential theory. Nonlinear viscous heave damping was calculated by solving Navier-Stokes equation based on the finite difference method. These two were then combined via an iterative procedure. It was concluded that the heave resonant response can be considerably reduced by alternative hull shapes via increasing the damping mechanism and keeping the natural heave period outside the range of wave energy.

With the advance of the wave-current interaction theory, it was revealed that the wave drift damping [74], which is the second order potential force proportional to the low forward speed of the platform, was considered as another important damping source for slow drift motions. This damping comes from the added resistance to motion in the presence of waves versus the resistance in no waves. This means solving a diffraction-radiation problem for a body with small forward speed and computing the added resistance. The solution must be performed in time domain because the wave drift damping force is coupled with the input wave as well as the output motion [36]. A quasi-analytic solution was given by Emmerhoff and Emmerhoff and Sclavounos [75]. Simple expressions for the wave drift damping [74] have been developed for infinite water depth and for bodies constrained to respond to the waves. These expressions have been reported to be quite accurate when compared to the more rigorous preceding procedure [75]. Weggel [11] developed equations for calculating the mean drift forces. These equations represent curve fitting of results obtained from second order diffraction theory due to the first order potential. These equations were substituted in the expressions [74] to find the wave drift damping for free-body cylinders. A more general account of wave drift damping is available in some diffraction codes such as SWIM [76].

For finding out the importance of the wave drift damping and viscous forces to be included in the dynamic analysis of spar platforms, Alok et al. [77] compared the analytically predicted motions of a spar buoy platform with the results of wave tank experiments. They used extreme wave conditions in both the Gulf of Mexico and the

North Sea. In their numerical model they combined nonlinear diffraction loads and a linear, multi-degree-of-freedom model of the spar stiffness and damping characteristics. They investigated the effect of wave drift damping and the viscous forces on the spar motions. By including these two effects to the numerical model, the predicted results were found to improve the agreement with the model test results.

2.4.3 Mooring lines

This category discusses the studies related to investigations on the analysis methods of the station keeping systems. Under the assumption of neglecting the inertia of mooring system as well as the additional drag force that may increase the damping of the total system, Ansari [78] presented an analysis to determine the tension displacement characteristics of a slack mooring line made up of anchors, clump weights, chains and cables and showed how the effect of cable behavior can be included in the dynamic analysis of a moored offshore vessel. In deriving the various configuration equations, use was made of the catenary relationships pertaining to a static mooring system configuration and, where necessary, continuity of slope and displacement was incorporated with due regard for force equilibrium and anchor holding power consideration.

According to the same assumption, an iterative numerical scheme for the quasi-static analysis of multi-component mooring lines for horizontal excursion was presented by Agarwal and Jain [79]. The material and geometry nonlinearities were taken into consideration with no hydrodynamic effects taken into account. Further improvement of this method namely the quasi-static analysis of multi-component mooring lines for vertical excursion was developed [80].

Quasi-static analysis ignores the effect of line dynamics which, in some situations, as Ansari and Khan [81] have shown, may prove to be significant element in the dynamic analysis of a moored offshore vessel. In an effort to predict mooring system behavior in a way that is realistically feasible as well as useable, Khan and Ansari [82] modeled each mooring line as a multi-segment, discrete dynamic system. The equations of motions were formulated based on Lagrange equations and then

numerically solved to develop tension-displacement characteristics. This information was then used in providing nonlinear restoring forces in the dynamic analysis of the moored offshore structure, as shown by Ansari and Khan [81].

As water depth increases, the damping contribution from the mooring lines and risers can be significant. In addition to the damping effect, the mooring system may affect the motions of the platform due to the line dynamics (inertia effect). These effects cannot be predicted in a conventional quasi-static analysis. Coupled analysis, which simultaneously solves the dynamics of the platform and the mooring system, can handle such a vessel/mooring/riser coupling including all effects. There are few useful coupled analysis software available for the engineering analysis. Pauling and Webster [83] analyzed the large amplitude motion of the TLP using a coupled platform-tether system model. They used a slender rod theory to model the tendons of the TLP [84] and Morison equation to calculate hydrodynamic forces on the TLP. Kim et al. [85] developed a coupled time domain analysis program for TLP tether analysis, using nonlinear beam theory and updated Lagrangian formulation. The integration scheme requires iteration and coordinate transformation between local coordinate in the beam element and the global coordinates at each time step, which require significant computation effort.

With the awareness of the importance of coupling effect between the mooring system and the platform in deepwater, a Joint Industry Project sponsored by several major oil companies (Shell, Amoco, Molbil, etc.) and offshore engineering companies (Aker, Brown & Root, etc.) was started in the ocean engineering program Texas A&M University in 1994. The goal of the project was to develop an efficient hydrodynamics program (WINTCOL) for column-based floating structures and a coupled platform/ riser/mooring dynamic analysis program (WINPOST) with a finite element model which can deal with the dynamics of most types of mooring system and risers [86].

Methods used for cable dynamic analysis are either in frequency domain or time domain. Traintafyllou et al. [87] conducted many mooring dynamic analyses in the frequency domain. His study laid a foundation for some commonly used mooring design tools in the frequency domain. Time domain methods are based on either a

lumped mass method or finite element method. Van den Boom [88] performed dynamic analysis of mooring lines using the lumped mass method. He examined the mechanism of the dynamic behavior of mooring lines. He developed a computer algorithm based on the lumped mass method and compared the predictions with results of harmonic oscillation tests for various lines and water depths at different model scales. Results from this study clearly showed the importance of dynamic analysis for various mooring configurations. A commercial code, known as OrcaFlex [89], also uses the lumped mass method. Brown [90] and Mavrakos made a comparison of mooring line dynamic loading computed by fifteen different numerical programs in frequency domain or time domain. One study [91] made a comparison of spar motions and the mooring dynamic tensions by using coupled dynamic analysis in time domain and frequency domain. WINTCOL and WINPOST were used for this purpose. The results showed that generally time domain analysis produces larger wave frequency and slowly varying responses and mooring tensions (except for wave-frequency top tension) than the corresponding frequency domain results, which implies that the viscous damping is likely to be overestimated by stochastic linearization in the frequency domain.

Nonlinear motion equations of cable was reduced with the assumption of linear constitutive relation, and simplified further according to propagation characters of stress wave [92]. The loading acting on quasi-static cables were analyzed and the detailed expressions were given. The displacement, stress and strain in mooring line in deep water were calculated. The results showed that, the stress in cable propagating from exciting end to fixed end and there is a difference in phase. At the same time, the strain in cable different point is also different. At the point with maximum tension, the normal motion is double-period and the tangential motion is quasi-periodic. The tension in cable is effected by tangential and normal drag.

A coupled dynamic analysis program called COUPLE was developed [93]. This program is applicable for spar and TLPs. It has two options for computing wave potential forces, namely second order diffraction/radiation theory or Morison equation using HWMs to compute the nonlinear wave kinematics. It also has two options for

modeling mooring/tendon/riser system, namely quasi-static and coupled dynamic approach.

A six DOF FE code was developed for the nonlinear static and dynamic analysis of mooring lines and marine risers by [94]. The geometric and the environmental load nonlinearities were considered. The Newton iteration method was selected to solve the mooring line nonlinear algebraic governing differential equations while for dynamic problems, the first order differential equations were solved by the first order Adams-Moulton method. The reliability and accuracy of the program were demonstrated by comparing numerical solutions with the analytical solutions, experimental data and numerical results by other programs.

Beside numerical simulations, model tests are the other important simulation method in the design of a floating system. The design of the mooring system in deepwater presents a challenge to the model tests in wave basins. Water depths around 1000 m can be modeled in the largest test basins in the world by typical scales ranging from 1:50 to 1:100 in the past [95]. Due to the limitation of the depth of existing wave basins, either the model is made in very small scale, or the mooring system has to be distorted. It is truncated vertically and sometimes horizontally due to the limited horizontal dimensions of the a basin [96]. Truncated mooring line model tests showed that line dynamic tensions of a truncated mooring system are very different from those of a full-depth (undistorted) mooring system [97]. Ormberg et al. [98] has proposed a hybrid method to extrapolate a truncated mooring model test to the corresponding full depth mooring system with the aid of numerical simulations based on coupled dynamic analysis.

The coupled dynamic analysis is much more accurate than the quasi-static approach in predicting the motions of a hull and tensions in the mooring lines. However, it is also computationally intensive, which hinders its application as a common design tool. A three-hour simulation of a moored floating structure may take much longer time to perform using a couple analysis [95].

2.4.4 Spar platform generations development

The first spar production platform, Neptune spar (24 m in diameter and 198 m draft) was installed in 610 m deep water in 1996 [99-100]. This spar and its first generation successors are called the “classic” spars. They are essentially deep draft, vertical steel cylinders. Neptune spar was followed by Genesis (37 m diameter and 198 m draft) in 790 m water depth in 1998, and Diana (37 m diameter and 198 m draft) in 1310 m water depth in 1999 [86]. The recent generations of the spar platform are considered to be more cost effective.

Many improvements have been made on the first spar generation, including the hull form optimization and the applications of other offshore technologies such as heave plate configurations. Generally speaking, those improvements were mainly in terms of fabrication and installation complexities. The truss spar production platform is the second development concept that replaces the cylindrical lower section of a classic spar with an open truss structure that includes heave plates. When the storage capacity of a classic spar is not a requirement and the current is a major factor, the truss spar (second generation) provides a lighter, more cost effective alternative that still maintains the same motion characteristics of a classic spar [101-102].

Truss spar platform consists of a top “hard” and bottom “soft” tanks separated by a truss mid-section. Horizontal heave plates are fitted across the truss bays to reduce heave motion by increasing both the added mass and the viscous damping. In addition, truss spar has a much lower drag area than the classic spar mid-section so that the current and associated mooring loads are reduced [70, 103].

All the truss spar projects are associated with numerical and experimental studies. Datta et al. [104] presented comparisons of numerical predictions of motions and loads using TDSIM software [105] to typical truss spar model test results. The purpose of this comparison was to calibrate hydrodynamic coefficients, which were to be used for the design of a new truss spar platform for Amoco. The results agreed very well over a wide range of wave frequencies. It also proved that the numerical program could be used with high confidence for spar design. The first truss spar installed outside Gulf of Mexico is Kikeh truss spar, which is located 120 Km

northwest of the island of Labuan, East Malaysia, in approximately 1330 m water depth. various numerical and experimental studies were performed to arrive at the design of Kikeh [106]. MLTISM [107], which is a time domain simulation program, was used for the numerical predictions. Theckumpurath et al. [108] conducted a time domain coupled dynamic analysis for the “Horn Mountain” truss spar, which was deployed in the Gulf of Mexico in 1650 m water depth, by using COUPLE software. The simulated results were compared with the corresponding field measurements made during Hurricane Isidore. Satisfactory agreement between the simulation and the measurements was achieved.

The cell spar is a new design that has several physical characteristics different from those of the classic and truss spars. Its upper portion is composed of six outer cells surrounding a center cell to provide the buoyancy, while the lower portion is formed by extending three of the outer cells down to the keel. This concept was put forward basically in consideration of the reduction of fabrication difficulty and cost, as the standard rolling technique could be taken in. Some studies were conducted on cell spar concept. As an example, an experimental study [109] on the motion characteristics of cell spar was performed. During the experiments, it was observed that the pitch motions became unstable at a certain time range. The authors thought that kinetic energy was transferred from heave mode to pitch mode due to the nonlinearity. The experimental results agreed well with the numerical predictions except for the time range of unstable pitch motion. Some model basin tests [7] of the cell spar indicate that multiple cells forming a column can be less susceptible to vortices as the spacing between them permits interstitial flow of water through their spaces. An experimental study [6] on the effect of heave plates on the hydrodynamic performance of cell spar platform was conducted. A variation of the cell spar concept with the lower part fitted with a truss section and several heave plates, was modeled and tested. Different types of heave plates were used to investigate various design aspects of the plates.

The newest spar configuration is the cell-truss spar. This new concept was introduced by the State Key Laboratory of Ocean Engineering (SKLOE) in Shanghai Jiaotong University (SJTU), intending to take advantage of both the typical truss spar

and cell spar. A nonlinear time domain dynamic coupled analysis program, named SESAM (developed by DNV software), was used to investigate the global performance and mooring line tensions of the new spar concept [110]. A basic test with a 1:100 scale model was also conducted in the wave basin of SKLOE to calibrate the numerical approach. It was found that this new configuration has inherited the advantages of its former generations of spar and its motions could be restrained in a satisfactory region. As the research on cell-truss spar was going on in SKLOE at SJTU, the new concept has been subjected to numerous studies. A model test of cell-truss spar based on hybrid model testing technique was conducted for cell-truss spar [111]. By using this method for experiments, full-depth mooring/riser system should be truncated according to model scale and available work depth of the basin and model test results need to be calibrated and extrapolated by numerical software. The numerical predictions agreed well with the experimental measurements. In addition to the preceding studies on cell-truss spar at SJTU, a comparison between three numerical schemes, including frequency domain analysis, time domain semi-coupled and fully-coupled analysis, and experimental data have been performed for cell-truss spar [112]. The aim of these comparisons was to find the applicability of the different approaches to predict the motions and mooring line tensions for cell-truss spar.

A new type of Spar platform named S-Spar was presented [113]. Its midsection is a cylinder with the same diameter as the centre well. And the centre well and midsection was designed as an integrated structure. Heave plates are attached appropriately along the connection section. With the unique midsection, S-Spar is suitable for operating at the special oceanic environment and ultra-deep water depth in South China Sea. The structural design and hydrodynamic analysis for this structure were discussed. Detail motion analysis results showed that the platform offers excellent motion characteristics, and optimizing to carry large payloads in ultra-deep water. Finally, the effect of potential and viscous damping in different region has been analyzed.

2.5 Critical literature review

In this section, the conclusions made from the literature survey related to the study are presented.

Second order slow drift responses

This part explains the analytical methods used for determining the slow drift motions of spar platforms. Most of the numerical studies that investigated the second order slow drift motions were applied to the first generation classic spar only and used the JIP spar experimental data [18] for the purpose of validation.

The reported studies on the nonlinear difference frequency forces began by using second order diffraction theory [21-22]. The shortcoming of this method is the intensive computations required. For slender offshore structures like spar, slender body approximation method [25] was found more efficient compared to the second order diffraction theory in the calculation of the second order difference frequency forces. The assessment of the effect of these forces on the spar motions was demonstrated by using second order diffraction theory [33-34] and the slender body approximation method [29-31] which assumes that the presence of the structure does not alter the wave field. All the nonlinear effects were incorporated in [33-34] while in [29-31], the second order temporal acceleration is not considered in the analysis.

With regard to the wave kinematics, hybrid wave model [28] differs from the other theories by considering the decomposition of the wave elevations into free waves up to the second order, while in the other theories, the wave elevations are considered to be linear combinations of individual sinusoids. The differences between the various methods have been investigated in [42]. This wave decomposition was considered only in [27], [28], [41] and [42].

Time domain analysis was found to be appropriate for response predictions in survival conditions while frequency domain analysis was found suitable for operation conditions [14]. The difference between these two methods in determining the slow drift motions of spar has been studied in [49].

Second order difference frequency forces and its effects on the slow drift motions of classic spar platform were studied elaborately. The second spar generation, truss spar, did not receive enough attention in this research area. Furthermore, only few published studies [86] addressed the effect of current and wind forces on the motion characteristics of truss spar platform.

Damping and added mass

As the significant spar motions are caused by the nonlinear difference frequency forces, damping plays a great part in reducing these slow drift motions. For the spar, there are four sources of damping known as radiation damping, viscous damping, wave drift damping and mooring line damping. The last three sources have more significant effect on the resonant responses compared to the radiation damping [114].

Viscous damping is commonly predicted by using Morison equation [58]. As the nature of this damping is nonlinear, many studies [59-60] propose statistical linearization for the velocity squared drag force for inertia dominated structures. In order to increase this damping especially in the heave direction, number of researchers studied the effect of damping-augmenting devices on the heave motion [65] to [69]. A study by Magee et al. [5] showed that the square plates in the truss spar platform significantly reduced the heave motion by increasing the added mass and the viscous damping.

Wave drift damping is usually predicted by using second order diffraction theory. One of the most important equations used for this purpose, was developed by Weggel [11]. These equations represent curve fitting of results for fixed-body and free-body cylinders.

Mooring lines

Mooring lines form an integral part of floating offshore structures. Many researches have been conducted on its effect on the structure motions. In general, methods of analysis of mooring line can be classified into two main categories known as quasi-static analysis and dynamic analysis. The main difference between these two methods, is the effect of fluid mooring line interaction, which is considered only in the dynamic analysis.

Under the assumption of the insignificance of the generated drag and inertia forces on the mooring line due to its motion, Ansari [78] used the catenary equations for conducting static analysis for multi component mooring line. Under the same assumption, Agarwal and Jain [79] developed an iterative numerical scheme that can be used for predicting the mooring line restoring force vs excursion relationship which is required for solving the equation of motion.

Many studies considered the dynamic effects of the mooring line. These studies followed two methods. First, the semi-coupled dynamic analysis in which a separate program based on either finite element method or lumped mass method [88] is required to predict mooring line tension. Second, the fully coupled analysis [86] in which the structure with its mooring lines was considered as a coupled structural system. In comparison with the quasi-static analysis and semi-coupled analysis, the fully coupled analysis is more accurate and it is computationally intensive.

Considerable research has been done in this area. However, the amount of research considering the fully coupled dynamic analysis is very few compared to the other mentioned methods for mooring line analysis. On the other hand, the effects of the phenomena of mooring line failure and strengthening of mooring line system on the motion characteristics of truss spar platform have not been considered either experimentally or numerically in the published literature.

CHAPTER 3

SECOND ORDER SLOWLY VARYING DRIFT FORCES

3.1 Introduction

Different wave kinematics theories and the boundary conditions are reviewed first in this chapter. The design wave environments and mean drift forces are discussed subsequently. Finally, the calculations for the second order wave forces are derived and presented. In this chapter, the second order slow varying drift forces formulae were derived considering the inclination of the structure during the dynamic analysis by using the extended Morison equation for an inclined cylinder for predicting the wave forces and hyperbolic extrapolation for calculating the wave kinematics.

3.2 Wave theories

Most of the wave theories which are applicable to a variety of environments and are used in the design of offshore structures are dependent upon water depth, wave height and wave period. In developing a wave theory, a boundary value problem (BVP) consisting of a differential equation with boundary conditions describing the various boundaries is solved in an approximate way. There are two general types of approximate theory: one is developed around the wave height as a perturbation parameter (e.g. in deep water) while the other is developed as a function of the water depth (e.g. in shallow water).

3.2.1 Governing equation and boundary conditions

In developing the wave theories, water is assumed to be incompressible and

irrotational and the continuity of the flow is assumed. The continuity equation, which states that the mass of the fluid is conserved, can be written in terms of fluid velocities as

$$\frac{\partial u}{\partial x} + \frac{\partial v}{\partial z} + \frac{\partial w}{\partial y} = 0 \quad (3.1)$$

in which u , v , w are the three components of a fluid particle velocity in a rectangular Cartesian coordinate system, $oxyz$. The coordinate system is chosen such that the origin, o , is at mean water level (MWL), x is positive in the direction of the wave propagation, z is positive upwards and y forms a right-handed system with x and z .

The continuity equation can be equivalently written in terms of the velocity vector as

$$\nabla \cdot V = 0 \quad (3.2)$$

where $V = ui + vj + wk$ and the operator, ∇ , is defined as $\nabla = \frac{\partial}{\partial x}i + \frac{\partial}{\partial z}j + \frac{\partial}{\partial y}k$

If a rotational vector is introduced such that

$$\omega = \frac{1}{2} \nabla \times V \quad (3.3)$$

then the three components of the rotational vector are given by

$$\omega_1 = \frac{1}{2} \left(\frac{\partial w}{\partial z} - \frac{\partial v}{\partial y} \right) \quad (3.4)$$

$$\omega_2 = \frac{1}{2} \left(\frac{\partial u}{\partial y} - \frac{\partial w}{\partial x} \right) \quad (3.5)$$

$$\omega_3 = \frac{1}{2} \left(\frac{\partial v}{\partial x} - \frac{\partial u}{\partial z} \right) \quad (3.6)$$

The motion is considered irrotational if $\omega_1 = \omega_2 = \omega_3 = 0$. By define a function named velocity potential, ϕ , such that

$$u = \frac{\partial \phi}{\partial x}, \quad v = \frac{\partial \phi}{\partial z} \quad \text{and} \quad w = \frac{\partial \phi}{\partial y} \quad (3.7)$$

and by inserting these values of the velocity components in Eqs 3.4 to 3.6, it can be shown that $\omega_1 = \omega_2 = \omega_3 = 0$. Thus the existence of the velocity potential, ϕ , implies that the motion is irrotational.

Substituting Eq. 3.7 in Eq. 3.1, the well-known Laplace equation is obtained as

$$\nabla^2 \phi = \frac{\partial^2 \phi}{\partial x^2} + \frac{\partial^2 \phi}{\partial y^2} + \frac{\partial^2 \phi}{\partial z^2} = 0 \quad (3.8)$$

In order to solve for the kinetics (e.g., pressures and forces) of the waves, Bernoulli equation is used. The Navier-Stokes equation [115] can be written in vector form as

$$\rho \frac{\partial V}{\partial t} + \rho(\nabla \times V) \times V - \mu \nabla^2 V + \nabla \left(p + \rho g z + \rho \frac{V^2}{2} \right) = 0 \quad (3.9)$$

in which ρ = mass density of wave, μ = dynamic viscosity of wave, g = acceleration due to gravity, z = vertical coordinate, p = pressure and V = velocity vector.

By applying the assumptions of ideal fluid (i.e. inviscid ($\mu=0$), incompressible and irrotational ($\nabla \times V = 0$)), and inserting the value of V in terms ϕ in the local inertia term, $\rho \partial V / \partial t$, the unsteady form of Bernoulli equation can be written as

$$\rho \frac{\partial \phi}{\partial t} + p + \rho g y + \frac{1}{2} \rho \left[\left(\frac{\partial \phi}{\partial x} \right)^2 + \left(\frac{\partial \phi}{\partial y} \right)^2 + \left(\frac{\partial \phi}{\partial z} \right)^2 \right] = f(t) \quad (3.10)$$

where $f(t)$ = an arbitrary function of time.

It is assumed that the waves are two dimensional in the xz plane and the seabed is flat out of undisturbed depth from the MWL. Parameters used to define the progressive wave are shown in Figure 1.4.

As the waves are assumed two dimensional, the governing equation (Eq. 3.8) can be written as

$$\frac{\partial^2 \phi}{\partial x^2} + \frac{\partial^2 \phi}{\partial z^2} = 0 \quad (3.11)$$

The BVP in the two-dimensional case may be summarized as follows:

$$\text{Bottom boundary condition: } \frac{\partial \phi}{\partial z} = 0 \text{ at } z = -d \quad (3.12)$$

$$\text{Free surface kinematic condition: } \frac{\partial \eta}{\partial t} + \frac{\partial \phi}{\partial x} \frac{\partial \eta}{\partial x} - \frac{\partial \phi}{\partial z} = 0 \text{ at } z = \eta \quad (3.13)$$

$$\text{Free surface dynamic condition: } \frac{\partial \phi}{\partial t} + \frac{1}{2} \left[\left(\frac{\partial \phi}{\partial x} \right)^2 + \left(\frac{\partial \phi}{\partial z} \right)^2 \right] + g\eta = 0 \text{ at } z = \eta \quad (3.14)$$

where η is the wave elevation. The velocity potential, ϕ , must satisfy the governing equation 3.11 and the three boundary conditions (Eqs 3.12 - 3.14). The perturbation approach is used in this study for solving Eq. 3.11 with the three boundary conditions up to the second order.

3.2.2 Wave theories kinematics

One of the most useful theories in calculating the kinematics of a progressive wave (Figure 1.4) is Linear Airy theory (LAT) which is based on the assumption that the wave height (H) is small compared to the wave length (L) or water depth (d). This assumption allows the free surface boundary conditions to be linearized by dropping wave height terms, which are beyond the first order and also to be satisfied at the mean water level (MWL), rather than at the oscillating free surface. The solution for velocity potential, ϕ , is assumed to take the form of

$$\phi = \sum_{n=1}^{\infty} \varepsilon^n \phi^n \quad (3.15)$$

where ε is a nondimensional perturbation parameter, defined as $\varepsilon = \frac{kH}{2}$, k is a wave number, defined as $k = \frac{2\pi}{L}$ and ϕ^n is the n^{th} order solution for ϕ . Similarly, the wave

elevation, η , is defined as

$$\eta = \sum_{n=1}^{\infty} \varepsilon^n \eta_n \quad (3.16)$$

Since LAT is directed toward a first order solution, only the first term of the series in Eqs 3.15 and 3.16 is considered. For unidirectional regular wave, the general solution of the two directional Laplace equation (Eq. 3.11) were derived by [116] with the use of the boundary conditions (Eqs 3.12 – 3.14) and the first terms in Eqs 3.15 and 3.16. As a result, the first order velocity potential can be written as

$$\phi^{(1)} = \frac{ag}{\omega} \frac{\cosh ks}{\cosh kd} \sin \theta \quad (3.17)$$

where ω = wave frequency, a = wave amplitude, $\theta = kx - \omega t$.

The wave elevation is

$$\eta = \frac{H}{2} \cos \theta \quad (3.18)$$

The water- particle velocities and accelerations in the x and z directions are

$$u = \frac{H}{2} \omega \frac{\cosh ks}{\sinh kd} \cos \theta \quad (3.19)$$

$$v = \frac{H}{2} \omega \frac{\sinh ks}{\sinh kd} \sin \theta \quad (3.20)$$

$$\frac{\partial u}{\partial t} = \frac{H}{2} \omega \frac{\cosh ks}{\sinh kd} \sin \theta \quad (3.21)$$

$$\frac{\partial v}{\partial t} = -\frac{H}{2} \omega \frac{\sinh ks}{\sinh kd} \cos \theta \quad (3.22)$$

From Eq. 3.10, the first order dynamic pressure, p , can be written as

$$p = \rho \frac{\partial \phi^{(1)}}{\partial t} + \frac{1}{2} \rho \left[\left(\frac{\partial \phi^{(1)}}{\partial x} \right)^2 + \left(\frac{\partial \phi^{(1)}}{\partial z} \right)^2 \right] \quad (3.23)$$

The resultant kinematics for the irregular waves is obtained by applying these equations to each wave component and then summing up the individual effects.

Linear Airly theory (LAT) predicts wave kinematics only up to the MWL. However, waves above MWL may produce significant structure responses and may not be ignored. If LAT is used, then the theory is modified to account for the free surface effect. Generally, there are two types of modifications that have been proposed:

A. Stretching:

In these formulations, the kinematics at the MWL are assumed to be applicable at the free surface. Two stretching formulae used this technique are:

1. Wheeler [9]: The effective water depth, s , in the LAT kinematics is replaced by

$$\frac{s}{1 + \frac{\eta}{d}}, \text{ for } -d \leq z \leq \eta$$

2. Chakrabarti [10]: The water depth, d , in the LAT kinematics is replaced by $d + \eta$

B. Extrapolation:

Here, the wave kinematics below MWL follow the same kinematics as for LAT while those at the free surface are predicted by using some approximate functional expansions about this value. Three types of extrapolations are generally used:

1. Hyperbolic: In these formulations, the wave kinematics up to the free surface are assumed to follow the same hyperbolic variations with depth as in LAT up to MWL.

2. Linear: The elevation z between the MWL and free surface is expanded in a Taylor series, and the first two terms are retained (Rodenbush [117]);

$$\text{i.e., } \cosh(k(z+d)) \approx \cosh(kd) + kz \sinh(kd) \text{ and } \sinh(k(z+d)) \approx \sinh(kd) + kz \cosh(kd), \text{ this is for } 0 \leq z \leq \eta$$

3. Uniform: The wave kinematics at the free surface are assumed same as the ones at the MWL; i.e., $z = 0$ for $0 \leq z \leq \eta$

3.3 Design wave environment

There are two basic approaches considered in selecting the design wave environment for an offshore structure, single wave method and wave spectrum.

3.3.1 Single wave method

Here, the design wave is represented by a wave period (T) and a wave height (H). The reason for using this approach is the simplicity in the design analysis and easy prediction of the responses due to extreme wave conditions.

3.3.2 Wave spectrum

In this case, a suitable wave spectrum model is chosen representing an appropriate density distribution of the sea waves at the site under consideration. The most suitable spectrum is a measured design wave spectrum at the site, although such a spectrum is seldom available. As an alternative, there are various theoretical spectrum models that can be used to represent the wave energy.

3.3.2.1 JONSWAP spectrum

The most common theoretical spectrum models used in the dynamic analysis of offshore structures are Pierson-Muskowitz (PM) and the more generalized Joint North Sea Wave Project (JONSWAP) spectrum model (Figure 3.1) which was developed by Hasselman [118]. In this study, the latter model is used for wave simulation because it is more versatile and represents the spectral peakedness better than PM spectrum.

According to JONSWAP spectrum, the wave energy spectral density formula is

$$S(\omega) = \alpha H_s^2 \left(\frac{\omega_0^4}{\omega^5} \right) \exp \left(-1.25 \left(\frac{\omega_0}{\omega} \right)^4 \right) \gamma^{\exp \left(-\frac{(\omega - \omega_0)^2}{2\sigma^2 \omega_0^2} \right)} \quad (3.24)$$

where H_s = significant wave height.

ω_0 = frequency at spectral peak

γ = peakedness parameter and may vary from 1 to 7 (=2, here)

α = is a constant called Phillip's constant

$$= \frac{0.0624}{0.23 + 0.0336\gamma - \frac{0.185}{1.9 + \gamma}}$$

σ = shape parameter

=0.07 , for $\omega \leq \omega_0$

=0.09, otherwise.

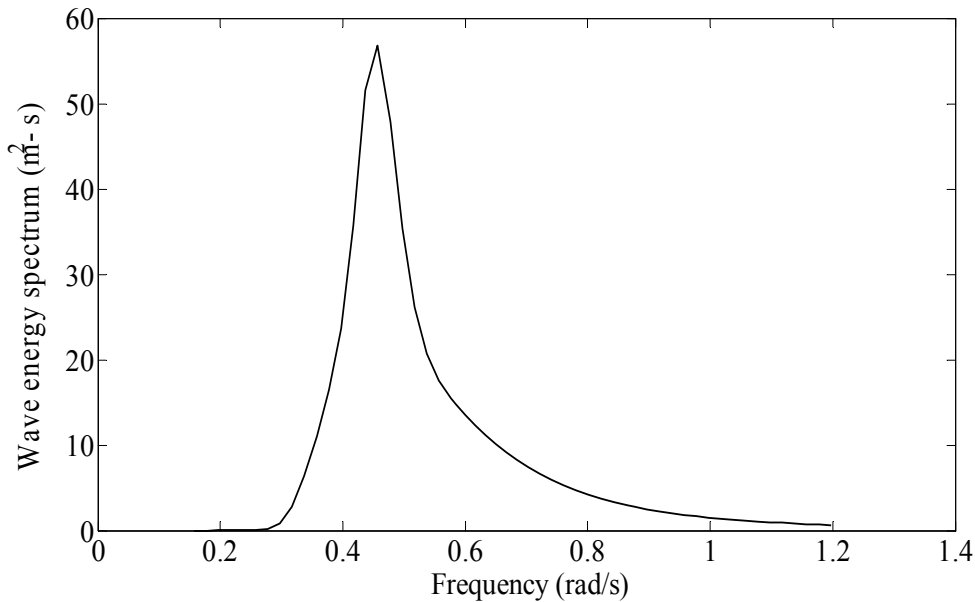


Figure 3.1: JONSWAP energy density spectrum for a given $H_s = 12.7$ m and $\omega_0 = 0.45$ rad/s

The amplitudes of the individual wave components (i) are calculated as

$$a_i = \sqrt{2S(\omega_i)\Delta\omega} \quad (3.25)$$

Once amplitudes are known, the wave-elevation time series can be generated from

$$\eta(t) = \sum a_i \cos(k_i x - \omega_i t + \beta_i) \quad (3.26)$$

3.4 Mean drift forces

Mean drift forces are a function of the first order velocity potential and, as a result, solutions have been obtained analytically by Weggel [11] for the simple geometry of a bottom-mounted circular cylinder (presented in Chakrabarti [116]).

There are two types of drift forces:

1. Fixed- body forces:

In this type, the quadratic products of the first order body motion are ignored. Equations represent curve fitting for the fixed-body mean drift forces for surge and pitch are

$$F_s = \rho g R \frac{H^2}{4} [2.15 \varepsilon^3] \quad \text{for } 0 < \varepsilon \leq 0.2 \quad (3.27)$$

$$F_s = \rho g R \frac{H^2}{4} [0.125 - 1.35 \varepsilon + 4.57 \varepsilon^2 - 2.7 \varepsilon^3] \quad \text{for } 0.2 < \varepsilon \leq 1 \quad (3.28)$$

$$F_s = \rho g R \frac{H^2}{4} [0.651] \quad \text{for } 1 < \varepsilon \leq 5 \quad (3.29)$$

$$F_p = \rho g R^2 \frac{H^2}{4} [2.08 \varepsilon^3] \quad \text{for } 0 < \varepsilon \leq 0.2 \quad (3.30)$$

$$F_p = \rho g R^2 \frac{H^2}{4} [0.012 - 0.258 \varepsilon + 1.65 \varepsilon^2 - 1.29 \varepsilon^3] \quad \text{for } 0.2 < \varepsilon \leq 0.8 \quad (3.31)$$

$$F_p = \rho g R^2 \frac{H^2}{4} [0.218 - 0.0251 \varepsilon] \quad \text{for } 0.8 < \varepsilon \leq 5 \quad (3.32)$$

where R , F_s and F_p are cylinder radius, surge and pitch mean drift forces respectively. All the above equations are valid for diameter/draft ratios from 0.05 to 1.6.

2. Free-body forces:

This type considers the quadratic products of first order body motion. Equations that represent curve fitting for the free-body mean drift forces for surge and pitch are:

$$F_s = \rho g R \frac{H^2}{4} [-0.102 \varepsilon + 0.51 \varepsilon^2 - 0.147 \varepsilon^3] \quad \text{for } 0 < \varepsilon \leq 2 \quad (3.33)$$

$$F_s = \rho g R \frac{H^2}{4} [0.645] \quad \text{for } 2 < \varepsilon \leq 4 \quad (3.34)$$

$$F_p = \rho g R^2 \frac{H^2}{4} [0.02 \varepsilon + 0.609 \varepsilon^2 - 0.411 \varepsilon^3] \quad \text{for } 0 < \varepsilon \leq 1 \quad (3.35)$$

$$F_p = \rho g R^2 \frac{H^2}{4} [0.261 - 0.0389 \varepsilon] \quad \text{for } 1 < \varepsilon \leq 4 \quad (3.36)$$

These expressions are valid for (diameter/draft) ratios from 0.2 to 1.2. A simple expression for the wave drift damping as given by Clark [74] is:

$$B_{11_{wd}}(\omega, \beta) = - \left(\frac{\omega^2}{g} \frac{\partial \bar{F}_d}{\partial \omega} + \frac{4\omega}{g} \bar{F}_d \right) \cos \beta + \frac{2\omega}{g} \frac{\partial \bar{F}_d}{\partial \beta} \sin \beta \quad (3.37)$$

This, for a single cylinder in unidirectional waves, reduces to

$$B_{11_{wd}}(\omega) = - \frac{\omega^2}{g} \frac{\partial \bar{F}_d}{\partial \omega} - \frac{4\omega}{g} \bar{F}_d \quad (3.38)$$

where β is the incident wave heading angle and \bar{F}_d is the surge mean drift forces.

By substituting Eqs 3.33 and 2.34 into Eq. 3.38 a simple expression for the waft drift damping can be obtained as:

$$B_{11_{wd}} = \rho \omega R \frac{H^2}{4} [-0.612 \varepsilon + 4.08 \varepsilon^2 - 1.47 \varepsilon^3] \quad \text{for } 0 < \varepsilon \leq 2 \quad (3.39)$$

$$B_{11_{wd}} = \rho \omega R \frac{H^2}{4} [2.58] \quad \text{for } 2 < \varepsilon \leq 4 \quad (3.40)$$

3.5 Second order difference frequency wave forces

As mentioned earlier, the truss spar platforms are designed to have natural frequencies of vibration much lower than the dominant wave frequencies, so that the second order difference frequency forces should be considered in the dynamic analysis of truss spar platform. This section discusses the second order effects which are caused by:

1. Structural displacement,
2. Axial divergence,
3. Free-surface fluctuation,
4. Convective acceleration and
5. Temporal acceleration due to second order velocity potential.

For slender structures like truss spars, typical values of the $\left(\frac{\text{Structure Diameter}}{\text{Wave Length}} \right)$ ratio are less than 0.2. As such, the use of Morison equation is considered to be valid for truss spar platforms and has been used in several previous studies.

Formulae used to evaluate these effects are derived based on the principles for the extension of Morison equation for an inclined cylinder and the hyperbolic extrapolation for predicting the wave kinematics.

The wave forces are decomposed into two components; normal and tangential to the structure. The normal component is calculated using an extension of the Morison equation for an inclined cylinder which is based upon normal velocities and accelerations as shown in Figure 3.2.

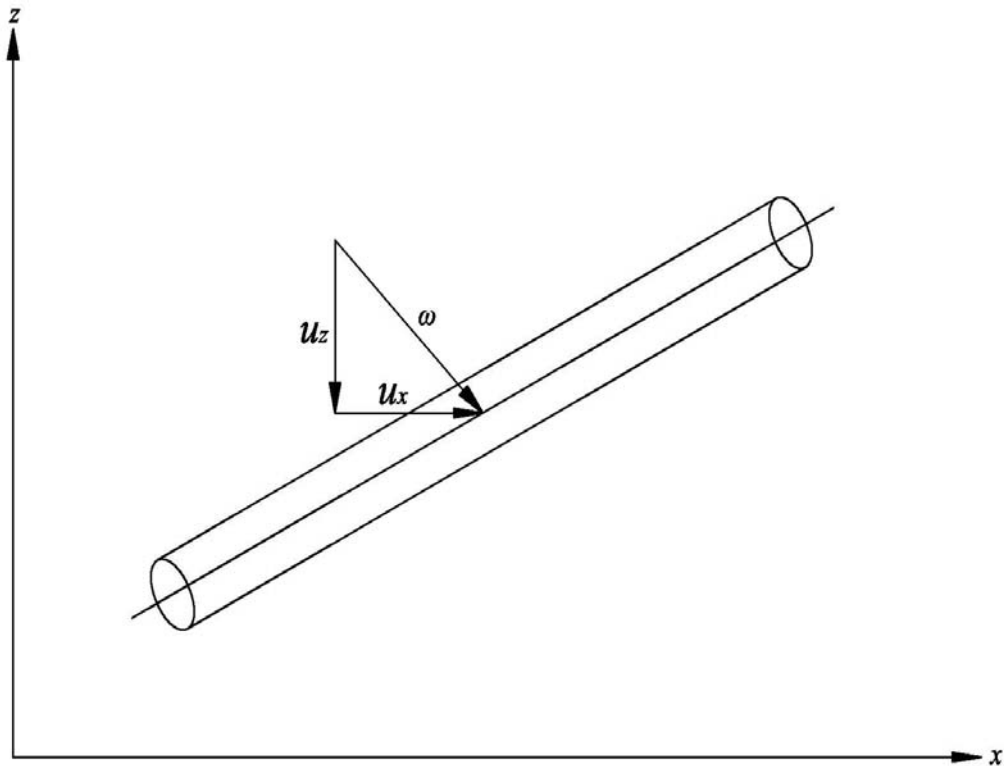


Figure 3.2: Wave kinematics components on a segment on inclined cylinder

Wave velocity components along x and z coordinates are

$$\begin{aligned} u_x &= u - C_x (C_x u + C_z v) \\ u_z &= v - C_z (C_x u + C_z v) \end{aligned} \quad (3.41)$$

where C_x and C_z are x and z components of the unit vector C which is acting along the cylinder axis directed up or down. Two coordinate systems are illustrated in Figure 3.3, the global axis (xoz) is fixed at MWL and the local axis (ζGn) is fixed at the centre of gravity of the structure.

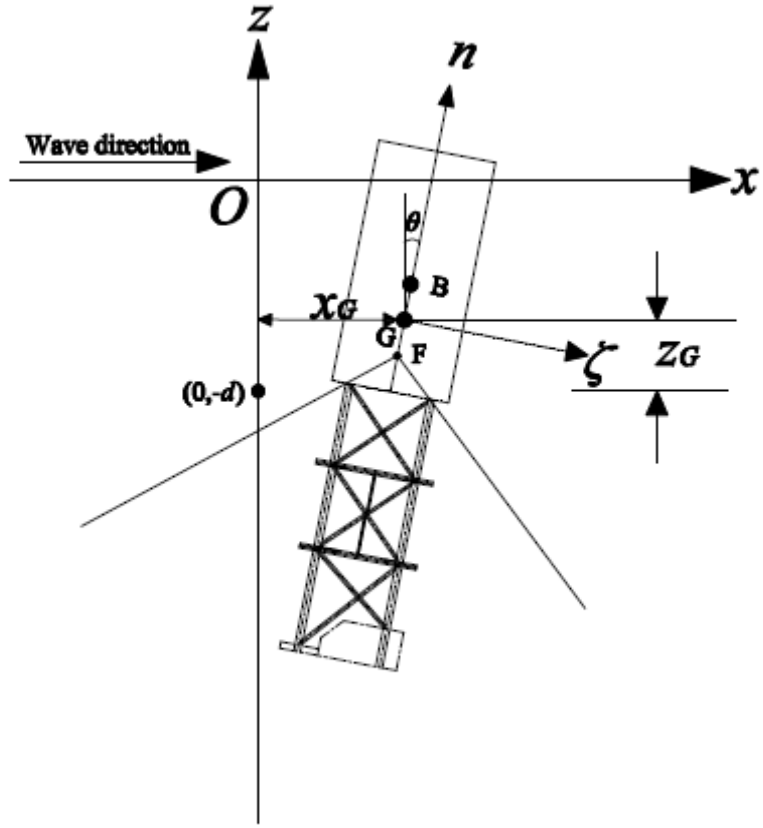


Figure 3.3: Global and local coordinates used for dynamic analysis

The normal wave force component per unit length can be written as

$$f = \rho C_M A \frac{\partial w}{\partial t} + \frac{1}{2} \rho C_D D |w| w + \rho C_m A w \tau^T V \tau \quad (3.42)$$

where C_M , C_D and C_m are the inertia, drag and added mass coefficients respectively, A and D are the cross-sectional area and structure diameter respectively and w is the relative normal velocity. The first two terms in Eq. 3.42 give the inertia and drag forces respectively.

$$\tau = \begin{bmatrix} \sin \vartheta \\ \cos \vartheta \end{bmatrix}, \text{ where } \vartheta \text{ is the pitch angle.} \quad (3.43)$$

The last term in Eq. 3.42 represents the normal axial divergence in which the velocity gradient matrix is given by

$$V = \begin{bmatrix} \frac{\partial u}{\partial x} & \frac{\partial u}{\partial z} \\ \frac{\partial v}{\partial x} & \frac{\partial v}{\partial z} \end{bmatrix} \quad (3.44)$$

The tangential component is predicted by carrying out a double integration of the dynamic pressure on the bottom surface of the structure B which is derived from Bernuolli equation and the potential velocity.

$$F_{Ext} = \iint \left[\begin{aligned} & \rho g a \frac{\cosh(ks)}{\cosh(kd)} \cos \theta + \frac{3}{4} \rho g \frac{\pi H^2}{L} \frac{1}{\sinh(2kd)} \times \left[\frac{\cosh 2ks}{\sinh^2 kd} - \frac{1}{3} \right] \cos 2\theta \\ & - \frac{1}{4} \rho g \frac{\pi H^2}{L} \frac{1}{\sinh 2kd} \times [\cosh 2ks - 1] \end{aligned} \right] \partial B \quad (3.45)$$

The potential velocity for the interaction between the wave components within a random wave was derived up to the second order by Longuet -Higgins and Stewart [119] using a conventional perturbation approach.

$$\begin{aligned} \phi = \sum \left\{ A_i \frac{\cosh(k_i s)}{\cosh(k_i d)} \sin \theta_i + A_{ii} \frac{\cosh(2k_i s)}{\sinh^4(k_i d)} \sin 2\theta_i \right\} \\ + \\ \sum \sum \left\{ \begin{aligned} & A_{i-j} \frac{\cosh[(k_i - k_j) s]}{\cosh[(k_i - k_j) d]} \sin(\theta_i - \theta_j) \\ & + A_{i+j} \frac{\cosh[(k_i + k_j) s]}{\cosh[(k_i + k_j) d]} \sin(\theta_i + \theta_j) \end{aligned} \right\} \end{aligned} \quad (3.46)$$

The first Σ , in $\Sigma\Sigma$, indicates a summation over i^{th} waves and the second Σ is a summation over j^{th} interacting waves for $\omega_i > \omega_j$ only.

also $A_{ii} = 3a_i^2 \omega_i / 8$, $\lambda = \omega_j / \omega_i$, $\alpha_i = \coth(k_i d)$,

$$A_{i-j} = a_i a_j \omega_i (\alpha_i \alpha_j - 1) / 2 [2\lambda(1-\lambda)(\alpha_i \alpha_j + 1) - \lambda^3(\alpha_j^2 - 1) + \alpha_i^2 - 1] / [(\alpha_i - \lambda \alpha_j)^2 - (1 - \lambda)^2]$$

for A_{i+j} , only the signs for α_j and ω_j will be changed.

The first term in Eq. 3.46 represents the first order potential velocity, whereas the second, third and fourth terms stand for second order potential velocity working at a

frequency twice that of the linear term, difference frequency and sum frequency respectively.

As mentioned earlier, floating structures, like spar, have natural frequencies lower than the incident ocean wave frequencies so that the third term in Eq. 3.46 is the most important term in studying the effects of the second order forces on spar.

The inertia and drag forces in this study are calculated in the displaced position of the structure and the effect of the free surface fluctuation is also considered. In addition, the convective acceleration is added to the first and second order temporal accelerations to obtain the total wave acceleration for the inertia force calculations.

3.5.1 Inertia force

Because spar platforms have low Keulegan-Carpenter parameter (KC), the contribution of drag force is small compared to the inertia force. Up to the second

order, the normal inertia force can be written as

$$F_I = \int_{n_b} \rho C_M A \frac{\partial(w_{SD})}{\partial t} \cdot \hat{n} + \int^n \rho C_M A \frac{\partial(w_{FS})}{\partial t} \cdot \hat{n} + \int_{n_b} \rho C_M A w'_{CA} \cdot \hat{n} + \int_{n_b} \rho C_M A \frac{\partial(w_{TA}^{(2)})}{\partial t} \cdot \hat{n} \quad (3.47)$$

where the first, second, third and fourth parts of the Eq. 3.47 are for the second order difference frequency inertia forces due to the structural displacement, free surface

fluctuation, convective and temporal accelerations respectively, \int_{n_b} is the integration

between the bottom and the top of the structure/member (up to MWL), and \int^n is the

integration between MWL and the instant free surface.

3.5.1.1 Structural displacement

The forces on the structure must be calculated at the displaced position instead of the mean position. This adds nonlinear force on the spar (Li and Kareem [120]). By

expanding the horizontal and vertical wave accelerations in Taylor series and retaining the first two terms, the horizontal and vertical wave particle accelerations up to the second order can be written as

$$\begin{aligned} \frac{\partial u}{\partial t} = & \Sigma a_i \omega_i^2 \left[\frac{\cosh(k_i s)}{\sinh(k_i d)} \right] \sin \theta_i \\ & + \left[\Sigma \Sigma \left\{ x_{Gim} a_j \omega_j^2 k_j \left[\frac{\cosh(k_j s)}{\sinh(k_j d)} \right] - x_{Gjm} a_i \omega_i^2 k_i \left[\frac{\cosh(k_i s)}{\sinh(k_i d)} \right] \right\} \right. \\ & \left. + n \Sigma \Sigma \left\{ \gamma_{im} a_j \omega_j^2 k_j \left[\frac{\cosh(k_j s)}{\sinh(k_j d)} \right] - \gamma_{jm} a_i \omega_i^2 k_i \left[\frac{\cosh(k_i s)}{\sinh(k_i d)} \right] \right\} \right] \frac{\sin(\theta_i - \theta_j)}{2} \end{aligned} \quad (3.48)$$

$$\begin{aligned} \frac{\partial v}{\partial t} = & -\Sigma a_i \omega_i^2 \left[\frac{\sinh(k_i s)}{\sinh(k_i d)} \right] \cos \theta_i \\ & + \left[\Sigma \Sigma \left\{ x_{Gim} a_j \omega_j^2 k_j \left[\frac{\sinh(k_j s)}{\sinh(k_j d)} \right] + x_{Gjm} a_i \omega_i^2 k_i \left[\frac{\sinh(k_i s)}{\sinh(k_i d)} \right] \right\} \right. \\ & \left. + n \Sigma \Sigma \left\{ \gamma_{im} a_j \omega_j^2 k_j \left[\frac{\sinh(k_j s)}{\sinh(k_j d)} \right] + \gamma_{jm} a_i \omega_i^2 k_i \left[\frac{\sinh(k_i s)}{\sinh(k_i d)} \right] \right\} \right] \frac{\cos(\theta_i - \theta_j)}{2} \end{aligned} \quad (3.49)$$

where x_{Gm} , γ_m are surge and pitch amplitudes respectively. The first terms in Eqs 3.48 and 3.49 correspond to the wave horizontal and vertical accelerations at the mean position which are used to predict the first order inertia force. The second term represents the nonlinear structural displacement effect. When $i = j$, Eq. 3.49 contributes to the mean force.

3.5.1.2 Axial divergence

Morison equation has been modified by Rainey [121] who added a new term to the original formula. This term, which is sometimes known as Rainey axial divergence correction, represents a second order velocity in addition to Morison equation. This normal velocity is given by

$$\begin{aligned}
w\tau^T V\tau = & \left[\left(u - \frac{\partial x}{\partial t} \right) - C_x \left(C_x \left(u - \frac{\partial x}{\partial t} \right) + C_z \left(v - \frac{\partial z}{\partial t} \right) \right) \right] \tau^T V\tau \cos \vartheta \\
& - \left[\left(v - \frac{\partial z}{\partial t} \right) - C_z \left(C_x \left(u - \frac{\partial x}{\partial t} \right) + C_z \left(v - \frac{\partial z}{\partial t} \right) \right) \right] \tau^T V\tau \sin \vartheta
\end{aligned} \tag{3.50}$$

in which

$$\begin{aligned}
\left(u - \frac{\partial x}{\partial t} \right) \tau^T V\tau = & AD_{hr1} \sin^2 \vartheta + (AD_{hr2} + AD_{hrMean2}) \sin \vartheta \cos \vartheta \\
& + (AD_{hr3} + AD_{hrMean3}) \sin \vartheta \cos \vartheta + AD_{hr4} \cos^2 \vartheta
\end{aligned} \tag{3.51}$$

$$AD_{hr1} = \sum \sum \omega_i \omega_j \left\{ \begin{array}{l} a_i a_j \frac{\cosh k_i s \cosh k_j s}{\sinh k_i d \sinh k_j d} (k_j - k_i) \\ + a_j k_j (x_{Gim} + n\gamma_{im}) \left[\frac{\cosh k_j s}{\sinh k_j d} \right] \\ - a_i k_i (x_{Gjm} + n\gamma_{jm}) \left[\frac{\cosh k_i s}{\sinh k_i d} \right] \end{array} \right\} \frac{\sin(\theta_i - \theta_j)}{2} \tag{3.52}$$

$$AD_{hr2} = \sum \sum \omega_i \omega_j \left\{ \begin{array}{l} a_i a_j \frac{k_j \sinh k_j s \cosh k_i s + k_i \sinh k_i s \cosh k_j s}{\sinh k_i d \sinh k_j d} \\ + a_j k_j (x_{Gim} + n\gamma_{im}) \left[\frac{\sinh k_j s}{\sinh k_j d} \right] \\ + a_i k_i (x_{Gjm} + n\gamma_{jm}) \left[\frac{\sinh k_i s}{\sinh k_i d} \right] \end{array} \right\} \frac{\cos(\theta_i - \theta_j)}{2} \tag{3.53}$$

$$AD_{hr3} = AD_{hr2} \tag{3.54}$$

$$AD_{hr4} = \sum \sum \omega_i \omega_j \left\{ \begin{array}{l} a_i a_j \frac{\cosh k_i s \cosh k_j s}{\sinh k_i d \sinh k_j d} (k_i - k_j) \\ + a_i k_i (x_{Gjm} + n \gamma_{jm}) \left(\frac{\cosh k_i s}{\sinh k_i d} \right) \\ - a_j k_j (x_{Gim} + n \gamma_{im}) \left(\frac{\cosh k_j s}{\sinh k_j d} \right) \end{array} \right\} \frac{\sin(\theta_i - \theta_j)}{2} \quad (3.55)$$

$$\left(v - \frac{\partial z}{\partial t} \right) \tau^T V \tau = (AD_{vr1} + AD_{vrMean1}) \sin^2 \vartheta + (AD_{vr2} + AD_{vrMean2}) \sin \vartheta \cos \vartheta \quad (3.56)$$

$$+ (AD_{vr3} + AD_{vrMean3}) \sin \vartheta \cos \vartheta + (AD_{vr4} + AD_{vrMean4}) \cos^2 \vartheta$$

$$AD_{vr1} = - \sum \sum \omega_i \omega_j a_i a_j \left[\frac{\sinh k_j s}{\sinh k_j d} k_i \frac{\cosh k_i s}{\sinh k_i d} + \frac{\sinh k_i s}{\sinh k_i d} k_j \frac{\cosh k_j s}{\sinh k_j d} \right] \frac{\cos(\theta_i - \theta_j)}{2} \quad (3.57)$$

$$+ \sum \sum \left[a_j k_j \omega_j \frac{\cosh k_j s}{\sinh k_j d} Z_{Gim} - a_i k_i \omega_i \frac{\cosh k_i s}{\sinh k_i d} Z_{Gjm} \right] \frac{\sin(\theta_i - \theta_j)}{2}$$

$$AD_{vr2} = \sum \sum \omega_i \omega_j a_i a_j \frac{\sinh k_i s \sinh k_j s}{\sinh k_i d \sinh k_j d} (k_j - k_i) \frac{\sin(\theta_i - \theta_j)}{2} \quad (3.58)$$

$$+ \sum \sum \omega_i \omega_j \left[a_i k_i \frac{\sinh k_i s}{\sinh k_i d} Z_{Gjm} + a_j k_j \frac{\sinh k_j s}{\sinh k_j d} Z_{Gim} \right] \frac{\cos(\theta_i - \theta_j)}{2}$$

$$AD_{vr3} = AD_{vr2} \quad (3.59)$$

$$AD_{vr4} = \sum \sum \omega_i \omega_j a_i a_j \left[\frac{\cosh k_i s}{\sinh k_i d} k_i \frac{\sinh k_j s}{\sinh k_j d} + \frac{\cosh k_j s}{\sinh k_j d} k_j \frac{\sinh k_i s}{\sinh k_i d} \right] \frac{\cos(\theta_i - \theta_j)}{2} \quad (3.60)$$

$$+ \sum \sum \left[a_i k_i \omega_i \omega_j \frac{\cosh k_i s}{\sinh k_i d} Z_{Gjm} - a_j k_j \omega_i \omega_j \frac{\cosh k_j s}{\sinh k_j d} Z_{Gim} \right] \frac{\sin(\theta_i - \theta_j)}{2}$$

where Z_{Gm} is the heave amplitude. Since some of the above equations have difference frequency cosine terms, there will be a contribution to the mean force. This will occur when $i = j$.

$$AD_{hrMean2} = \frac{1}{2} \sum \omega_i^2 a_i k_i \left[\frac{\sinh k_i s}{\sinh k_i d} \right] \left\{ a_i \frac{\cosh k_i s}{\sinh k_i d} + x_{Gim} + n\gamma_{im} \right\} \quad (3.61)$$

$$AD_{hrMean3} = AD_{hrMean2} \quad (3.62)$$

$$AD_{vrMean1} = -\frac{1}{2} \sum a_i^2 \omega_i^2 k_i \left[\frac{\sinh k_i s \cosh k_i s}{\sinh^2 k_i d} \right] \quad (3.63)$$

$$AD_{vrMean2} = \frac{1}{2} \sum a_i \omega_i^2 k_i \frac{\sinh k_i s}{\sinh k_i d} Z_{Gim} \quad (3.64)$$

$$AD_{vrMean3} = AD_{vrMean2} \quad (3.65)$$

$$AD_{vrMean4} = \frac{1}{2} \sum a_i^2 \omega_i^2 k_i \frac{\sinh k_i s \cosh k_i s}{\sinh^2 k_i d} \quad (3.66)$$

3.5.1.3 Free surface fluctuation

The integration of the first order accelerations from the MWL to the wave free surface gives another source of the nonlinear difference frequency forces. The integration of the corresponding second order horizontal and vertical accelerations leads to

$$\int \frac{\partial u}{\partial t} \cdot \partial n = \frac{g}{\cos \vartheta} \sum \sum a_i a_j (k_i - k_j) \frac{\sin(\theta_i - \theta_j)}{2} \quad (3.67)$$

$$\int \frac{\partial v}{\partial t} \cdot \partial n = -\frac{g}{\cos \theta} \left\{ \sum \frac{a_i^2 k_i}{2} + \sum \sum a_i a_j (k_i + k_j) \frac{\cos(\theta_i - \theta_j)}{2} \right\} \quad (3.68)$$

As in the axial divergence effect, there is also a contribution to the mean force when putting $i = j$ in Eq. 3.68.

3.5.1.4 Convective acceleration

The total wave particle acceleration is caused by the change of the wave particle velocity with time and space. The change with time is known as temporal acceleration while the change with space is known as convective acceleration. The horizontal and vertical wave particle convective accelerations up to the second order can be written as

$$\left(u \frac{\partial u}{\partial x} + v \frac{\partial u}{\partial z}\right) = -\Sigma \Sigma a_i a_j \omega_i \omega_j (k_i - k_j) \left\{ \frac{\cosh(k_i + k_j)s}{\sinh k_i d \sinh k_j d} \right\} \frac{\sin(\theta_i - \theta_j)}{2} \quad (3.69)$$

$$\begin{aligned} \left(u \frac{\partial v}{\partial x} + v \frac{\partial v}{\partial z}\right) &= \Sigma a_i^2 \omega_i^2 k_i \left[\frac{\cosh k_i s \sinh k_i s}{\sinh^2 k_i d} \right] \\ &+ \Sigma \Sigma a_i a_j \omega_i \omega_j \left\{ (k_i + k_j) \left[\frac{\sinh(k_i + k_j)s}{\sinh k_i d \sinh k_j d} \right] \right\} \frac{\cos(\theta_i - \theta_j)}{2} \end{aligned} \quad (3.70)$$

The first part of Eq. 3.70 contributes to the mean force.

It is interesting to compare the free surface effect with the convective acceleration using Eqs. 3.67- 3.70 for this purpose. For near values of ω_i and ω_j (thus k_i and k_j), and for small pitch angle which is applicable for spar, and for ultra deep water ($\tanh kd \approx 1$), Eqs 3.69 and 3.70 for the hard tank of the truss spar can be written as

$$\int_{n_b} \left(u \frac{\partial u}{\partial x} + v \frac{\partial u}{\partial z}\right) \cdot \partial n \cong -\frac{g}{\cos \vartheta} \Sigma \Sigma a_i a_j (k_i - k_j) \frac{\sin(\theta_i - \theta_j)}{2} \left\{ 1 - \frac{\sinh 2k_i s'}{\sinh 2k_i d} \right\} \quad (3.71)$$

$$\begin{aligned} \int_{n_b} \left(u \frac{\partial v}{\partial x} + v \frac{\partial v}{\partial z}\right) \cdot \partial n &\cong \int_{-d}^n \Sigma a_i^2 \omega_i^2 k_i \left[\frac{\cosh k_i s \sinh k_i s}{\sinh^2 k_i d} \right] \cdot \partial n \\ &+ \frac{g}{\cos \vartheta} \Sigma \Sigma a_i a_j (k_i + k_j) \frac{\cos(\theta_i - \theta_j)}{2} \left\{ 1 - \frac{2 \cosh^2 k_i s'}{\sinh 2k_i d} \right\} \end{aligned} \quad (3.72)$$

By comparing Eq. 3.67 with Eq. 3.71, and Eq. 3.68 with Eq. 3.72, one can observe that the exciting force due to the convective acceleration is slightly less than the negative of that due to free surface fluctuation. That is, these two second order effects are opposite to each other.

3.5.1.5 Temporal acceleration

For the spars, the second order wave particle accelerations, which are derived from the second order potential velocity at the difference frequency, have significant contribution to the forces at the natural frequencies. The horizontal and vertical wave particle temporal accelerations up to the second order can be written as

$$\frac{\partial u^{(2)}}{\partial t} = \sum \sum \left\{ \frac{\frac{(\omega_i - \omega_j)}{\omega_i \omega_j} k_i k_j [1 + \tanh k_i d \tanh k_j d] + (k_i^2 \operatorname{sech}^2(k_i d) / \omega_i - k_j^2 \operatorname{sech}^2(k_j d) / \omega_j) / 2}{g(k_i - k_j) \tanh((k_i - k_j) d) - (\omega_i - \omega_j)^2} \right\} \quad (3.73)$$

$$\times a_i a_j (\omega_i - \omega_j) g^2(k_i - k_j) \left[\frac{\cosh((k_i - k_j) s)}{\cosh((k_i - k_j) d)} \right] \sin(\theta_i - \theta_j)$$

$$\frac{\partial v^{(2)}}{\partial t} = - \sum \sum \left\{ \frac{\frac{(\omega_i - \omega_j)}{\omega_i \omega_j} k_i k_j [1 + \tanh k_i d \tanh k_j d] + (k_i^2 \operatorname{sech}^2(k_i d) / \omega_i - k_j^2 \operatorname{sech}^2(k_j d) / \omega_j) / 2}{g(k_i - k_j) \tanh((k_i - k_j) d) - (\omega_i - \omega_j)^2} \right\} \quad (3.74)$$

$$\times a_i a_j (\omega_i - \omega_j) g^2(k_i - k_j) \left[\frac{\sinh((k_i - k_j) s)}{\cosh((k_i - k_j) d)} \right] \cos(\theta_i - \theta_j)$$

As in the above equations, $\frac{\partial v^{(2)}}{\partial t}$ contributes to the mean force when $i = j$.

3.5.2 Drag force

In the case of inertia force dominant systems, such as spar, the system may be approximated with reasonable accuracy as a linear system in calculating the drag force and a linearization method may be adopted.

The linear approximation for the drag force per unit length is

$$f_D = \frac{1}{2} \rho C_D D \sqrt{\frac{8}{\pi}} \sigma_{wr} w_r \quad (3.75)$$

where σ_{wr} is the standard deviation of the relative normal velocity and w_r is the relative normal velocity.

$$\sqrt{\frac{8}{\pi}} \sigma_{wr} w_r = \sqrt{\frac{8}{\pi}} \left\{ \begin{aligned} & [(\sigma_{ur} u_r) - C_x (C_x (\sigma_{ur} u_r) + C_z (\sigma_{vr} v_r))] \cos \vartheta \\ & - [(\sigma_{vr} v_r) - C_z (C_x (\sigma_{ur} u_r) + C_z (\sigma_{vr} v_r))] \sin \vartheta \end{aligned} \right\} \quad (3.76)$$

$$\begin{aligned} \sqrt{\frac{8}{\pi}}\sigma_{ur}u_r &= \sqrt{\frac{8}{\pi}} \times \sqrt{\sum \left(\omega_i \left\{ a_i \left[\frac{\cosh k_i s}{\sinh k_i d} \right] - x_{Gim} - n\gamma_{im} \right\} \right)^2 / 2} \\ &\times \left[\sum a_i \omega_i \left[\frac{\cosh k_i s}{\sinh k_i d} \right] \cos \theta_i - \sum \omega_i (x_{Gim} + n\gamma_{im}) \sin \theta_i \right] \end{aligned} \quad (3.77)$$

$$\begin{aligned} \sqrt{\frac{8}{\pi}}\sigma_{vr}v_r &= \sqrt{\frac{8}{\pi}} \times \sqrt{\sum \left(\omega_i \left\{ a_i \left[\frac{\sinh k_i s}{\sinh k_i d} \right] - Z_{Gim} \right\} \right)^2 / 2} \\ &\times \left[\sum a_i \omega_i \left[\frac{\sinh k_i s}{\sinh k_i d} \right] \sin \theta_i - \sum \omega_i Z_{Gim} \sin \theta_i \right] \end{aligned} \quad (3.78)$$

In Eqs 3.77 and 3.78, the first part contributes to the excitation force and the second part to the damping of the system. Although these equations represent the linear approximation of the drag force, there are two sources for the second order slow varying difference frequency forces involved. One is due to the integration of the wave forces at the displaced position and the other is due to free surface fluctuation effect.

3.5.2.1 Structural displacement

Just like the inertia force, calculation of the drag force at the displaced position of the structure adds a second order term as follows

$$\begin{aligned} \sqrt{\frac{8}{\pi}}\sigma_{ur}u_r &= -\sqrt{\frac{8}{\pi}} \times \sqrt{\sum \left(\omega_i \left\{ a_i \left[\frac{\cosh k_i s}{\sinh k_i d} \right] - x_{Gim} - n\gamma_{im} \right\} \right)^2 / 2} \\ &\times \left[\sum \sum \left\{ \begin{aligned} &a_i \omega_i k_i (x_{Gjm} + n\gamma_{jm}) \left[\frac{\cosh k_i s}{\sinh k_i d} \right] \\ &+ a_j \omega_j k_j (x_{Gim} + n\gamma_{im}) \left[\frac{\cosh k_j s}{\sinh k_j d} \right] \end{aligned} \right\} \frac{\cos(\theta_i - \theta_j)}{2} \right] \end{aligned} \quad (3.79)$$

$$\begin{aligned}
\sqrt{\frac{8}{\pi}} \sigma_{vr} v_r = & -\sqrt{\frac{8}{\pi}} \times \sqrt{\sum \left(\omega_i \left\{ a_i \left[\frac{\sinh k_i s}{\sinh k_i d} \right] - Z_{Gim} \right\} \right)^2 / 2} \\
& \times \left[\sum \sum \left\{ \begin{array}{l} a_i \omega_i k_i (x_{Gjm} + n \gamma_{jm}) \left[\frac{\sinh k_i s}{\sinh k_i d} \right] \\ - a_j \omega_j k_j (x_{Gim} + n \gamma_{im}) \left[\frac{\sinh k_j s}{\sinh k_j d} \right] \end{array} \right\} \frac{\sin(\theta_i - \theta_j)}{2} \right] \quad (3.80)
\end{aligned}$$

As Eq. 3.79 includes a difference frequency cosine term, there will contribution to the mean forces when $i = j$.

3.5.2.2 Free surface fluctuation

As for the inertia force, there is an important source for the second order difference frequency forces developing from the integration of the linearized drag force up to the free surface. The expression up to the second order is

$$\begin{aligned}
F_D^{FS} = & \sqrt{\frac{8}{\pi}} \rho C_D \frac{D}{2\sqrt{2}} \sqrt{\sum \left\{ \omega_i \left(\frac{a_i}{\tanh k_i d} - x_{Gim} - \gamma_{im} \right) \right\}^2} \\
& \times \sum \sum a_i a_j \left(\frac{\omega_i}{\tanh k_i d} + \frac{\omega_j}{\tanh k_j d} \right) \frac{\cos(\theta_i - \theta_j)}{2} \quad (3.81)
\end{aligned}$$

Also Eq. 3.81 contributes to the mean forces due to difference frequency cosine term involved.

3.5.2.3 Mean drag force

As for the inertia force, there will be a contribution to the mean force when $i = j$ in Eqs 3.79 and 3.81. These equations for the mean force can be written as

$$\sqrt{\frac{8}{\pi}} \sigma_{ur} u_r = -\frac{1}{2} \sqrt{\frac{8}{\pi}} \times \sqrt{\sum \left(\omega_i \left\{ a_i \left[\frac{\cosh k_i s}{\sinh k_i d} \right] - x_{Gim} - n \gamma_{im} \right\} \right)^2} / 2 \quad (3.82)$$

$$\times \sum \left\{ a_i \omega_i k_i (x_{Gim} + n \gamma_{im}) \left[\frac{\cosh k_i s}{\sinh k_i d} \right] \right\}$$

$$F_{D(mean)}^{FS} = \sqrt{\frac{8}{\pi}} \rho C_D \frac{D}{2\sqrt{2}} \sqrt{\sum \left\{ \omega_i \left(\frac{a_i}{\tanh k_i d} - x_{Gim} - \gamma_{im} \right) \right\}^2} \Sigma a_i^2 \left(\frac{\omega_i}{\tanh k_i d} \right) / 2 \quad (3.83)$$

3.6 Qualitative comparison between second order inertia and drag forces

At this stage, it is interesting to note the qualitative differences between the second order difference frequency forces induced by inertia and drag. They are

1. For the inertia force, the horizontal components have $\sin (\theta_i - \theta_j)$ terms while the vertical components have $\cos (\theta_i - \theta_j)$ terms and the opposite is true in the case of the drag force. It means that the harmonics they represent are at an angle $\pi/2$ out of phase with each other.
2. Even though, the truss spar has low KC number, the linearized drag force is very important due to the second order difference frequency terms involved.
3. The vertical and the horizontal components of the second order difference frequency inertia and drag forces respectively contribute to the mean force.

3.7 Chapter summary

In this chapter, the common wave theories which are used in the offshore engineering were described in details showing the governing equations and the boundary conditions. The design wave environment which is used for the dynamic analysis was classified and defined. Mean drift forces were presented for fixed and free bodies and accordingly, the wave drift damping were given. The second order difference frequency wave forces were derived and presented including inertia and drag forces.

Finally, qualitative comparisons between second order inertia and drag forces were presented.

CHAPTER 4

TIME DOMAIN FORMULATIONS

4.1 Introduction

The equations of motion of offshore floating structures such as truss spar platform consist of the force vector, which are derived in the previous chapter, based on hyperbolic extrapolation and the principles of the extension of Morison equation for an inclined cylinder. On the other hand, stiffness, mass and damping matrices are obtained from the usual concepts of structural dynamic analysis as illustrated in this chapter. These equations define the instantaneous structure motions in the considered degrees of freedom and hence this is a time domain problem.

In this study, the problem is formulated in time domain. This is because the frequency domain analysis gives only the steady state responses. In the subsequent chapters, time domain analysis will be used to predict the structure responses under different environmental loads and compared with experimental data.

Truss spar platform is connected to sea bed by using taut mooring line system. These mooring lines contribute to the structure motion by providing restoring forces to restrain the system, particularly in surge and pitch directions. There are various methods, which can be used to analyze mooring lines. The most common one is the quasi-static analysis. Here, the mooring lines are modeled as linear/nonlinear springs and their contribution to the system damping is assumed small and can be neglected. Dynamic mooring line analysis, which is another approach, considers the effect of line dynamics which, in some situations, may prove to be a significant element in predicting mooring line tensions.

In Section 4.2, the governing equations of motion are derived from Newton's second law of motion. Time domain formulation using Morison equation is discussed. This is followed by the numerical solution scheme which is adopted to predict the structure responses.

Quasi-static analysis is treated in Section 4.3. Assumptions made for the mooring line analysis is presented. The approximate modeling of mooring lines as linear/nonlinear spring is discussed.

Section 4.4 discusses in detail the mooring lines dynamic analysis approach. This approach uses lumped mass method and implementing time domain simulation for the mooring line using fairlead motions as input to predict the dynamic tension.

Finally in Sections 4.5 and 4.6, the effect of the combination of wave, current and wind loads are discussed. Current velocity is added to the horizontal wave velocity and therefore contributes to the drag force as well as to the structural damping. On the other hand, wind acts on the structure above water and contributes to the mean force.

4.2 Numerical solution of the equation of motion

4.2.1 Equation of motion

The resultant force on truss spar comprise of a number of components, which are:

1. Exciting force due to wave, current and wind,
2. Restoring forces due to hydrostatic effects and mooring lines,
3. Damping force due to drag force on the structure and mooring lines, radiation and wave drift damping and
4. Inertial force due to structure mass and added mass.

Applying Newton's second law at the center of gravity, the governing equations of motion for a rigid body are derived. Equations of motion usually represented in matrix form and the number of equations are based on the degrees of freedom considered. In

this study, truss spar buoy is modeled as a rigid body with three degrees of freedom, surge, heave and pitch.

Therefore, the conventional equation of motion can be written as

$$\{M\} \left[\frac{\partial^2 x_G}{\partial t^2} \right] + \{C\} \left[\frac{\partial x_G}{\partial t} \right] + \{K\} [x_G] = [F(t)] \quad (4.1)$$

where $\{M\} \left[\frac{\partial^2 x_G}{\partial t^2} \right]$ is 3×3 body mass and added mass matrix multiply by the structural acceleration vector in surge, heave and pitch directions. The resultant forces can be defined as

$$\{M\} \left[\frac{\partial^2 x_G}{\partial t^2} \right] = \left\{ \begin{array}{l} \left[\begin{array}{ccc} m & 0 & 0 \\ 0 & m & 0 \\ 0 & 0 & I \end{array} \right] + \left[\begin{array}{ccc} m_{11} & m_{12} & m_{13} \\ m_{21} & m_{22} & m_{23} \\ m_{31} & m_{32} & m_{33} \end{array} \right] \\ \text{Mass matrix} \qquad \qquad \text{Added mass matrix} \end{array} \right\} \left[\begin{array}{c} \frac{\partial^2 x_G}{\partial t^2} \\ \frac{\partial^2 z_G}{\partial t^2} \\ \frac{\partial^2 \vartheta}{\partial t^2} \end{array} \right] \quad (4.2)$$

where m and I denote body mass and mass moment of inertia about the y -axis respectively. The added mass is determined by integrating the added mass from the bottom of the structure/member to the instantaneous surface elevation. The computations of added mass forces and moments are as follows

$$\begin{aligned}
m_{11} &= \int_{n_b}^{n_t} \rho C_m A \cdot \delta n \cos \vartheta \cos \vartheta \\
m_{12} = m_{21} &= - \int_{n_b}^{n_t} \rho C_m A \cdot \delta n \sin \vartheta \cos \vartheta \\
m_{13} = m_{31} &= \int_{n_b}^{n_t} \rho C_m A n \cdot \delta n \cos \vartheta \\
m_{22} &= \int_{n_b}^{n_t} \rho C_m A \cdot \delta n \sin \vartheta \sin \vartheta \\
m_{23} = m_{32} &= - \int_{n_b}^{n_t} \rho C_m A n \cdot \delta n \sin \vartheta \\
m_{33} &= \int_{n_b}^{n_t} \rho C_m A n^2 \cdot \delta n
\end{aligned} \tag{4.3}$$

$\{C\} \left[\frac{\partial x_G}{\partial t} \right]$ is the structure damping matrix multiply by body velocity vector in the

considered degrees of freedom. The resultant forces can be defined as

$$\{C\} \left[\frac{\partial x_G}{\partial t} \right] = \begin{bmatrix} c_{11} & 0 & 0 \\ 0 & c_{22} & 0 \\ 0 & 0 & c_{33} \end{bmatrix} \begin{bmatrix} \frac{\partial x_G}{\partial t} \\ \frac{\partial z_G}{\partial t} \\ \frac{\partial \vartheta}{\partial t} \end{bmatrix} \tag{4.4}$$

Damping sources can be identified as structural, radiation, wave drift and mooring lines. The significant contribution comes from the drag force on the truss spar when using Morison equation as mentioned in Section 3.5.2. The structural damping of the system is small compared to the other forces. That is due to the low natural frequencies of the system in all degrees of freedom. The computations of the structure damping elements are as follows

$$\begin{aligned}
c_{11} &= 2 \xi_s \omega_{ns} m \\
c_{22} &= 2 \xi_h \omega_{nh} m \\
c_{33} &= 2 \xi_p \omega_{np} I
\end{aligned} \tag{4.5}$$

where the subscripts s , h and p stand for surge, heave and pitch respectively. ξ is the damping ratio in the specified direction of motion and ω_n is the natural frequency of

the system in the specified degree of freedom. Wave drift damping, which is defined in section 3.4, can be added to the C matrix as

$$\{C\} = \begin{bmatrix} c_{11} + B_{11_{wd}} & 0 & z_G \times B_{11_{wd}} \\ 0 & c_{22} & 0 \\ z_G \times B_{11_{wd}} & 0 & c_{33} + z_G^2 \times B_{11_{wd}} \end{bmatrix} \quad (4.6)$$

where z_G is z-coordinate of the center of gravity.

In addition to the aforementioned damping, heave plates greatly increase the heave added mass and viscous damping as follows

$$F = \frac{1}{2} \rho U |U| L^2 C_D + \rho \frac{\partial U}{\partial t} L^3 C_A \quad (4.7)$$

where C_D and C_A are drag and added mass coefficients for heave plates, respectively. U and $\frac{\partial U}{\partial t}$ represent the velocity and acceleration of the plate perpendicular to its plane respectively.

$\{K\}[x_G]$ is the system stiffness matrix multiplied by displacement vector. The stiffness matrix is composed of two main components, hydrostatic and mooring line stiffness matrices. The mooring lines, which are represented here by linear/nonlinear massless spring attached at the spar fairleads, are the only source of stiffness in the direction of surge motion. The hydrostatic buoyancy force provides the heave restoring force. Both kinds of stiffness contribute to the pitch stiffness. The resultant restoring force can be defined as

$$\{K\}[x_G] = \left[\underbrace{\begin{bmatrix} 0 & 0 & 0 \\ 0 & k_2 & 0 \\ 0 & 0 & k_3 \end{bmatrix}}_{\text{Hydrostatic}} + \underbrace{\begin{bmatrix} k_x & 0 & k_x h_2 \\ 0 & 0 & 0 \\ k_x h_2 & 0 & k_x h_2^2 \end{bmatrix}}_{\text{Mooring lines}} \right] \begin{bmatrix} x_G \\ z_G \\ \mathcal{G} \end{bmatrix} \quad (4.8)$$

where

$$k_2 = \pi \rho g (D/2)^2$$

$$k_3 = \text{buoyancy force} \times \text{distance from G to B}$$

k_x = horizontal spring stiffness

h_2 = distance from CG to fairlead

k_x is not necessarily constant throughout the analysis and generally it is a nonlinear function of the structure displacements. Thus the solution process involves updating the K matrix for each new displacement.

$[F(t)]$ is the force vector which is determined in this study by using Morison equation. As mentioned in section 3.5, the exciting forces are calculated, according to the local coordinate system $\zeta G \eta$, normal and tangential to the structure then transferred into spaced-fixed coordinate system xoz as

$$\begin{bmatrix} F_{EXx} \\ F_{EXz} \end{bmatrix} = \begin{Bmatrix} \cos \mathcal{G} & \sin \mathcal{G} \\ \sin \mathcal{G} & \cos \mathcal{G} \end{Bmatrix} \begin{bmatrix} F_{EXn} \\ F_{EXt} \end{bmatrix} \quad (4.9)$$

Therefore, this vector is

$$[F(t)] = \begin{bmatrix} F_{EXx} \\ F_{EXz} \\ M \end{bmatrix} \quad (4.10)$$

where M is the moment due to the normal forces. The vector $[F(t)]$ depends on the structural displacements and has to be updated iteratively till convergence is achieved at each time step. In addition to the dynamic forces, the force vector has to include mean drift forces to account for the mean offset of the truss spar they were discussed in section 3.4.

$$[F(t)] = \begin{bmatrix} F_{EXx} + F_{mean} \\ F_{EXz} \\ M + M_{mean} \end{bmatrix} \quad (4.11)$$

4.2.2 Numerical integration approach

The equations of motion can be solved in time domain using any of the several integration techniques available in the literature. In general, the solution approach should be executed through iteration, where the displacements obtained in the

preceding time steps are used to calculate the $[F(t)]$ and $[K]$ for the next steps and iteration is performed until satisfactory convergence is achieved.

In this study, in order to solve Eq. 4.1 in the time domain, the exciting forces at right hand side are evaluated at each time step at the instantaneous structure position and up to the free surface. The equations of motion are solved using unconditionally stable Newmark Beta integration method (explicit form) with constant average acceleration ($\beta = 1/4$ and $\gamma = 1/2$) [122]. A flow diagram illustrating the Newmark Beta procedure, is shown in Figure 4.1.

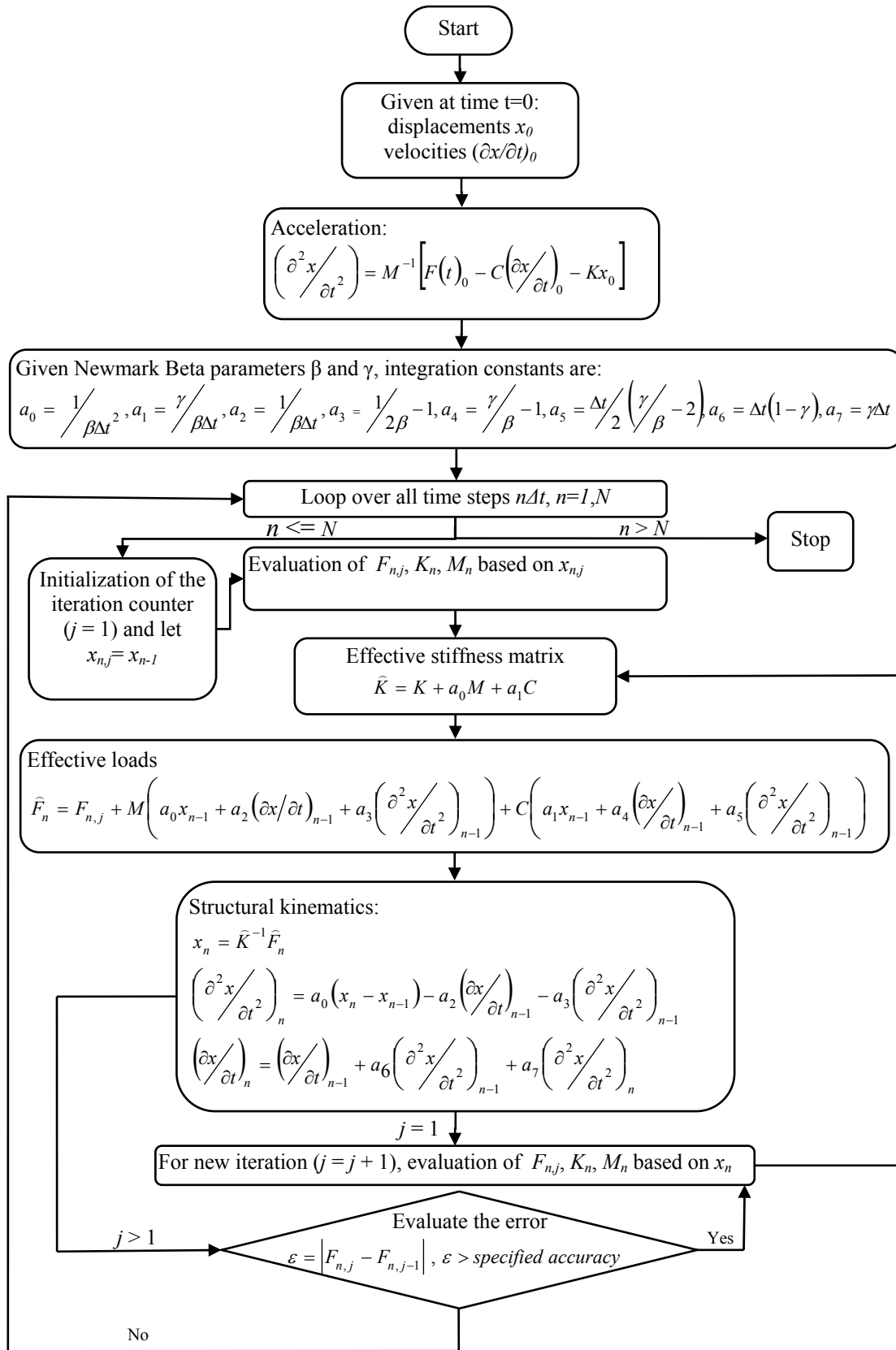


Figure 4.1: Flow chart of the Newmark Beta integration method

4.3 Quasi-static mooring line analysis

In this type of analysis, mooring lines are modeled as linear/nonlinear springs. In practical applications, the real force-displacement curve for the mooring system has to be matched in the lab tests. In this section, the nonlinear force-displacement equations [79] are presented.

The following assumptions are made for the analysis:

1. The sea floor has negligible slope
2. All mooring lines move very slow inside the water, so that the generated drag and inertia forces on the line due to the motion can be neglected.
3. The change in the line geometry and thereby in the line force due to direct fluid loading caused from wave/current is insignificant.
4. Initial length of the line is inclusive of the elongation due to the pretension force.
5. Anchor support does not move in any direction.
6. Only the horizontal excursion of the line is considered in the analysis.

Equations of catenary line are used to evaluate the force-displacement relationship of the mooring line. The horizontal and vertical projections of any segment hanging freely under its own weight W per unit length as shown in Figure 4.2 can be expressed as

$$\begin{aligned} Y &= \frac{H_t}{W} \cosh\left(\left[\sinh^{-1}(\tan \theta_t)\right] - \cosh\left[\sinh^{-1}(\tan \theta_b)\right]\right) \\ X &= \frac{H_t}{W} \left[\sinh^{-1}(\tan \theta_t) - \sinh^{-1}(\tan \theta_b)\right] \\ \tan \theta_b &= \frac{(V_t - WS)}{H_t} \\ V_t &= H_t \tan \theta_t \end{aligned} \tag{4.12}$$

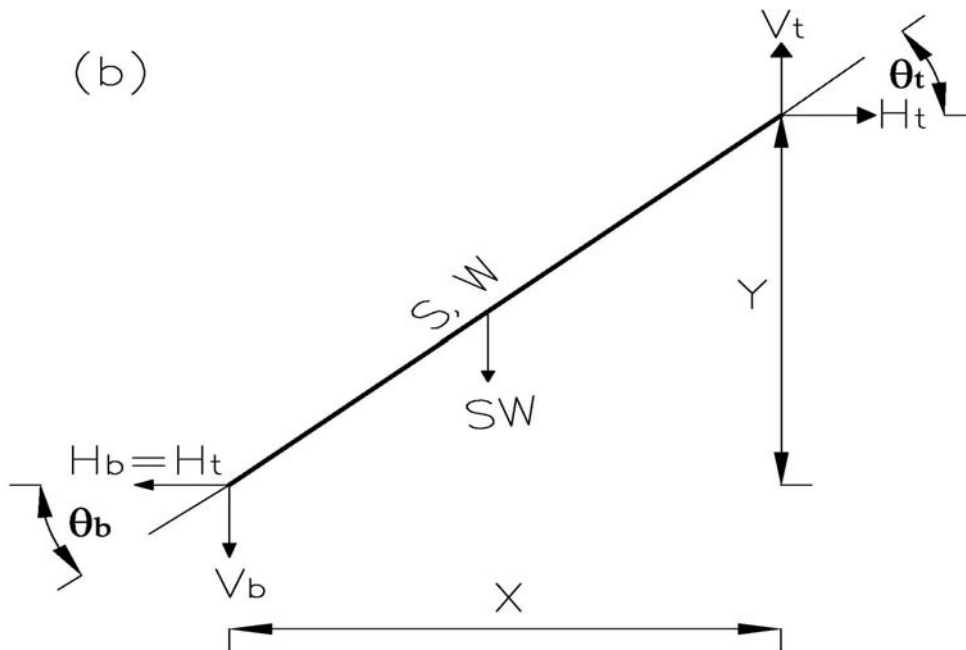
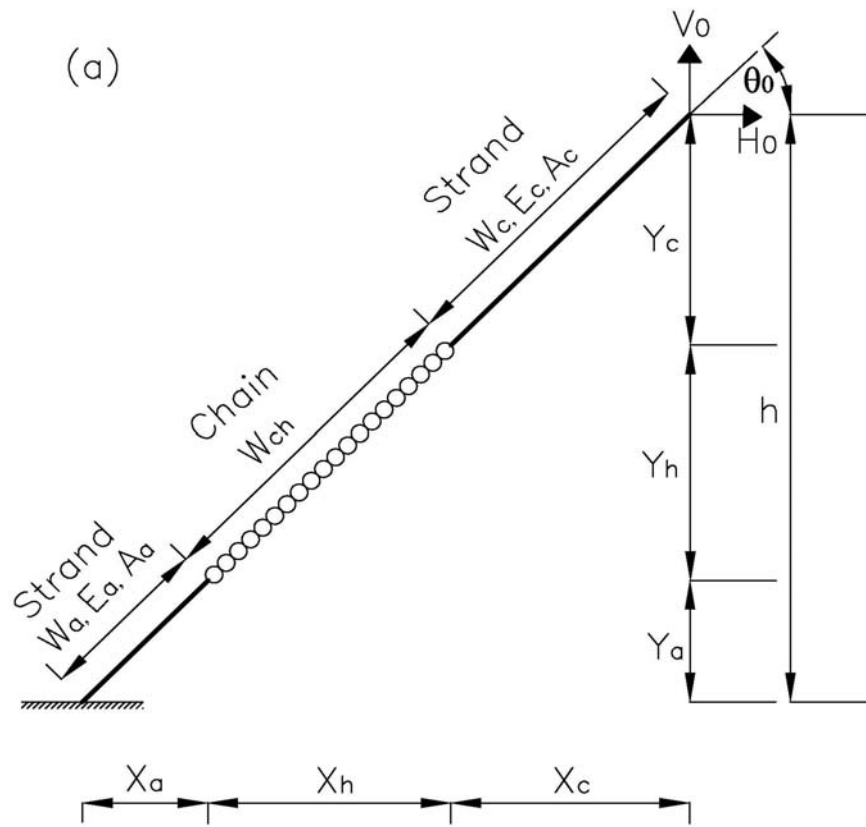


Figure 4.2: Multi-component taut mooring line: (a) Mooring line configuration; (b) Free body diagram of mooring line segment.

The new segment length due to increased line tension can be approximately evaluated as follows

$$S_i = S_{i-1} \left[1 + \frac{(T_i - T_{i-1})}{EA} \right] \quad (4.13)$$

where i is the line configuration number, T_i is the average segment tension and EA is the segment modulus of elasticity.

Even though the total segment weight (S_0W_0) remains same, the segment unit weight should be modified as

$$W_i = \frac{S_0W_0}{S_i} \quad (4.14)$$

Using Eq. 4.12, a numerical computer program was developed for generating the static tension-displacement characteristics of a single mooring line. This program performs static analysis of a mooring line with respect to structural horizontal displacement. A flow diagram illustrating the general procedure is shown in Figure 4.3.

The tension-displacement characteristics of the mooring lines are generated in the plan of symmetry of the mooring system. For structure horizontal excursion δ , the resultant horizontal restoring force is given by

$$Rf(\delta) = \sum_{j=1, p} H_j(\delta_j) \times \cos(\theta_j) \quad (4.15)$$

where p is the total number of mooring lines, θ_j is the angle between the j^{th} mooring line and the direction of excursion. δ_j is the excursion of the j^{th} mooring line which is equal to $\delta \times \cos(\theta_j)$ and $H_j(\delta_j)$ is the associated horizontal tension component for the j^{th} mooring line.

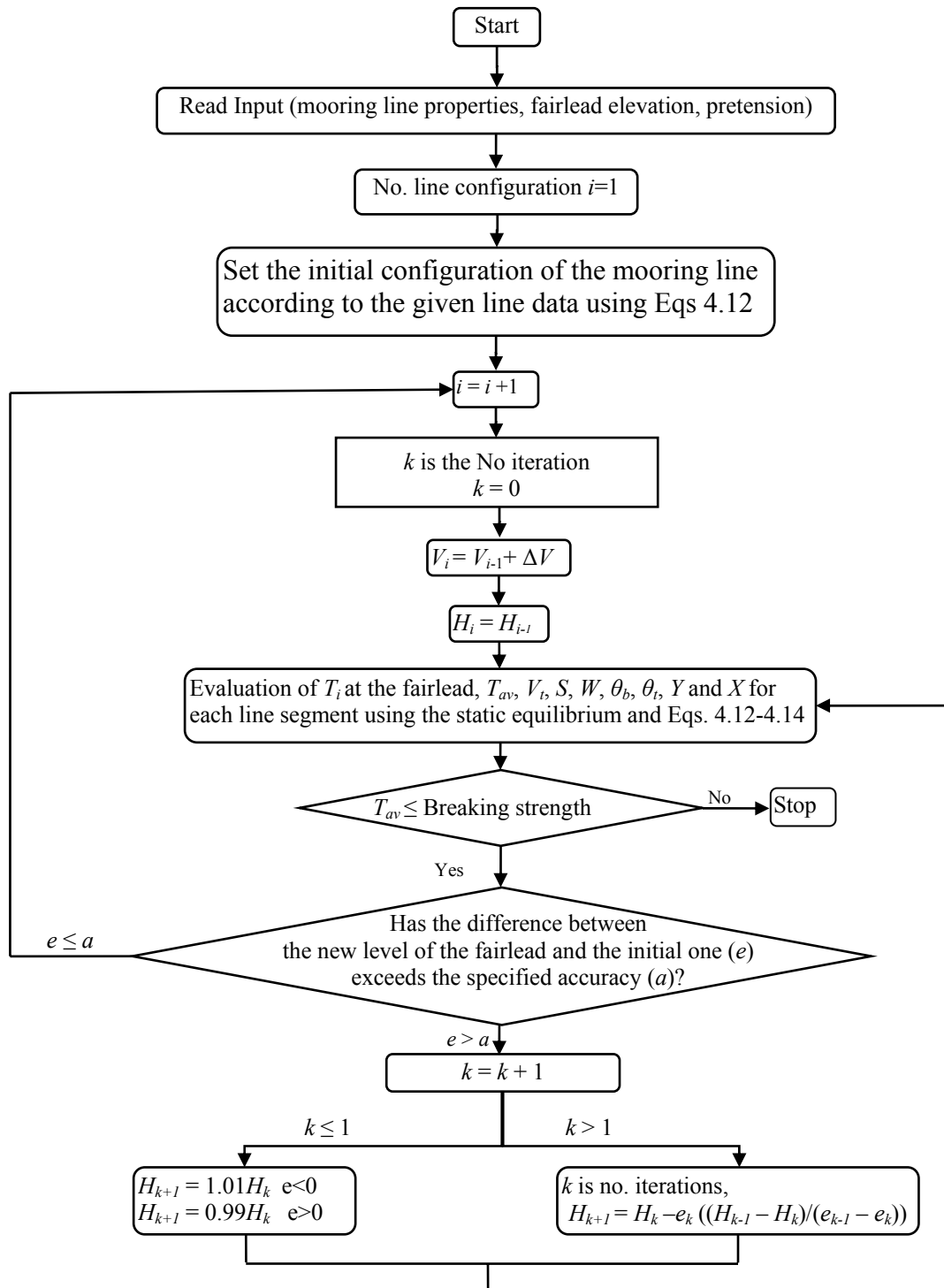


Figure 4.3: Flow chart of the quasi-static analysis of a mooring line

4.4 Dynamics of mooring lines

Floating offshore structures are maintained in the position by a variety of mooring line types and systems. For station keeping purpose, two types of mooring systems, the single-leg and multi-leg mooring systems have been used. The most common concept in deepwater oil fields is a multi-leg mooring system, which can be categorized by their shape as: catenary system, semi-taut, taut system and vertical tension tendons. The catenary and taut mooring systems generally use chain-wire-chain or chain-polyester-chain combination. Spar platforms which are generally installed in the ultra-deep oil fields, use taut system as catenary spread mooring lines having a large footprint.

In designing offshore mooring systems, the dynamic behavior of mooring lines is to be determined. In this study, the dynamic mooring line tension is predicted using lumped mass method. This numerical algorithm was developed by Boom [88]. The technique involves the lumping of all effects of mass, external forces and internal reactions at a finite number of points along the mooring line. By applying the equations of dynamic equilibrium and continuity (stress/strain) to each mass, a set of discrete equations of motion is developed. Boom [88] used finite difference techniques to solve these equations while in this study, Newmark Beta (constant average acceleration) method was adopted. The material damping, bending and torsional moments were neglected. Mooring line was modeled as a set of concentrated masses connected by massless springs.

A mooring line is subjected to line-end loads, weight, buoyancy, sea floor reaction forces (this is for catenary types) and fluid loading which may be divided as components proportional to the relative fluid acceleration (“added inertia”) and the components proportional to the relative velocity squared (“drag”). Only the current velocity is considered in the relative velocity since the wave velocities are normally small. In this procedure, the analysis of the dynamic motions of the structure and the behavior of mooring line are treated separately. The fairlead motion is considered as the boundary condition for the line motions. It is preferable to describe the fluid loading in a local system of coordinates along the line (tangential) and the normal

direction while describing the ultimate motions in an earth-fixed “global” system of coordinates.

The mathematical model is a modification of the lumped mass method as presented by Nakajima [123]. A developed computer program applies this method in two dimensions assuming that the mooring line remains in the vertical plane through both line ends. As shown in Figure 4.4, the mooring line is divided into finite nodes at which the forces are lumped. These nodes are connected by segments which are considered as massless springs accounting for the tangential elasticity of the line.

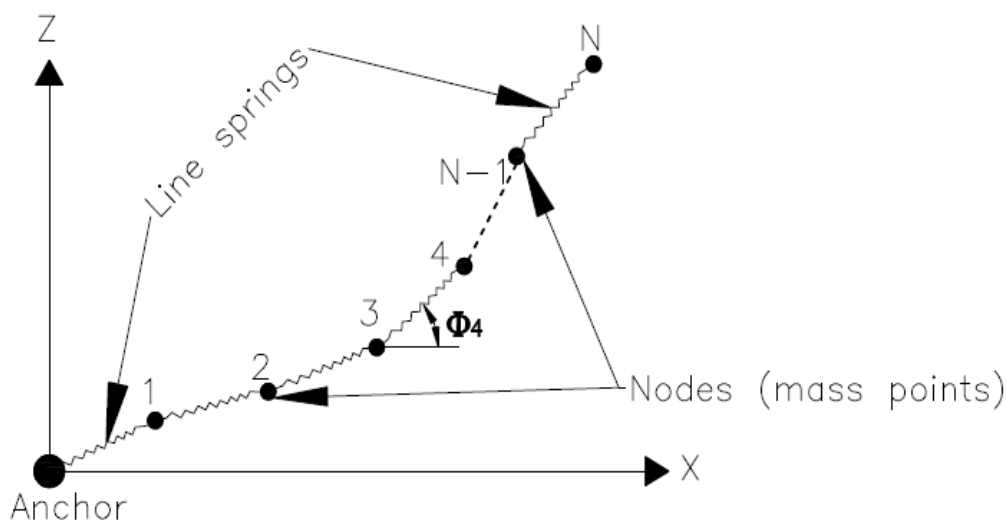


Figure 4.4: Discretization of mooring line by a lumped mass method

Applying Newton’s law in the global coordinate system, the governing equations for the j^{th} lumped mass are derived:

$$([M_j] + [m_j(t)]) \ddot{x}_j(t) = F_j(t) \quad (4.16)$$

where $[M_j]$ is the Mass matrix, $[m_j]$ is the added mass matrix, t is the time, x_j is the displacement vector and F_j is the external force vector.

The added mass matrix can be derived from the normal and tangential fluid forces by directional transformations:

$$[m_j(t)] = a_{nj}[\Lambda_{nj}(t)] + a_{tj}[\Lambda_{tj}(t)] \quad (4.17)$$

where a_{nj} and a_{tj} represent the normal and tangential added mass:

$$\begin{aligned} a_{nj} &= \rho C_{In} \frac{\pi}{4} D_j^2 l_j \\ a_{tj} &= \rho C_{It} \frac{\pi}{4} D_j^2 l_j \end{aligned} \quad (4.18)$$

$[\Lambda_{nj}]$ and $[\Lambda_{tj}]$ are directional matrices:

$$\begin{aligned} \Lambda_{nj} &= \begin{pmatrix} \sin^2 \bar{\phi}_j & -\sin \bar{\phi}_j \cos \bar{\phi}_j \\ -\sin \bar{\phi}_j \cos \bar{\phi}_j & \cos^2 \bar{\phi}_j \end{pmatrix} \\ \Lambda_{tj} &= \begin{pmatrix} \cos^2 \bar{\phi}_j & \sin \bar{\phi}_j \cos \bar{\phi}_j \\ \sin \bar{\phi}_j \cos \bar{\phi}_j & \sin^2 \bar{\phi}_j \end{pmatrix} \\ \bar{\phi}_j &= \frac{(\phi_j + \phi_{j+1})}{2} \end{aligned} \quad (4.19)$$

The nodal force vector $F_j(t)$ contains contributions from the segment tension T_j , the drag force F_{Dj} , buoyancy and weight F_{wj} .

$$F_j(t) = T_{j+1}(t)\Delta x_{j+1}(t) - T_j(t)\Delta x_j(t) + F_{Dj}(t) + F_{wj} \quad (4.20)$$

where:

$$\Delta x_j = (x_{j+1} - x_j)/l_j,$$

l_j is the original segment length

The drag forces are decomposed into normal and tangential force components:

$$\begin{aligned} F_{Dj}(t) &= [\Omega_j(t)] f_{Dj}(t) \\ f_{Dn}(t) &= \frac{1}{2} \rho C_{Dn} D_j l_j u_{nj}(t) |u_{nj}(t)| \\ f_{Dt}(t) &= \frac{1}{2} \rho C_{Dt} D_j l_j u_{tj}(t) |u_{tj}(t)| \\ u_j(t) &= [\Omega_j(t)] (c_j - x_j^*(t)) \end{aligned} \quad (4.21)$$

where f_{Dj} , u_j and c_j are the drag force, relative fluid velocity and current velocity

vector in local coordinates respectively. ρ , D and l are the fluid density, segment diameter and segment length respectively. C_{Dn} and C_{Dt} are the normal and tangential drag coefficients respectively. The directional matrix $[\Omega_j]$ is used to transform the drag force components from local to global axis and the global velocities into local velocities.

$$[\Omega_j] = \begin{bmatrix} -\sin \bar{\phi}_j & \cos \bar{\phi}_j \\ \cos \bar{\phi}_j & \sin \bar{\phi}_j \end{bmatrix} \quad (4.22)$$

As mentioned earlier the relations between nodal displacements, velocities and accelerations are approximated by Newmark Beta (Constant acceleration method):

$$\begin{aligned} \dot{x}_j(t + \Delta t) &= \dot{x}_j(t) + \frac{\Delta t}{2} \left(\ddot{x}_j(t) + \ddot{x}_j(t + \Delta t) \right) \\ x_j(t + \Delta t) &= x_j(t) + \Delta t \dot{x}_j(t) + \frac{\Delta t^2}{4} \left(\ddot{x}_j(t) + \ddot{x}_j(t + \Delta t) \right) \end{aligned} \quad (4.23)$$

The segment tension $T_j(t + \Delta t)$ is derived from the node positions by a Newton-Raphson iteration using the additional constraint equation for the constitutive stress-strain relation:

$$\begin{aligned} \psi_j(t) &= l_j^2(t) - \left\{ l_j(0) \left(1 + \frac{(T_j(t) - T_j(0))}{EA} \right) \right\}^2 \\ T^{k+1}(t + \Delta t) &= T^k(t + \Delta t) - [\Delta \psi^k(t)]^{-1} \psi^k(t) \end{aligned} \quad (4.24)$$

where ψ is the segment length error vector, T^k is the tentative segment tension vector at the k^{th} iteration and $\Delta \psi$ is the length error derivative matrix $[\partial \psi / \partial T]$.

For each time step the system of Eq. 4.24 is solved until acceptable convergence of $T^k(t + \Delta t)$ is obtained. The computer program flow chart is illustrated in Figure 4.5.

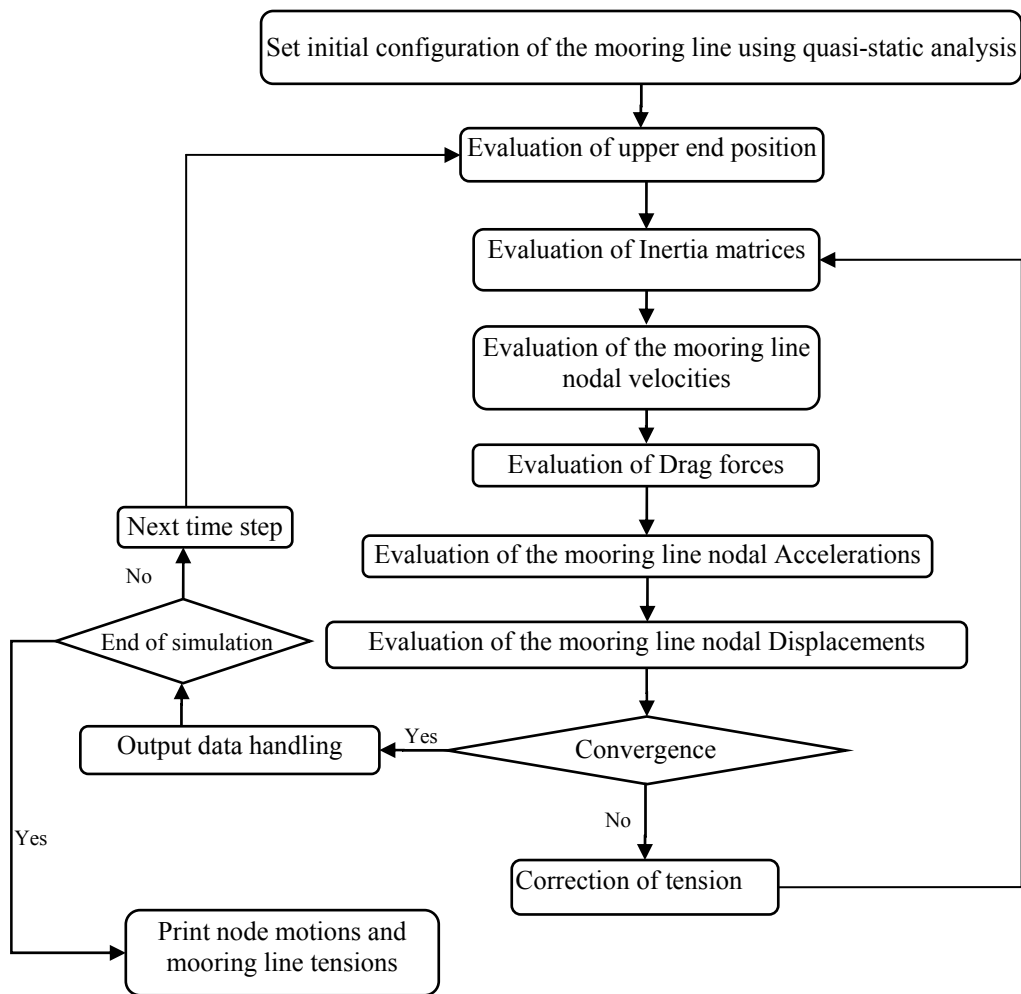


Figure 4.5: Lumped mass method flow chart

4.5 Effect of current

In practical situation waves are often associated with current. The current loads are as common as wave loads, and its appropriate modeling is necessary in order to predict structural displacements and mooring line tensions correctly.

Theory for current loads is not so well developed compared to the wave loads. However, some reasonable simplifications are often used in modeling current. The assumptions are:

1. Current velocity is steady.
2. Current velocity has the same profile over a reasonable distance.
3. The current and wave kinematics are independent.

Presence of current increases the incident wave frequency (ω_i) to the apparent frequency (ω_a) as given by

$$\omega_a = \omega_i + U_c k \quad (4.25)$$

where U_c and k are the current velocity and wave number respectively.

However, this effect has been neglected in this study for two reasons. First, the possible shift in frequency is not appreciable. Secondly, in the case of spar platforms the difference frequency forces are much more than the linear forces. As such, the shift ($\Delta\omega_i$) in one frequency would be offset by shift ($\Delta\omega_j$) in the other, resulting in very little change in ($\omega_i - \omega_j$).

Using the above assumptions, the current velocity, U_c , is incorporated in time domain by adding the average current velocity to the horizontal wave velocity in the drag term and carrying out the simulation process. As linearization of the drag force has been adopted in this study, the expressions derived by [124], which used for the linearization of drag force, was modified by incorporating the structure velocity.

Since the presence of current affects only the horizontal wave velocity, u , the relative vertical wave velocity component is same as in the wave-only case. Therefore, the subsequent equations focus only on the relative horizontal velocity, u_{re} . The horizontal drag force per unit length is written as

$$f_D(t) = C_D \rho \frac{D}{2} |u_{re}| u_{re} \quad (4.26)$$

where $u_{re} = u + U_c - (\partial x_G / \partial t + n \partial \gamma / \partial t)$

and

$$|u_{re}| u_{re} \approx c_0 + c_1 u_{re} \quad (4.27)$$

If $\mu_{u_{re}}$ is the mean value of u_{re} and $\sigma_{u_{re}}^2$ is its variance, then

$$c_0 = \sigma_{u_{re}}^2 \left\{ (1 - \lambda^2) [2Z(\lambda) - 1] + 2\lambda z(\lambda) \right\} \quad (4.28)$$

and

$$c_1 = 2\sigma_{u_{re}} \left\{ \lambda [2Z(\lambda) - 1] + 2z(\lambda) \right\} \quad (4.29)$$

where $\lambda = \mu_{u_{re}} / \sigma_{u_{re}}$ is a parameter measuring the strength of the current,

$$\mu_{u_{re}} = U_c \quad (4.30)$$

$$z(x) = \frac{e^{-x^2/2}}{\sqrt{2\pi}} \quad (4.31)$$

and

$$Z(x) = \int_{-\infty}^x \frac{e^{-x^2/2}}{\sqrt{2\pi}} dx = \int_{-\infty}^x z(x) dx \quad (4.32)$$

Eq. 4.26 shows that the horizontal component of the drag force in the presence of current has the following effects:

$$\text{Static force} = C_D \rho D/2 (c_0 + c_1 U_c) \quad (4.33)$$

$$\text{First and second order dynamic forces} = C_D \rho D/2 c_1 u(t) \quad (4.34)$$

$$\text{Surge and coupled surge-pitch damping forces} = C_D \rho D/2 c_1 (\partial x_G / \partial t + n \partial \gamma / \partial t) \quad (4.35)$$

The first and second order dynamic forces due to drag are greater than those for the wave-only case. The static force is important and causes large offsets. The damping forces in this case are larger than those for the wave-only case. This reduces the resonant response of the truss spar considerably.

4.6 Effect of wind

Wind is the main driving force for ocean waves. Just like current loads, wind loads are also integral part of the forces acting on offshore structures. Contrary to wave and current, winds act on the area above water. Due to its potentially high speed and the

magnitude of the moment-arm (as it acts way above the structural CG), wind loads may cause significant spar motions.

The wind load on a structure can be obtained by integrating the dynamic wind pressure over the surface it acts on. The velocity-squared term of the pressure equation is considered most important, and thus the dynamic pressure is approximated by

$\rho_d \cong \rho_w v^2 / 2$, where v is the wind velocity and ρ_w is the wind density.

The wind force is therefore the integral of this pressure over the structure's surface area from the mean water level to the tip. If W is the width of the structure at any point, then the total wind force is given by

$$F_w(t) \cong \int \rho_w v(t)^2 / 2 W \partial z \quad (4.36)$$

Here v and W are usually functions of z , but ρ_w is expected to remain constant.

Eq. 4.36 is easy to be implemented in the time domain. From test measurements, the time series $v(t)$ can be obtained. This can be used directly in Eq. 4.36 to get $F_w(t)$. It is common to replace the wind velocity $v(t)$ by the average velocity v_{avg} .

4.7 Chapter summary

In this chapter, the equation of motion and the numerical solution were discussed in details. Quasi-static analysis and dynamic analysis using lumped mass method, which are used for predicting mooring line tension, were presented. Finally, the current and wind forces calculations were given showing the assumptions used and their effects on the motion characteristics of the structure.

CHAPTER 5

EXPERIMENTAL STUDIES

5.1 Introduction

As indicated previously, the numerical models were developed for predicting the truss spar platform motions and the mooring line tensions. Therefore, it was decided to conduct the experimental studies in two phases. In the first phase, the experiments were carried out in the Marine Technology Laboratory of Universiti Teknologi Malaysia (UTM) at Skudai, Johor Baru. The numerical results were compared with the corresponding experimental measurements. These were preliminary experiments, which gave a general idea about the truss spar platform motion characteristics in the wave frequency exciting forces. In the second phase, the experiments were carried out in the Offshore Laboratory of the Universiti Teknologi PETRONAS (UTP). These comparisons mainly aimed to verify the numerical linear and nonlinear responses for truss spar platform with intact mooring and under mooring lines failure conditions. Sea-keeping tests were performed for regular and irregular waves. Linear structure responses were verified using regular waves while the irregular waves, which are the best representation of the ocean environments, provided a suitable platform to understand the nonlinear wave-structure interaction.

In this chapter, the laboratory tests are described. Modeling of the structure, mooring systems and environment are explained. Moreover, the instrumentation and data acquisition systems for the tests are described.

5.2 Experimental studies at UTM (Phase 1)

The purposes of these model tests were to investigate the performance of the truss

spar platform in the frequency range exciting wave forces and to provide experimental data for validation of the numerical results.

5.2.1 Test facilities and instrumentations

The Marine Technology Laboratory is equipped with a wave basin of 120 m length and 4 m width. The maximum water depth is 2.5 m. The waves are generated by a hydraulically driven flap type wave maker capable of generating waves up to a maximum height of 440 mm and a wave period less than 2.5 s. A beach at the far end of the basin absorbed the waves. The towing carriage is equipped with data acquisition system connected to the measured instrumentations. Figure 5.1 shows a cross-sectional and plan views for the wave tank.

In this experimental study, the wave environments were monitored with a wave probe on the upstream side of the model. The responses were measured with two accelerometers fitted on the deck, as shown in Figure 5.2. Tension in the wires was measured with four linear strain gauge type force transducers.

MARINE TECHNOLOGY LABORATORY LAYOUT PLAN

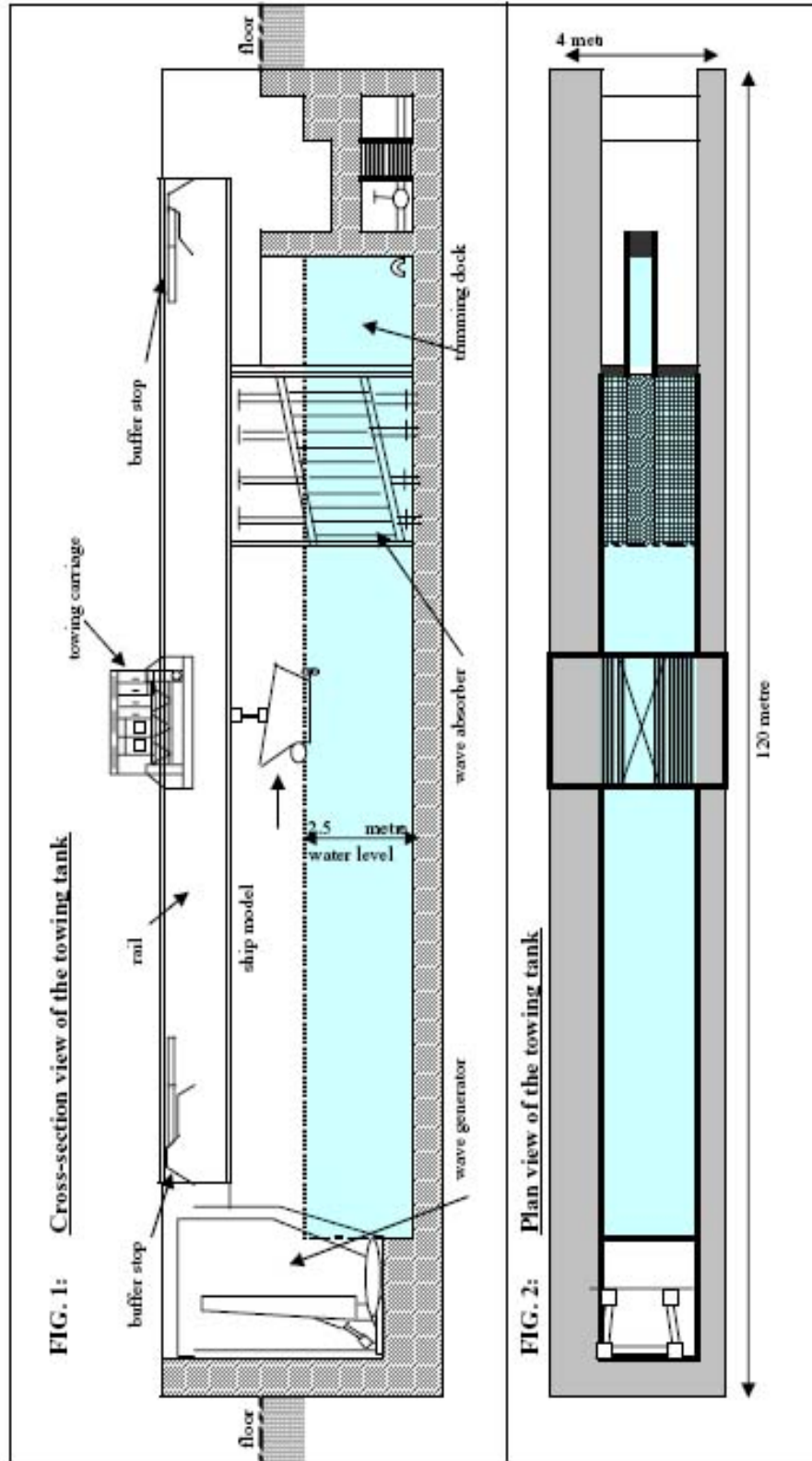


Figure 5.1: Schematic diagram for the Marine Technology Laboratory towing tank
 (Source: Marine Technology laboratory report No. MTL 056/2008)

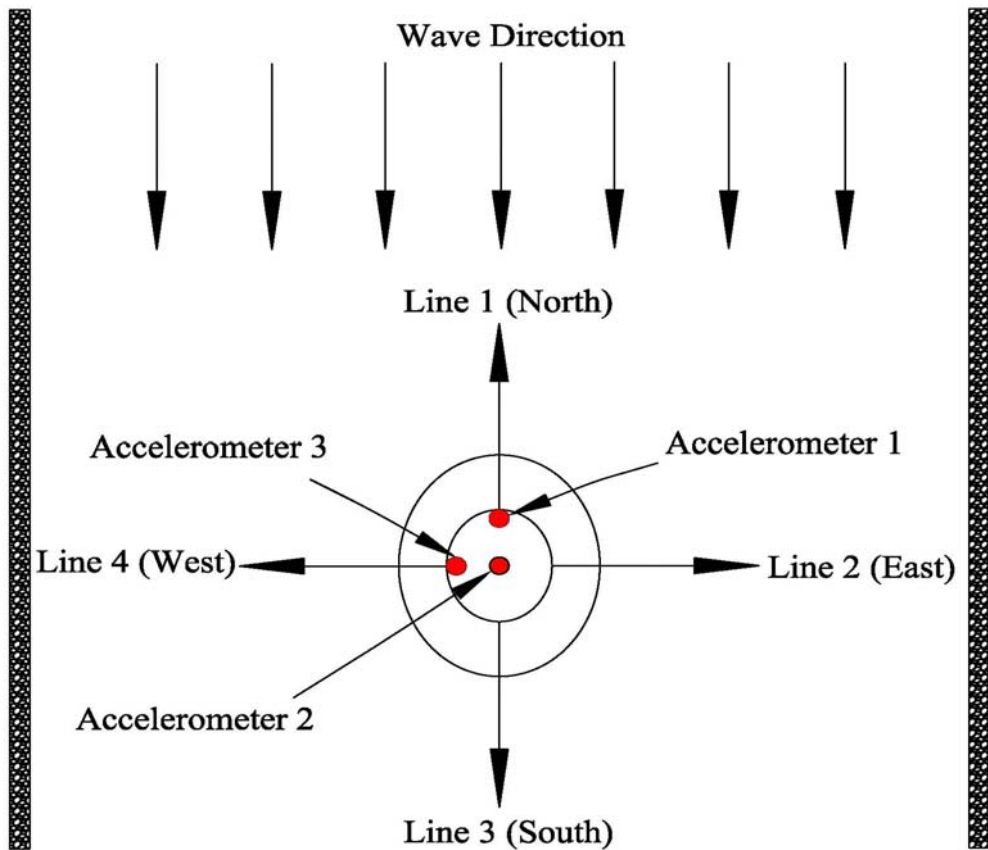


Figure 5.2: Model test arrangement in the wave basin (top view- Phase 1)

5.2.2 Model description

The model was designed and fabricated using galvanized steel. It comprised of two main sections; a conventional spar-shaped upper hull, and a lower truss section, as shown in Figure 5.3. The hull was 442 mm in diameter and 917 mm deep. The lower part of the spar was ballasted with water to bring the spar to a draft of 1.79 m. The truss was made up of three standard 312 mm × 312 mm × 312 mm bays, two 13 mm × 442 mm × 442 mm heave plates and a soft tank of 146 mm × 442 mm × 442 mm. The legs were 25 mm diameter and the horizontal and diagonal structural elements were 10 mm in diameter. The total length of the truss part was 1.021 m. Four horizontal wires combined with linear springs were used to provide restoring force for the model in the horizontal direction, as shown in Figure 5.4.



Figure 5.3: Truss spar model (Phase 1)

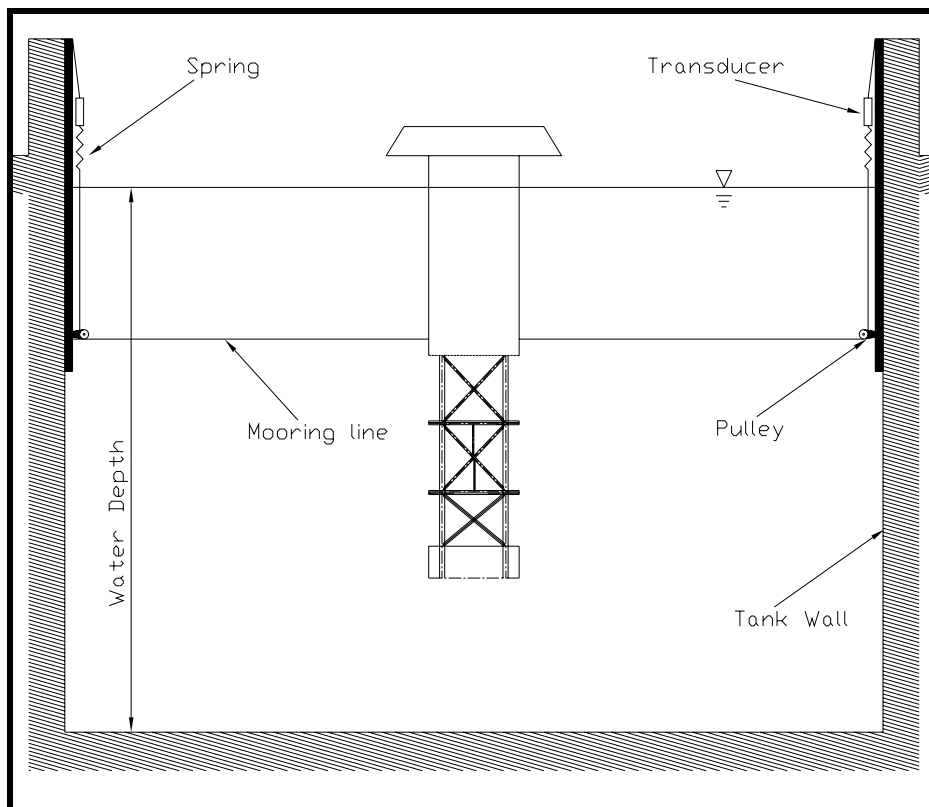


Figure 5.4: Truss spar model in the wave basin (Side view - Phase 1)

5.2.3 Experimental programs

As mentioned in Chapter 4, there is a need to obtain the mooring line restoring forces and the natural frequencies of the system in the considered degrees of freedom in order to solve the equations of motion of the system. For these purposes, static offset tests and free decay tests were conducted.

First, static offset test was conducted to estimate the stiffness of the mooring lines in the surge direction. The model was pulled horizontally from the downstream side. Accordingly, the horizontal movements and the readings from the transducers were recorded simultaneously. Using this data, the force-displacement relationship was constructed.

Then decay tests were conducted to calculate the damping ratio and the natural periods of the system in surge heave and pitch. The model was given an initial displacement and the subsequent motions were recorded. The damping ratio was computed using the logarithmic decrement formula:

$$\zeta \cong \frac{1}{2\pi} \cdot \ln \left[\frac{a_i}{a_{i+1}} \right] \quad (5.1)$$

where,

ζ = damping ratio, a_i and a_{i+1} = crest amplitude of the i^{th} and $(i+1)^{\text{th}}$ cycles, respectively.

Table 5.1 summarizes the regular waves, in model scale, that were created for sea keeping tests. Each regular wave test was run for a period of 1.5 minutes.

Table 5.1: Wave height and period of regular waves used for testing

Regular wave No.	Wave height (cm)	Wave period (sec)
Reg1	5.48	0.94
Reg2	6.98	1.05
Reg3	8.16	1.53
Reg4	5.52	1.64
Reg5	2.68	1.67
Reg6	7.02	1.86
Reg7	5.84	2

5.3 Experimental studies at UTP (Phase 2)

Comprehensive experimental studies have been conducted in the UTP offshore laboratory. These experiments were done for two structure cases:

Case 1: This case represents the truss spar with its intact mooring lines. The truss spar model was connected with four mooring lines as shown in Figure 5.5 and Figure 5.6.

Case 2: The same model with its mooring line system was modified to account for mooring line failure condition. This modification was performed by relaxing the upper stream mooring lines to obtain the migration surge distance caused due to mooring line failure.

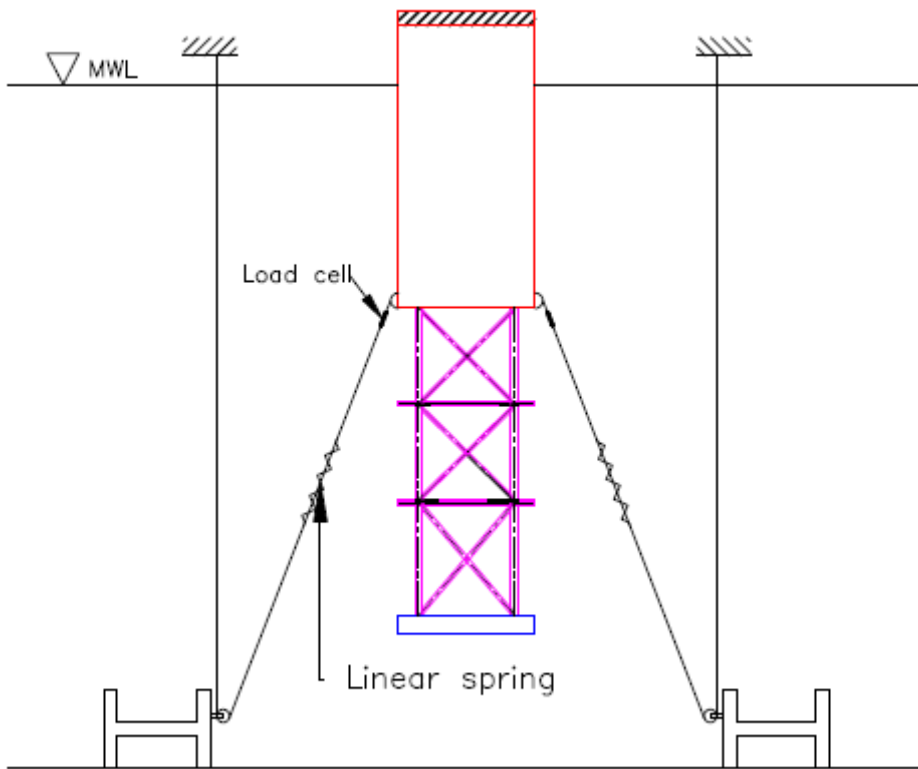


Figure 5.5: Sea keeping tests setup (side view - Phase 2)

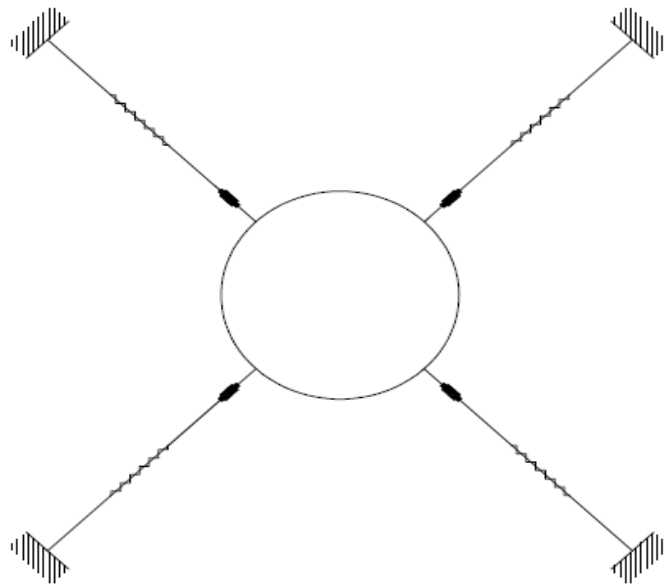


Figure 5.6: Model mooring line arrangement (Phase 2)

5.3.1 Test facilities and instrumentations

The offshore lab wave basin measures approximately 22 m long, 10 m wide and 1.5 m deep as shown in Figure 5.7. The wave maker system in this tank comprises of wave-maker, remote control unit, signal generation computer and dynamic wave absorption beach. The wave-maker comprises of a number of modules, each having eight individual paddles, which can move independently of one another. These paddles move backward and forward horizontally to generate waves in the basin.

The wave maker is capable of generating up to 0.3 m wave height and period as short as 0.5 s (model scale). Major random sea spectra, such as JONSWAP, ISSC, PM, Bretschneider, and Ochi-Hubble, can be simulated. Also, custom spectra can be added to the software and calibrated. The progressive mesh beach systems minimize interference from reflected waves during tests. UTP basin also includes a current making system capable of providing a current speed of 0.2 m/s at a water depth of 1 m (the speed varies with water depth). Figure 5.7 shows the plan and section of the UTP basin. Figure 5.8 shows UTP basin wave maker system.

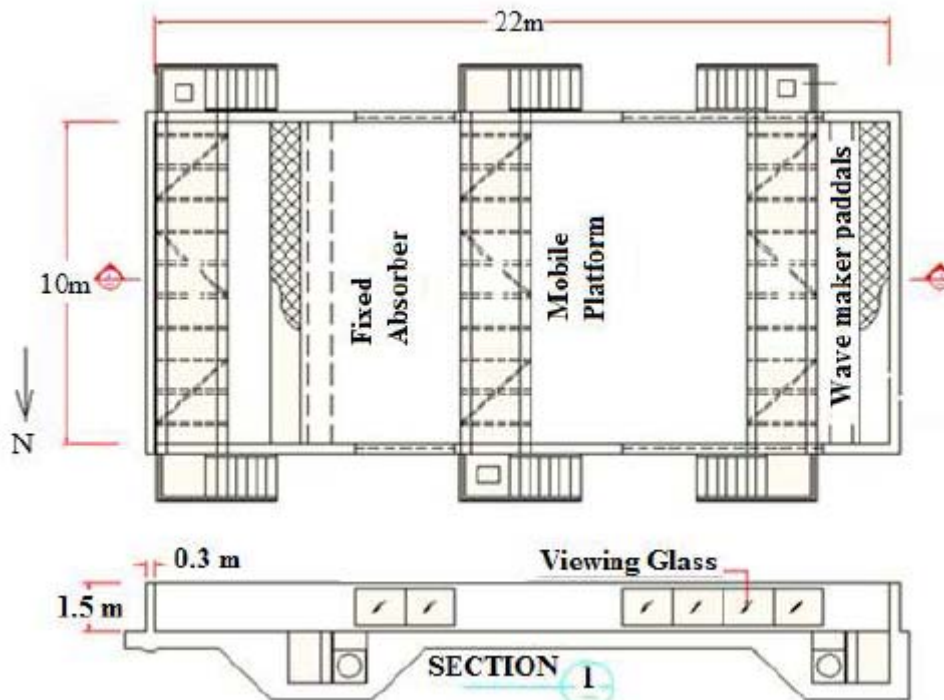


Figure 5.7: UTP wave basin



Figure 5.8: UTP basin wave maker system
(Source: UTP basin user manual, HR Wallingford, 2008)

The UTP basin beach consists of foamed filled plates fixed to a rigid framework. The beach efficiency has been verified by absorption coefficient test, it was found that the absorber coefficient decreased slightly with bigger waves, dropping from 98.1% to 97.4 % as wave height increase from 0.05 m to 0.30 m [125]. The following instrumentations were used during tests: 1) four-camera optical tracking (OptiTrack) system to measure 3 DOF (degrees of freedom) motions, 2) resistive HR's wave probes to measure the wave heights, 3) TML's load cells to measure the mooring system loads. The load cells were connected to TML's smart dynamic strain recorder (data logger) attached to Windows-based data acquisition and analysis program that is suitable for up to 64 analogue input channels. The remaining sensors were attached directly to the data acquisition system. This system consists of three modules: 1) calibration and scaling of inputs, 2) data acquisition and 3) data analysis.

The use of optical tracking (OptiTrack) system is a robust, real-time data, 3D system, in which markers can be attached to multiple objects in known patterns (rigid bodies) within specified volume, allowing them to be tracked in full 6 DOF (position and orientation).

The HR's wave probe comprises of two parallel stainless steel rods with a plastic head and foot. The head is fixed to calibration stem and a mounting block is supplied that allows the calibration stem to be fixed to any vertical surface. The wave probe is equipped with tripod for the use in the wave basin. The probe length is 900 mm and diameter of 6.0 mm. The wave probe is equipped with a simple monitor for measuring rapidly changing water levels. In addition, the TML's load cells used were tension/compression submersible low capacity (250N) cylindrical-shaped (80 mm diameter and 42 mm height) and light weight (0.45 kg) instruments. It can be used for high precision measurement.

The TML's smart dynamic strain recorder is a compact flash recording type 4-channel dynamic strain recorder and measures strain, DC voltage and thermocouples. At the same time of measurement, measured data are automatically stored on a compact flash card up to 2GB.

5.3.2 Choice of the scale and physical modeling law

The choice of scale of a model test often is limited by experimental facilities available. Modelling laws relate the behaviour of the prototype to that of a scaled model in a prescribed manner.

There are two generally accepted methods by which scaling laws relating two physical systems are developed. The first one is based on the inspectional analysis of the mathematical description of the physical system under investigation. The dynamics of the physical system are described by a system of differential equations. These equations are written in non-dimensional terms. Since the simulated physical system duplicates the full-scale system, these non-dimensional quantities in the differential equations must be equal for both. Thus, the equality of the corresponding non-dimensional parameters governs the scaling laws. This method assures similarity between the two systems but is dependent upon knowing explicitly the governing equations for both the prototype and model. The second method is based on well-known Buckingham Pi theorem. In this approach, the important variables influencing the dynamics of the system are identified first. Then, their physical dimensions are

noted. Based on Buckingham Pi theorem, an independent and convenient set of non-dimensional parameters is constructed from these variables. The equality of the pi terms for the model and prototype systems yields the similitude requirements or scaling laws to be satisfied. The model and prototype structural systems are similar if the corresponding pi terms are equal [126].

The principal types of forces encountered in the hydrodynamic model test are:

$$\text{Gravity force:} \quad F_G = Mg \quad (5.2)$$

$$\text{Inertia force:} \quad F_I = M (\partial u / \partial t) \quad (5.3)$$

$$\text{Viscous force:} \quad F_V = \mu A (\partial u / \partial y) \quad (5.4)$$

$$\text{Drag force:} \quad F_D = \frac{1}{2} CD \rho A u^2 \quad (5.5)$$

$$\text{Pressure force:} \quad F_P = \rho A \quad (5.6)$$

$$\text{Elastic force:} \quad F_e = EA \quad (5.7)$$

in which M = mass of the structure; u , $\partial u / \partial t$ = velocity and acceleration of fluid (or structure); y = vertical coordinates; A = area; and ρ = pressure fluid.

Hydrodynamic scaling laws are determined from the ratio of these forces. In most cases, the dynamic similitude between the model and the prototype is achieved from the satisfaction of only one of these scaling laws. Therefore, it is important to understand the physical process experienced by the structure and to choose the most important scaling law which govern this process. From the above forces, the following ratios may be defined:

1. Froude Number, F_r , F_I / F_G

2. Reynolds Number, Re , F_I / F_V

3. Iverson Modules, I_v , F_I / F_D

4. Euler Number, Eu , F_I / F_P

5. Cauchy Number, Cy , F_I / F_e

Since our problem is related to water flow with a free surface, the gravitational effect predominates. In this case, Froude's law is most applicable. By considering a

block of fluid having dimensions dx , dy and dz . The gravitation force on the block is given by:

$$W = \rho g \, dx \, dy \, dz \quad (5.8)$$

The inertia force is given by:

$$F_I = \rho \, dx \, dy \, dz \, (du/dt) \quad (5.9)$$

The ratio of the inertia force to the gravitation force is

$$\frac{F_I}{W} = \frac{u \, \partial u}{g \, \partial y} \quad (5.10)$$

Dimensionally, the Froude number is given by

$$F_r = \frac{F_I}{W} \rightarrow \frac{u^2}{gl} \quad (5.11)$$

The Froude number for the model and the prototype in waves can be expressed by

$$F_r = \frac{u_p^2}{gl_p} = \frac{u_m^2}{gl_m} \quad (5.12)$$

From geometric similarity, $l_p = \lambda \, l_m$ where p and m stand for prototype and model respectively and λ is the scale factor for the model. Then

$$u_p = \sqrt{\lambda} \, u_m \quad (5.13)$$

In this study, an assumption was made that the model follows the Froude's law of similitude. The scale factors for the common variables for the prototype and the model are listed in Table 5.2.

Table 5.2: Model to prototype multipliers for the variables under Froude scaling
(Source: *Offshore structure modeling, Chakrabarti, 1994*)

Variable	Unit	Scale factor
Geometry		
Length	L	λ
Area	L ²	λ^2
Volume	L ³	λ^3
Angle	None	1
Radius of gyration	L	λ
Area moment of inertia	L ⁴	λ^4
Mass moment of inertia	ML ²	λ^5
CG	L	λ
Kinematics and dynamics		
Time	T	$\lambda^{0.5}$
Acceleration	LT ⁻²	1
Velocity	LT ⁻¹	$\lambda^{0.5}$
Displacement	L	λ
Angular acceleration	T ⁻²	λ^{-1}
Angular velocity	T ⁻¹	$\lambda^{0.5}$
Angular displacement	None	1
Spring constant (linear)	MT ⁻²	λ^2
Damping coefficient	None	1
Damping factor	MT ⁻¹	$\lambda^{5/2}$
Natural period	T	$\lambda^{0.5}$
Displacement	L	λ
Wave mechanics		
Wave height	L	λ
Wave period	T	$\lambda^{0.5}$
Wave length	L	λ
Celerity	LT ⁻¹	$\lambda^{0.5}$
Particle velocity	LT ⁻¹	$\lambda^{0.5}$
Particle acceleration	LT ⁻²	1
Water depth	L	λ
Wave pressure	ML ⁻¹ T ⁻²	λ

5.3.3 Model description

A truss spar model was made of steel plates to the scale of 1:100 according to the dimensions shown in Figure 5.9. The constructed model undergoing tests is shown in Figure 5.10. Table 5.3 shows the summary of the general structural data of the freely-floating truss spar (full scale). The truss spar model was tested for the two cases, as mentioned above, in the wave tank of the UTP. The model motions and the restraining

mooring line tensions were measured by optical tracking system and load cells respectively. Data post processing program was prepared to evaluate the dynamic response spectra to random waves using the Fast Fourier Technique (FFT).

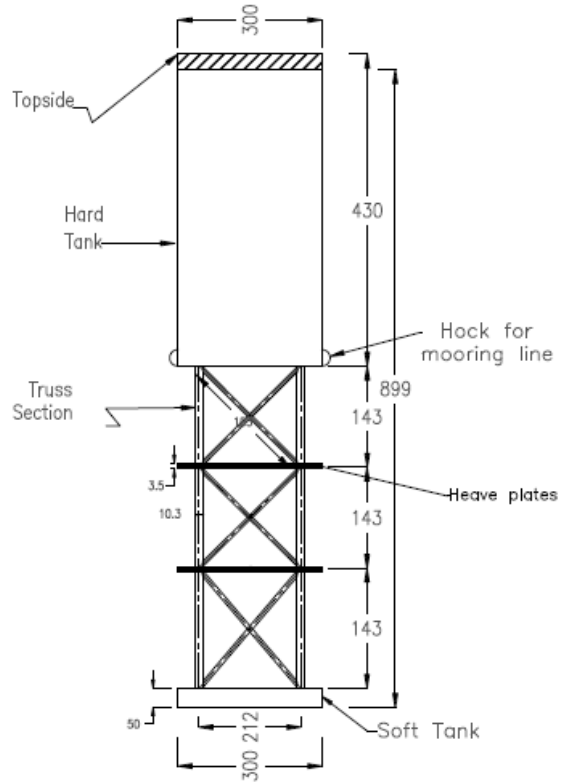


Figure 5.9: Truss spar model configuration (All dimensions are in mm - Phase 2)

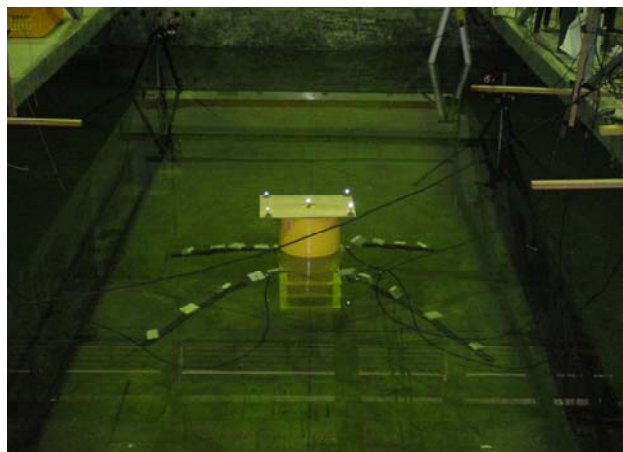


Figure 5.10: The truss spar model during tests (Phase 2)

Table 5.3: The truss spar data (full scale)

Description		Value
Diameter (m)		30
Overall length (m)		90.9
Draft (m)		70.4
Vertical center of gravity from the keel (m)		43.5
Vertical center of buoyancy from the keel (m)		48
Mass (ton)	Hard tank	8.5×10^3
	Truss members	1.6×10^3
	Heave plates	4.7×10^3
	Soft tank	3.3×10^3
	Other weights	2.86×10^3
	Total	20.96×10^3
Moment of inertia (Kg.m^2)		2.686×10^6
Water depth (m)		110

5.3.4 Mooring line system

Modeling of platforms involves modeling both the floating structure and the mooring system. Due to the limitations of the wave basin, it is common to model the mooring lines as springs and their effects are incorporated in the equation of motion by obtaining the static offset test results. The same procedure has been adopted in this study.

In the sea keeping tests, the cables with soft springs, as shown in Figure 5.5 - Figure 5.6, were used as mooring lines. Load cells were connected between the model and the spring for measuring mooring line tension in the fairlead. Small pieces of foam were attached to the springs and to the load cells to make them neutrally buoyant in water. It should be noted that the restraining system was pre-tensioned through pulley system and clamped in a way to ensure that no slacking of the wire occurred during the tests.

5.3.5 Experimental programs

Three different types of tests were conducted. Their details are as follows:

5.3.5.1 Quasi-static and free decay tests

Static offset tests were carried out to determine the mooring system stiffness. Load cells were attached to the up and down stream mooring lines. The same procedure used in Section 5.2.3 was followed in these tests for Cases 1 and 2. The measurements were taken for every 4 cm (model scale) horizontal displacement increment. Static forces were applied and the load cell readings were recorded accordingly.

In addition, free decay tests were conducted for Cases 1 and 2. The purpose of these tests was to predict the natural frequencies of the system in different conditions. By using Eq. 5.1, the structural damping of the system can be obtained. However, as mentioned earlier, this structural damping is small compared to the other damping sources.

5.3.5.2 Sea-keeping tests

For evaluating the sea-keeping characteristics of the model, it was tested for regular and random waves. Soft linear springs were attached to steel wires to form the mooring line system of the model. The general objectives of these tests were to measure the platform motions to regular and random waves. All random wave time series were transformed to the frequency domain using Fast Fourier Technique (FFT). Two model cases were considered in the experiments.

For measurements of the generated wave profiles, four wave probes were placed in the wave basin. Two were in front of the model and the other two at the back of the model. These remained in place during the whole experiments. The acquired data includes the model three DOF motions, mooring loads and the environmental variables (wave height and wave period).

Tests for regular waves were carried out for the range of the dominant wave frequencies. Table 5.4 summarizes the target and measured regular waves for the two cases. The test duration for each run was three minutes (model scale).

Table 5.4: Regular waves

Drive signal	Wave height (m)		Wave period (s)	
	Target	Measured	Target	Measured
RG1	4	3.8	6	6
RG2	4	3.7	7	7
RG3	5	4.8	8	8
RG4	6	5.9	9	9
RG5	7	6.85	10	10
RG6	8	7.9	12	12
RG7	9	8.85	14	14
RG8	10/8*	10/8*	16	16
RG9	11/8*	11.1/8*	18	18
RG10	12/8*	12.2/8*	20	20

*This wave height was used for mooring line damage condition

Storm waves were generated using JONSWAP spectra. During setup phase for the random wave tests, the data collection commenced 20 minutes (full scale) after the wave maker generated waves. This was to avoid the initial interval when the waves are in transition from calm to fully developed. A random wave with significant wave height $H_s = 5$ m and peak period $T_p = 12$ s (full scale) was selected for this experiment. The measured properties for this storm are $H_s = 4.7$ m and peak period $T_p = 11.5$ s.

5.4 Chapter summary

In this chapter, the model tests including quasi-static, free decay and station keeping tests conducted at UTM and UTP were described. The structural data, lab facilities and the related restraining system were given. Moreover, the procedure of choosing scale ratio was presented. For the experiments at UTM, the test details were given. These tests focused only on structure motions in the wave frequency region. In the experimental studies at UTP, the wave frequency and low frequency motions for the structure with intact mooring and mooring line failure were examined.

CHAPTER 6

RESULTS AND DISCUSSIONS

6.1 Introduction

In this chapter, the results of the numerical and experimental models are presented. The developed numerical scheme for predicting the dynamic responses of the platform is validated by comparisons with experimental results. These comparisons are arranged to cover the structure natural frequencies, wave frequency responses, low frequency responses and the effects of mooring line damage. The outcomes of the individual effects of the second order difference frequency wave forces are studied numerically. In addition, literature numerical data are used to validate the numerical model predictions in the case of combined wave, current and wind forces. Using the developed numerical model, a numerical study on strengthening of the station keeping system of the structure is presented. The discussions focus on its effects on the structure resonant responses. The developed numerical code based upon lumped mass method, is adopted for studying the dynamic effects on mooring line tension. This study is demonstrated by comparisons with literature experimental data. Finally, a parametric study on deepwater mooring line is presented showing the effects of pretension, cable unit weight and elongation on the nonlinear force-excursion relationship.

6.2 Experimental studies at UTM

In these experiments, all the experimental and numerical results are presented in model scale. From the results of the static offset test, the nonlinearity of the

force-displacement relationship of the mooring lines was approximated using multi-linear segments with different slopes as shown in Figure 6.1.

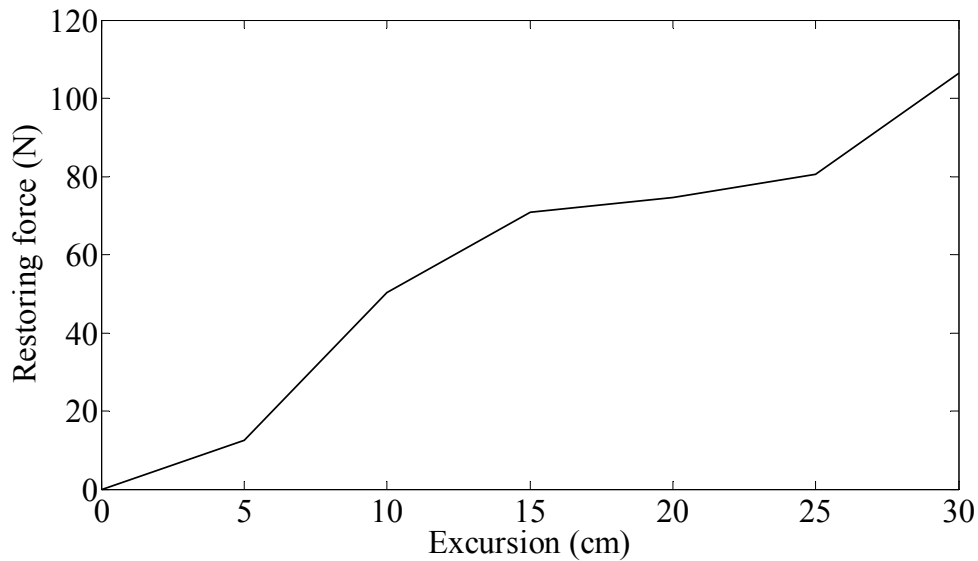


Figure 6.1: Static offset test results: Multi-segment force-displacement relationship

The natural periods of the model in heave, surge and pitch were predicted from the free decay tests and listed in Table 6.1.

Table 6.1: Natural periods of vibrations of the model

Motion type	Natural period (s)
Heave	2.47
Surge	2.41
Pitch	2.53

The responses of the truss spar model were determined numerically using the model parameters and the results were compared with the corresponding experimental measurements. The model dimensions and properties were used. The wave heights and wave periods corresponding to the generated waves in the basin were used for evaluating the wave force on the numerical model. All the dynamic responses are with respect to the CG.

The Response Amplitude Operators (RAOs) for surge, heave and pitch of the numerical model were compared with experimental measurements in Figure 6.2 -

Figure 6.4 respectively. The RAOs were determined as the ratio of response heights to wave heights.

As could be seen, the RAOs for surge, heave and pitch motions were fairly well predicted by the numerical model. The trend of the surge RAO agreed well with the measured values with a maximum difference of 20%. The heave RAOs agreed very well. For the pitch RAO, the simulation results followed the same trend as experimental results but it gave relatively lower values in wave frequencies between 0.55 – 0.8 Hz. This might be due to the effect of the reflection of the waves from the side walls of the wave flume on the model pitch motion.

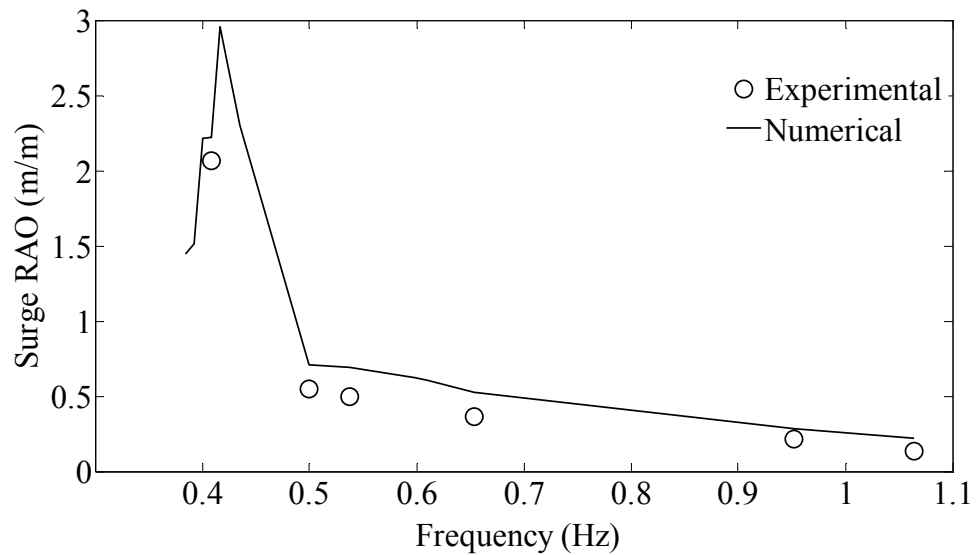


Figure 6.2: Comparison of surge motion RAO

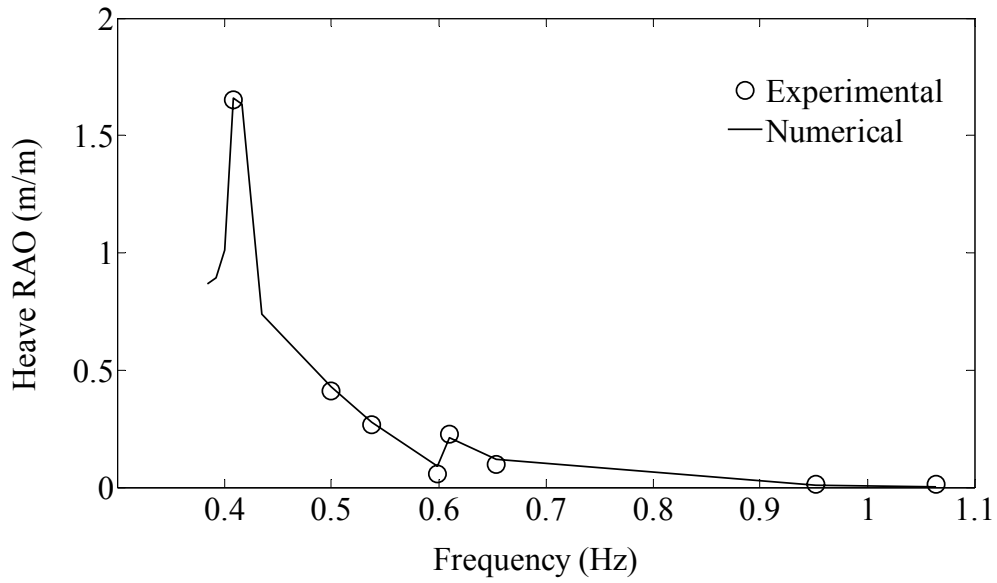


Figure 6.3: Comparison of heave motion RAO

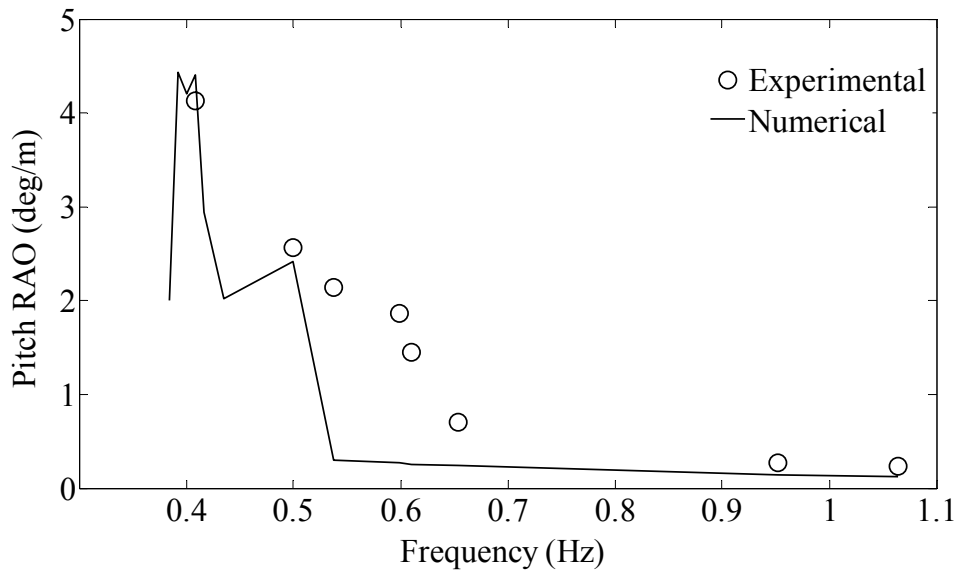


Figure 6.4: Comparison of pitch motion RAO

6.3 Experimental studies at UTP

These studies comprised of two main categories. First, the model in its normal condition was subjected to regular and random waves. Second, the model's mooring failure was simulated and the same environmental conditions were used to determine the structure dynamic responses in this condition.

6.3.1 Intact mooring lines condition

In this section, the numerical predictions were compared with the corresponding model test measurements (full scale) in terms of RAO for regular waves and response spectrum for random waves. In order to compare between the numerical and experimental results, mooring line stiffness, which was found from the static offset test, was used as input in the numerical model. In addition, free decay simulations were compared with the experimental measurements.

6.3.1.1 Static-offset test and free-decay results

In order to design the model with relatively low natural frequencies in all degrees of freedom, soft springs with 8.2 N/m stiffness (model scale) were used in the experiments to represent the mooring lines system. In Figure 6.5, a polynomial regression type with 4th order was chosen for the scatter static-offset test data.

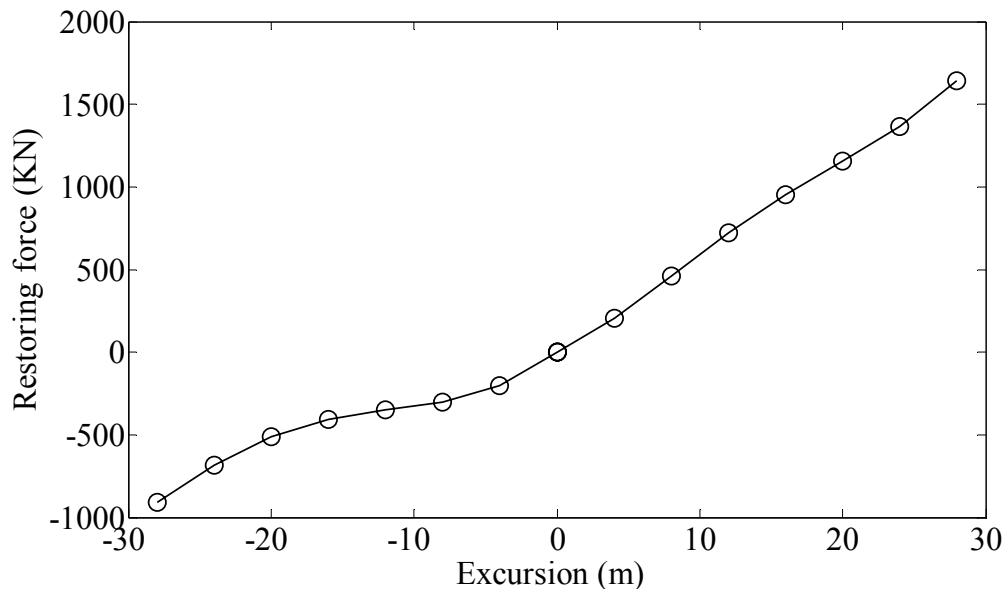


Figure 6.5: Static offset test results

Free-decay physical measurements and simulations for surge, heave and pitch are shown in Figure 6.6 - Figure 6.8 respectively. The numerical simulations gave good results when compared to the test results. Table 6.2 shows that the calculated natural periods and damping ratios (using Eq. (5.1)) were closed to the measurements. The differences were 5.6% for surge, 12.2% for heave and 24.2% for pitch.

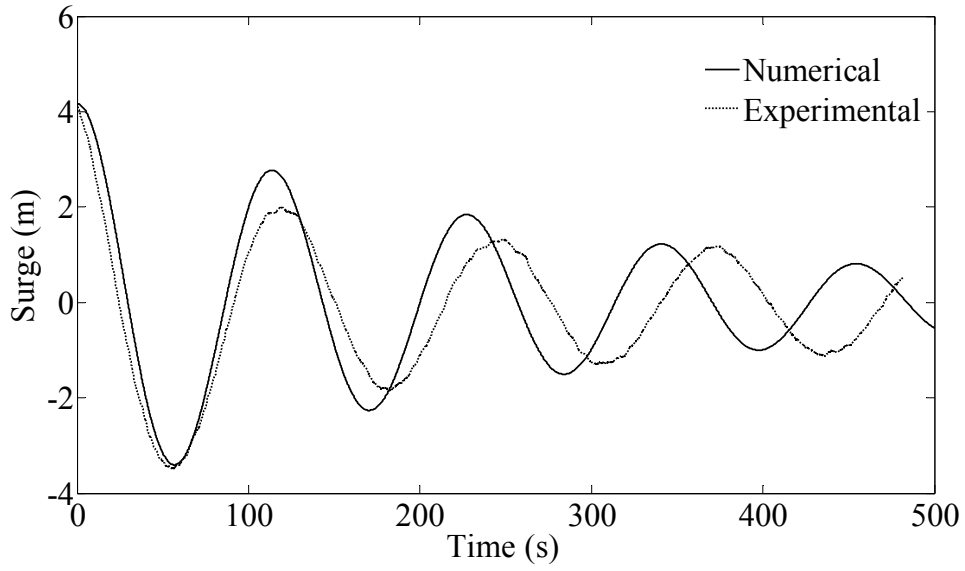


Figure 6.6: Surge free-decay results

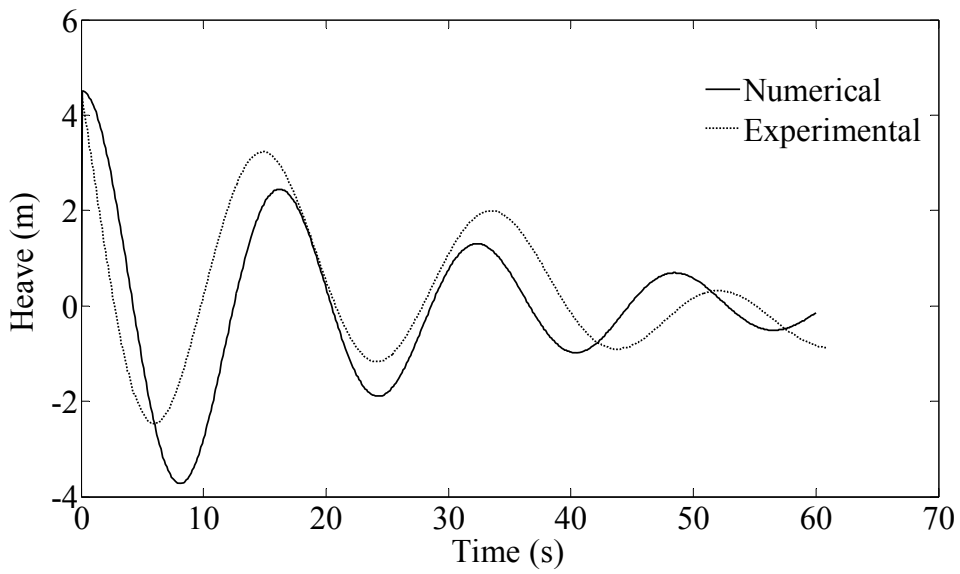


Figure 6.7: Heave free-decay results

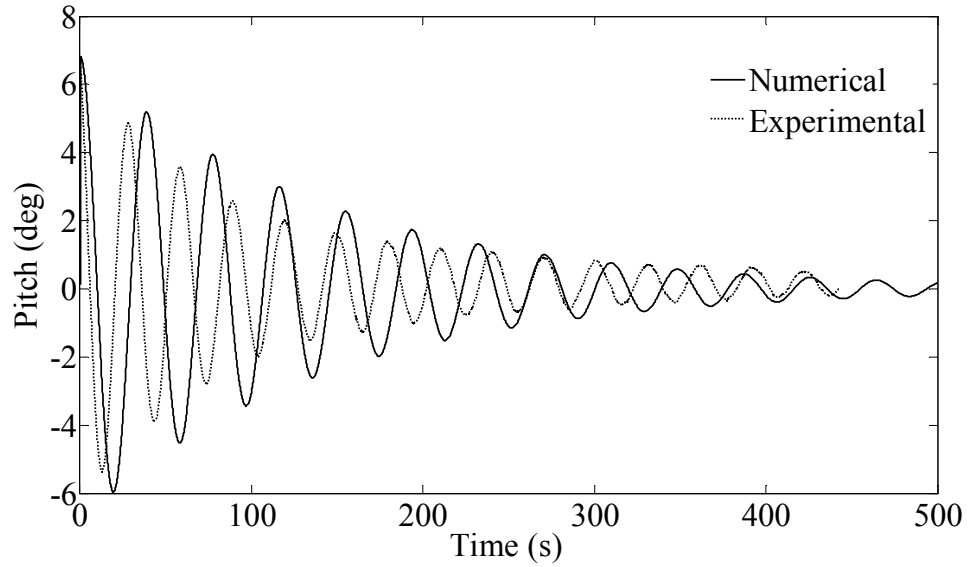


Figure 6.8: Pitch free decay results

Table 6.2: Comparison of natural periods and damping ratios

Motion type	Natural period (s)		Damping ratio (%)	
	Simulated	Measured	Simulated	Measured
Surge	114.5	121.25	6.6	6.9
Heave	16.25	18.5	10	7.7
Pitch	38.5	31	4.6	5.4

6.3.1.2 Wave frequency responses

The responses of the truss spar prototype were determined numerically using the structure dimensions, properties, draft and the generated wave characteristics (full scale) as input and the results were compared with the corresponding experimental data.

As shown in Figure 6.9 - Figure 6.11, the prototype RAOs for surge, heave and pitch of the numerical analysis were compared with the experimental processed

results for regular waves, which covered the dominant ocean wave frequencies (Table 5.4). The simulated results agreed well with the measurements. The trend of the surge RAO agreed well with the measured values with maximum difference of 25%. The numerical heave RAOs agreed very well with the experiments. For the pitch RAO, the simulation results followed the same trend as experimental results with maximum difference of 16.7%. Table 6.3 shows the Root Mean Square Deviation (RMSD) for the differences between the predictions and the measurements. The RMSD values for surge, heave and pitch indicate that the numerical model predict the truss spar motions with good accuracy.

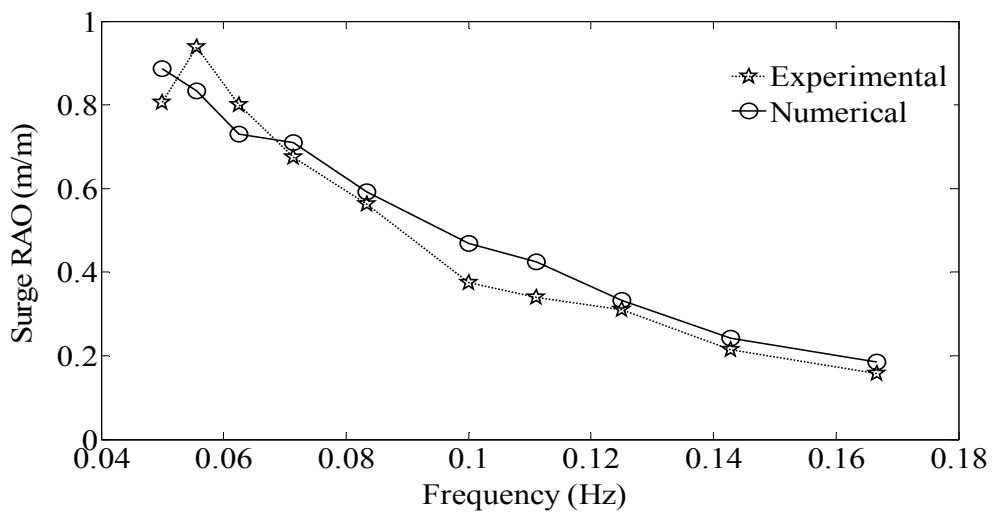


Figure 6.9: Surge RAOs

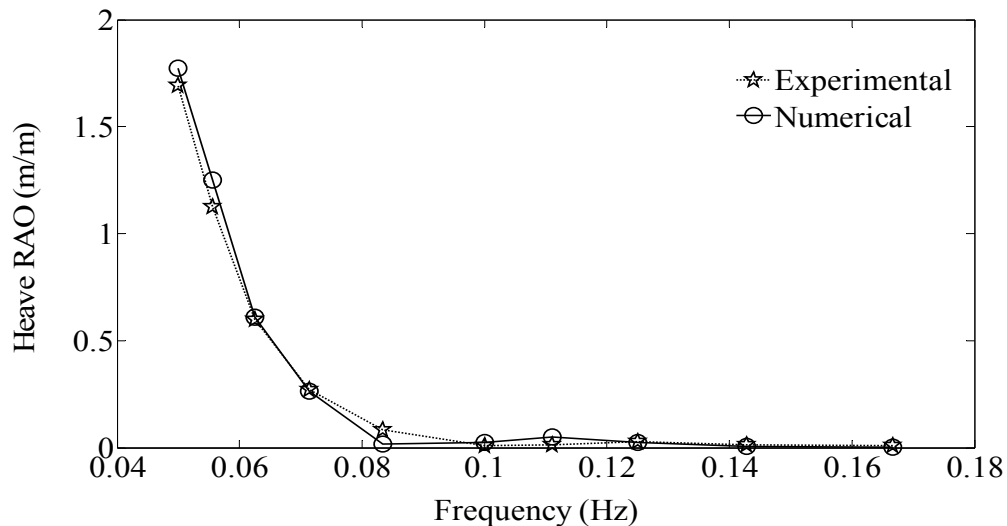


Figure 6.10: Heave RAOs

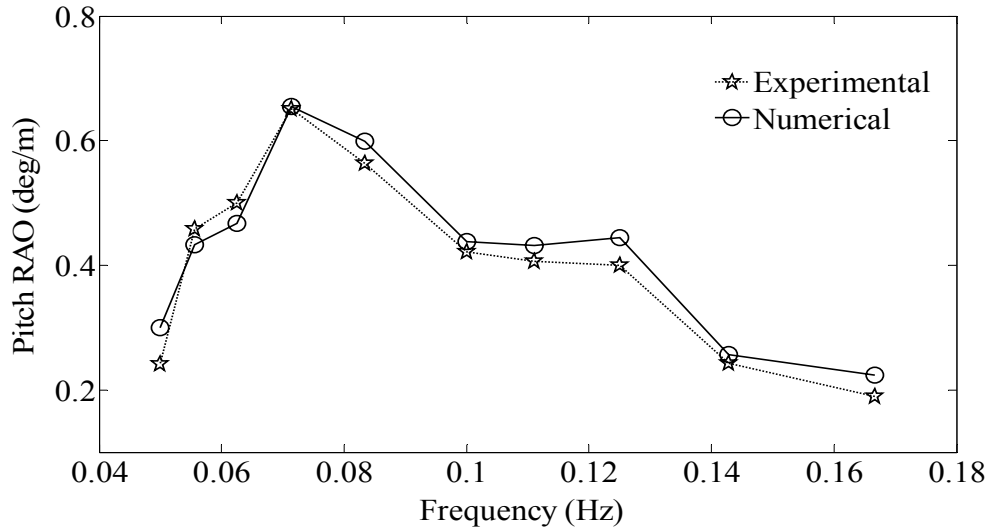


Figure 6.11: Pitch RAOs

Table 6.3: RMSD for dynamic motions due to regular waves

Dynamic motions	RMSD
Surge	0.0651
Heave	0.0532
Pitch	0.033

6.3.1.3 Low frequency responses

In this section, the low frequency responses due to random waves are presented in Figure 6.12 - Figure 6.14 for surge, heave and pitch respectively. In the simulation, all the derived equations (Eqs. 3.48 - 3.83) were incorporated in the numerical code to predict the slow drift responses. Both numerical predictions and the measurements show that the slow drift surge and pitch responses are significantly more than the wave frequency responses, while for heave motion the wave frequency response is dominant. From these figures, it can be seen that good agreement has been achieved between the numerical and experimental results. Table 6.4 shows the RMSD for the predicted and measured surge, heave and pitch motions in both low frequency (LFR)

and wave frequency (WFR) responses. The numerical results trend for WFR is relatively agreed well with the experiments compared to LFR predictions. However, both numerical results (WFR and LFR) have been fairly well predicted by the numerical model. With respect to the resonant and peak responses, which are extremely important in the design and the analysis for the system, the numerical algorithm was successfully estimated these responses with good accuracy. The percentage errors for surge, heave and pitch were found to be 9.5%, 13.7% and 11% respectively.

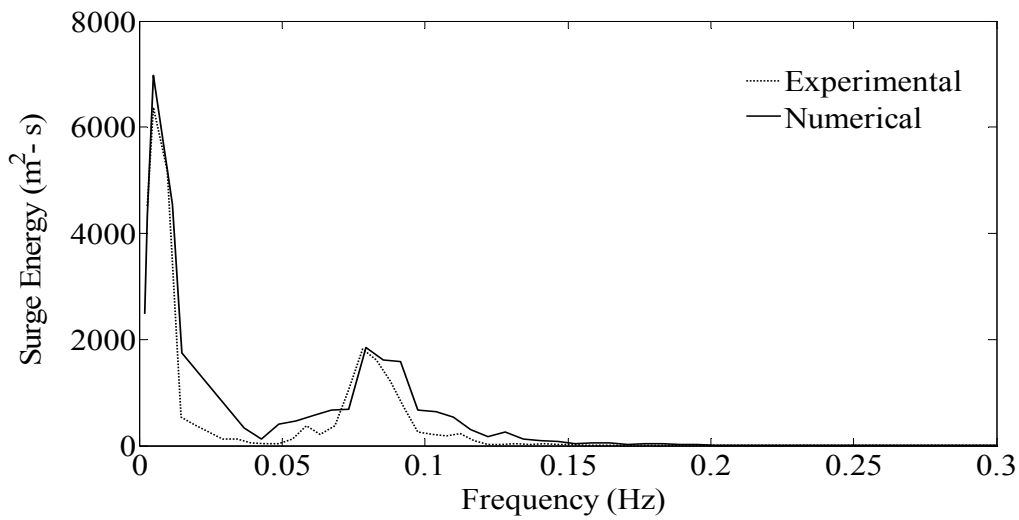


Figure 6.12: Surge spectra

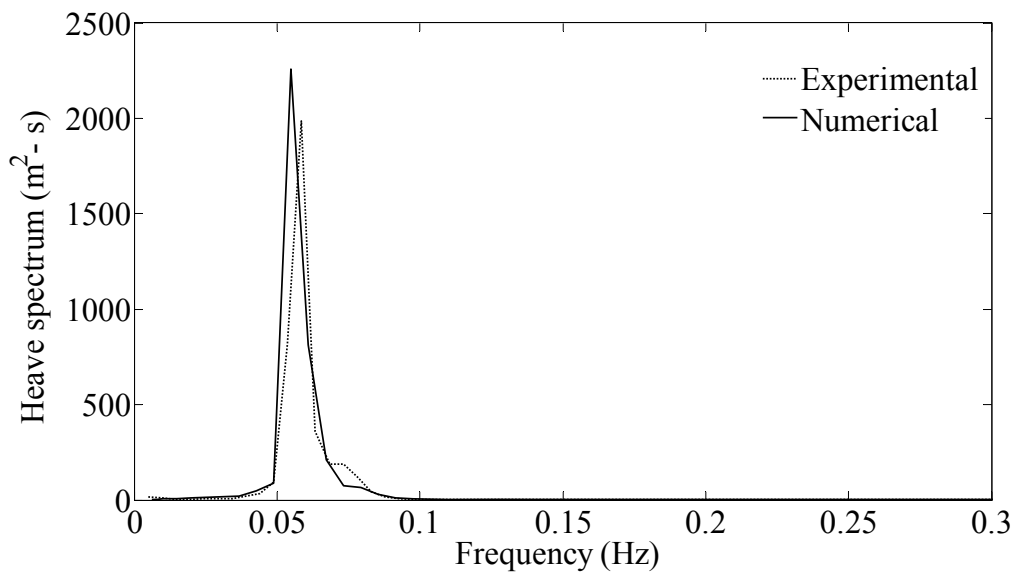


Figure 6.13: Heave spectra

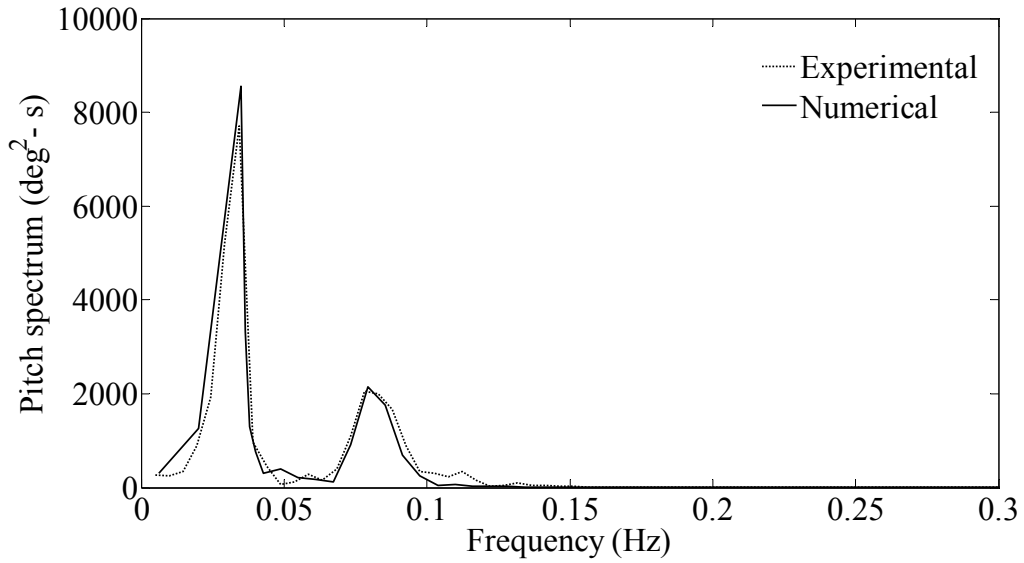


Figure 6.14: Pitch spectra

Table 6.4: RMSD for dynamic motions due to random waves

Dynamic motions	RMSD for LFR	RMSD for WFR
Surge	550.2	177.8
Heave	-	182.4
Pitch	499.6	109.9

6.3.2 Mooring lines damage condition

In the second phase of experimental tests, an attempt was made to investigate the effect of the mooring line failure phenomena on the motion characteristics of truss spar platform. This was made by relaxing the upper stream mooring lines and conducting the same sea keeping tests.

6.3.2.1 Static-offset test and free-decay results

The same procedure used earlier was adopted here to find the mooring line restoring forces. As could be seen from Figure 6.15, mooring line failure gave -35 KN (full scale) restoring force to the system at 0 m horizontal offset due to the unbalance between the resultant mooring line tensions at each sides. This restoring force caused the initial horizontal excursion for the structure. Also, it is expected to increase when more mooring lines are damaged. When comparing Figure 6.15 with Figure 6.5, another effect of mooring line failure on the mooring line restoring forces–horizontal excursion relationship can be observed. This is the substantial decrease in the magnitude of the restoring force of the system, which may cause increase in the structure dynamic responses.

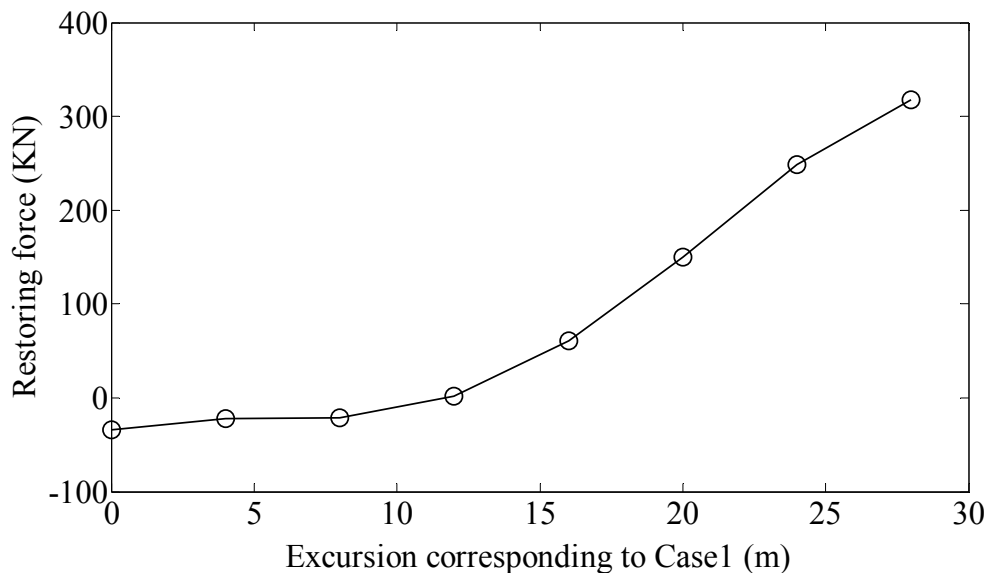


Figure 6.15: Static offset test results

Figure 6.16 - Figure 6.18 represent the comparison between the experimental measurements and the numerical predictions for surge, heave and pitch free decay respectively. In general, the numerical results agreed well with the experiments. Table 6.5 shows the natural periods and damping ratios of the prototype. The numerical predictions are close to the experimental results with differences of 5.06%, 9.4% and 24.3% for surge, heave and pitch natural periods respectively. From the comparisons

between Table 6.2 and Table 6.5, it can be observed that the failure of mooring line mostly affected the surge motion by increasing the corresponding natural period. This is because of decreasing mooring line stiffness, which is the only stiffness source of the system in the surge direction. Heave and pitch motions were affected by both mooring line and hydrostatic stiffnesses. However, the corresponding hydrostatic stiffness is large compared to the mooring line stiffness and therefore heave and pitch natural periods did not affect much by mooring line failure.

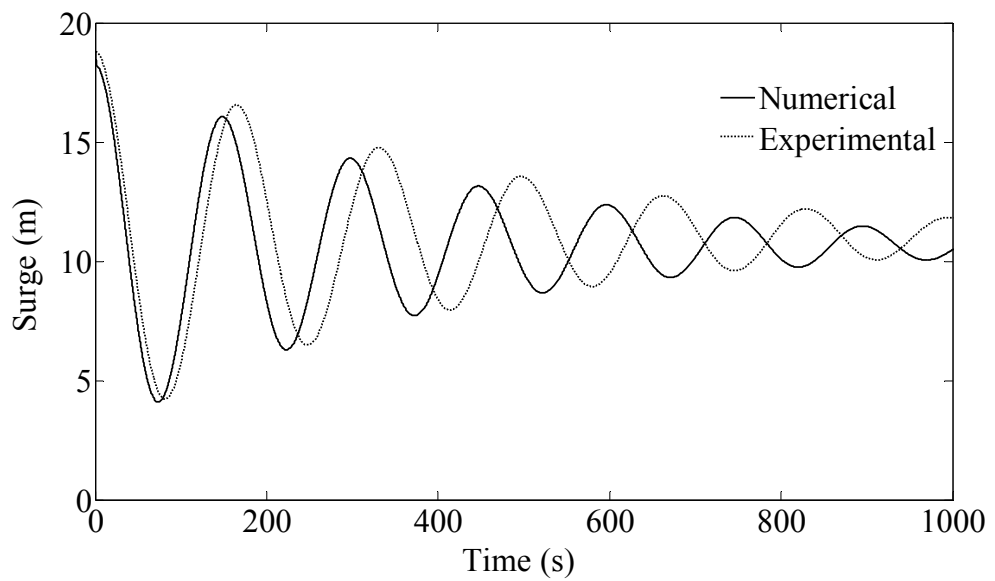


Figure 6.16: Surge free decay results

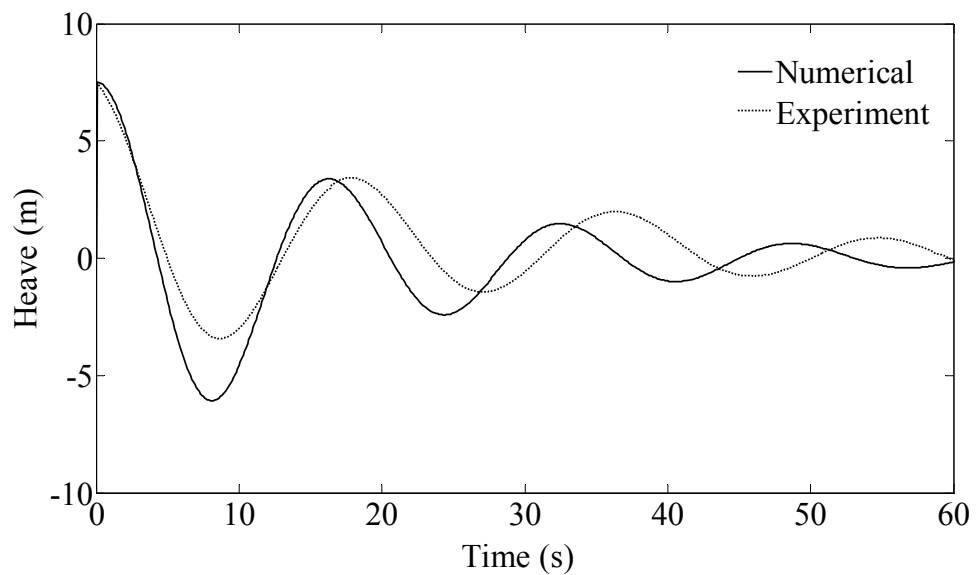


Figure 6.17: Heave free decay results

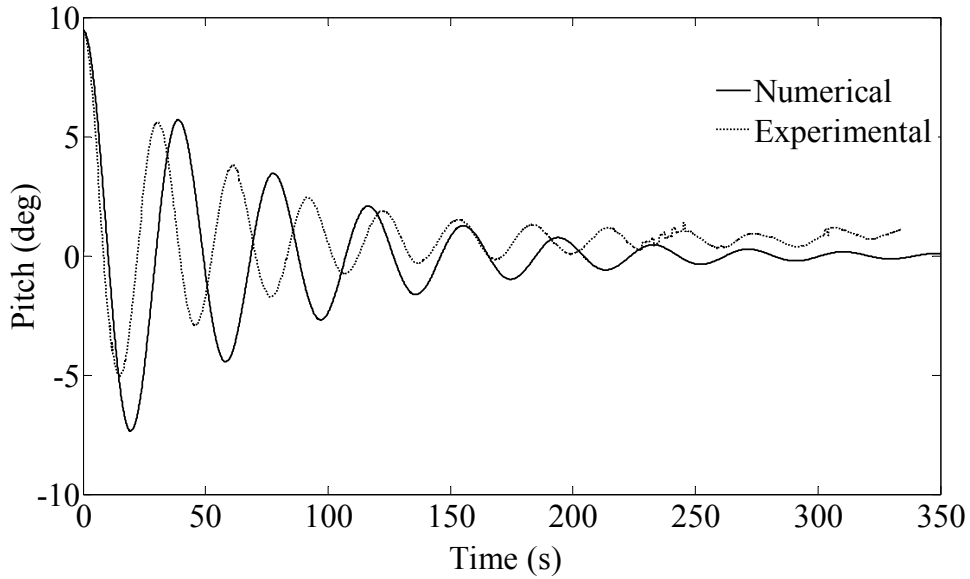


Figure 6.18: Pitch free decay results

Table 6.5: Comparison of natural periods and damping ratios

Motion type	Natural period (s)		Damping ratio (%)	
	Simulated	Measured	Simulated	Measured
Surge	150	158	1.3	1.41
Heave	16.3	18	12.9	8.6
Pitch	38.9	31.3	8	6.1

6.3.2.2 Wave frequency responses

Figure 6.19 - Figure 6.21 show the RAOs for surge, heave and pitch respectively for the structure under mooring line failure condition. For these three degrees of freedom, the numerical predictions agreed well with the experimental measurements. RMSD values in Table 6.6 support this observation as the numerical predictions were close to the measurements.

As the aim of this particular study is to examine the effect of the mooring line failure on the truss spar motion characteristics, the RAOs of the three degrees of

freedom in the two cases are compared. For surge motion (Figure 6.9 and Figure 6.19), the general performance of the prototype is almost same. However, for relatively low frequency regular waves, surge RAOs under mooring line failure is slightly lower than the normal case. This is because of the migration distance, which caused an increase in the mooring line stiffness of the structure in this case. For heave (Figure 6.10 and Figure 6.20) and pitch (Figure 6.11 and Figure 6.21) motions, the two cases are almost similar since the mooring line stiffness has insignificant effect on these motions.

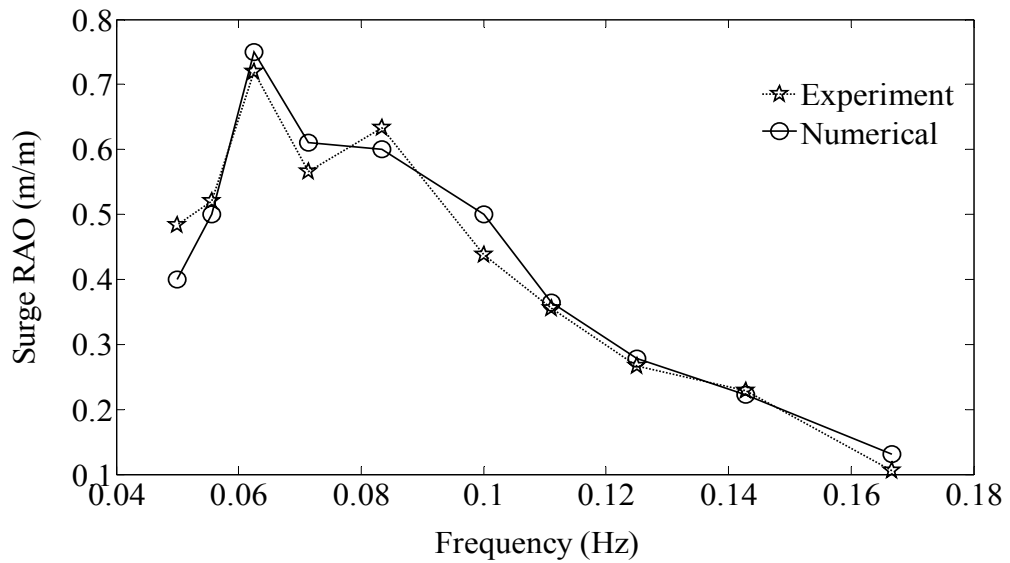


Figure 6.19: Surge RAOs

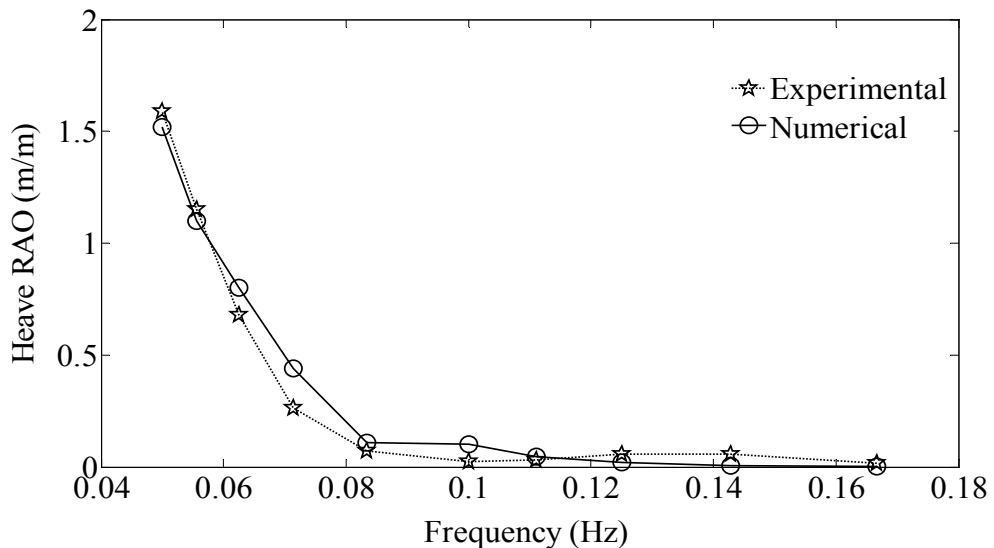


Figure 6.20: Heave RAOs

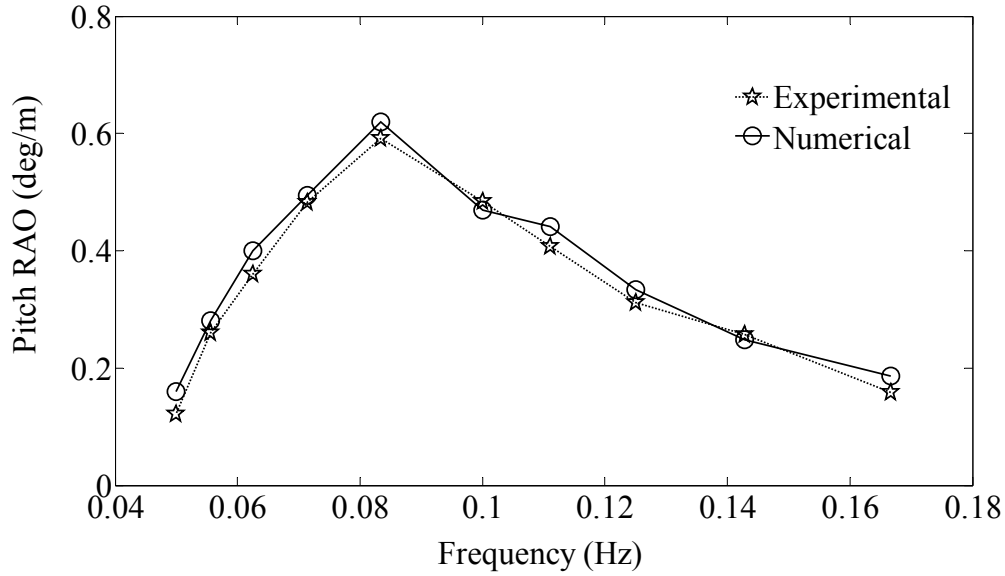


Figure 6.21: Pitch RAOs

Table 6.6: RMSD for dynamic motions due to regular waves

Dynamic motions	RMSD
Surge	0.04
Heave	0.08
Pitch	0.027

6.3.2.3 Low frequency responses

In this section, the effects of mooring line failure on the resonant responses for surge and pitch motions and the peak wave frequency response for heave motion are presented. As shown in Figure 6.22 - Figure 6.24, good agreement between the predictions and the measurements have been achieved in this particular condition. Table 6.7 shows the RMSD values for the numerical and experimental results for LFR as well as WFR. The same observation in the intact mooring line condition has been observed in this case where the predicted WFR trend is relatively agreed well with the measurements compared to the LFR. The developed numerical model estimated the

resonant and peak responses with a good accuracy. The differences were 15.1%, 11.4% and 17.3% for surge, heave and pitch respectively.

By conducting experimental comparisons between the two cases in surge (Figure 6.12 and Figure 6.22), heave (Figure 6.13 and Figure 6.23) and pitch (Figure 6.14 and Figure 6.24), it can be observed that a considerable increase in the surge resonant response ($6370 \text{ m}^2\cdot\text{s}$ to $8440 \text{ m}^2\cdot\text{s}$) and relatively insignificant increase in heave and pitch peaks responses ($1987 \text{ m}^2\cdot\text{s}$ to $2380 \text{ m}^2\cdot\text{s}$ for heave and $7715 \text{ deg}^2\cdot\text{s}$ to $8827 \text{ deg}^2\cdot\text{s}$ for pitch) have occurred due to mooring line failure. These observations confirm that the mooring line failure affect surge motion more than heave and pitch motions. This is because the main effect of mooring line failure is reducing the mooring line stiffness of the structure, which is the only source of stiffness in the surge direction as indicated in Eq. (4.8).

Another important effect of mooring line failure is reducing the mooring line damping, which has an important impact on the second order difference frequency responses as mentioned in the literature. However, this effect is not considered in this study by assuming truncated mooring lines in the model tests.

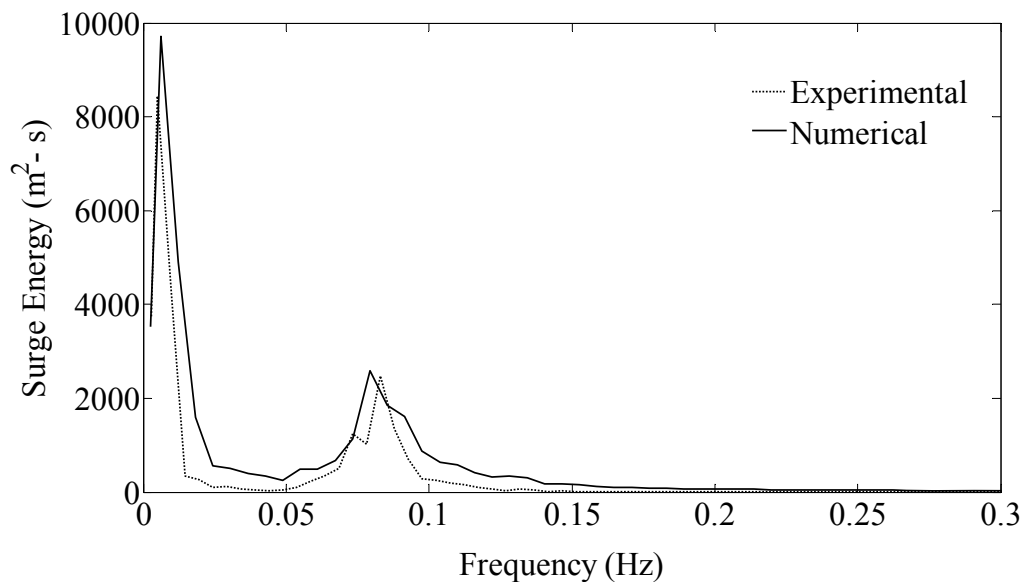


Figure 6.22: Surge spectra

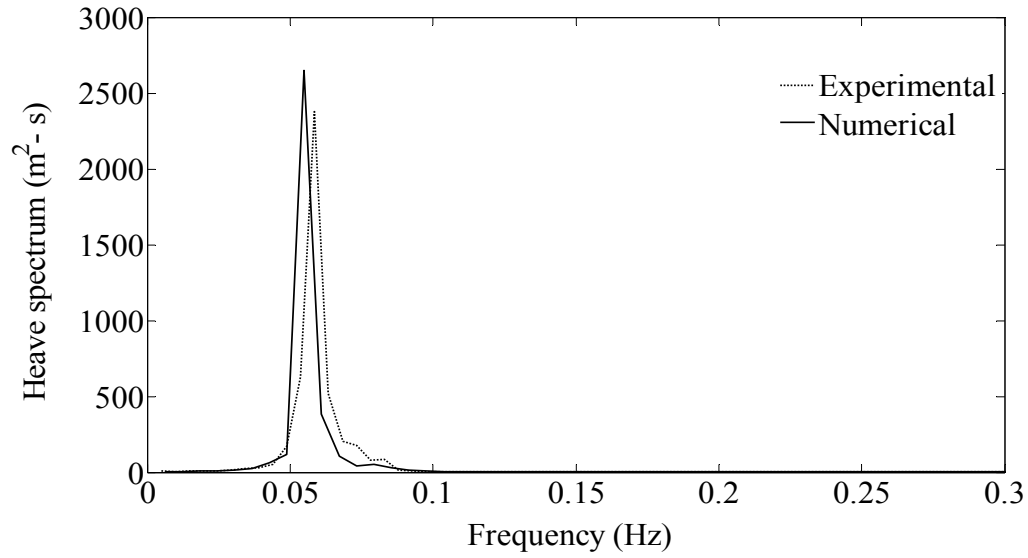


Figure 6.23: Heave spectra

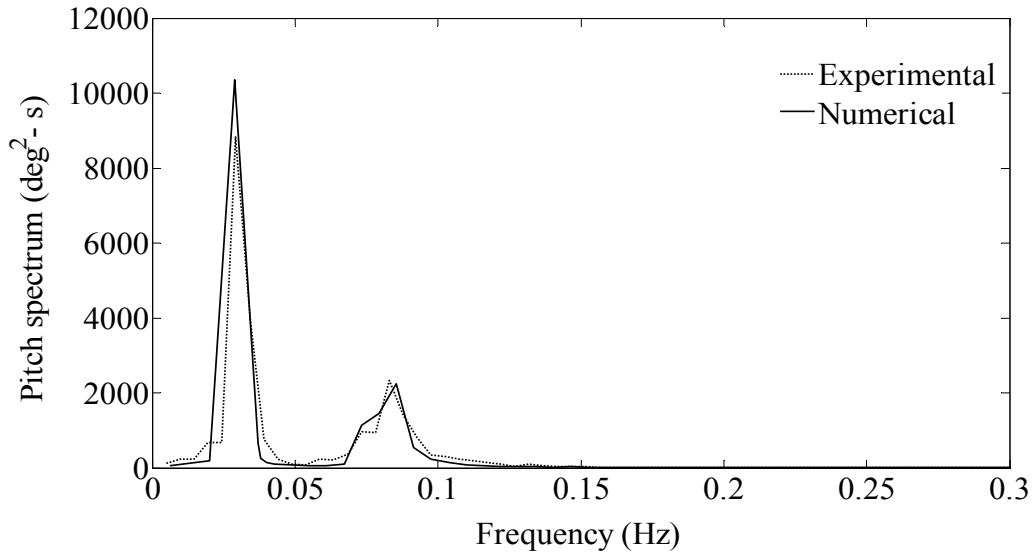


Figure 6.24: Pitch spectra\

Table 6.7: RMSD for dynamic motions due to regular waves

Dynamic motions	RMSD for LFR	RMSD for WFR
Surge	1074	323.6
Heave	-	239.2
Pitch	209.1	107.4

6.3.2.4 Mooring line failure mechanism for regular wave

As shown in the previous section, surge motion is most affected by the mooring line failure. In addition, regular wave response, with its sinusoidal trend, makes this study clearly than random wave response. Therefore, surge responses due to RG4 were selected to present the transition process from intact to mooring line failure condition.

The experimental surge measurements in the two conditions are shown in Figure 6.25 and Figure 6.26 while the whole process, which simulated the conversion from the intact mooring condition to the failure condition, is shown in Figure 6.27. In the simulation, the normal condition was considered up to 1000 s and then the mooring line failure was assumed. As could be seen, the effect of mooring line failure on surge motion was well predicted by the numerical model with small differences in the mean position of the structure in the two conditions. In the intact mooring condition, the numerical code gave 0.93 m mean position while the measurements showed 1.6 m. In the failure case, the mean position was 15.3 m and 16.4 m for the predictions and measurements respectively. These differences in the mean position are due to using Eqs. (3.33 – 3.36), which obtained from second order diffraction theory [11], to calculate the mean drift forces in the simulation rather than measuring these forces in the experiments.

At this point, it is interesting to recall Figure 6.15, which shows -35 KN mooring line restoring force at 0 m offset. This force affected the migration distance shown in Figure 6.27. In addition to the migration distance effect, Figure 6.27 shows transient surge response occurring immediately after failure. This transient response is very important in the analysis and design of mooring lines and risers.

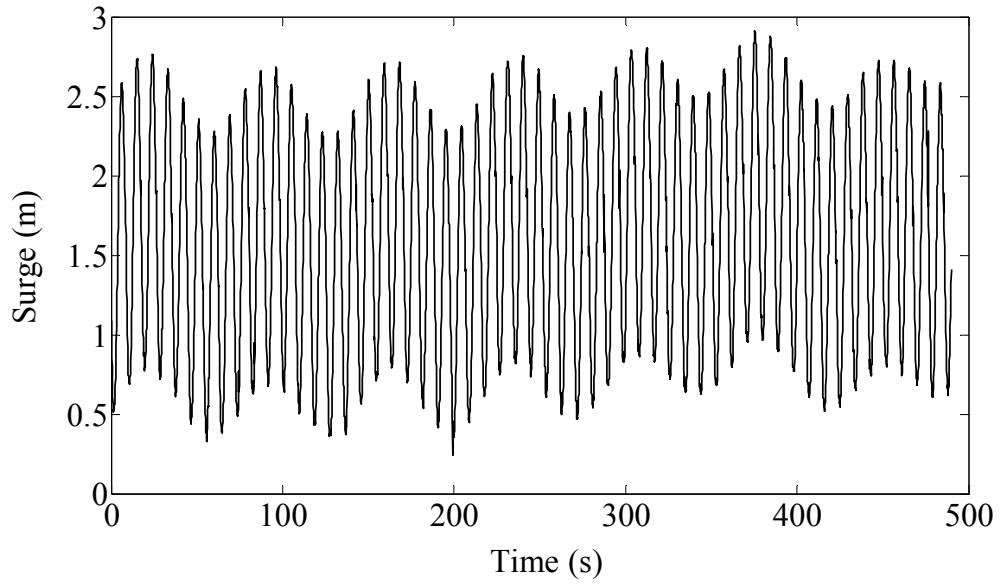


Figure 6.25: Surge time series for Case1 (experiment measurements)

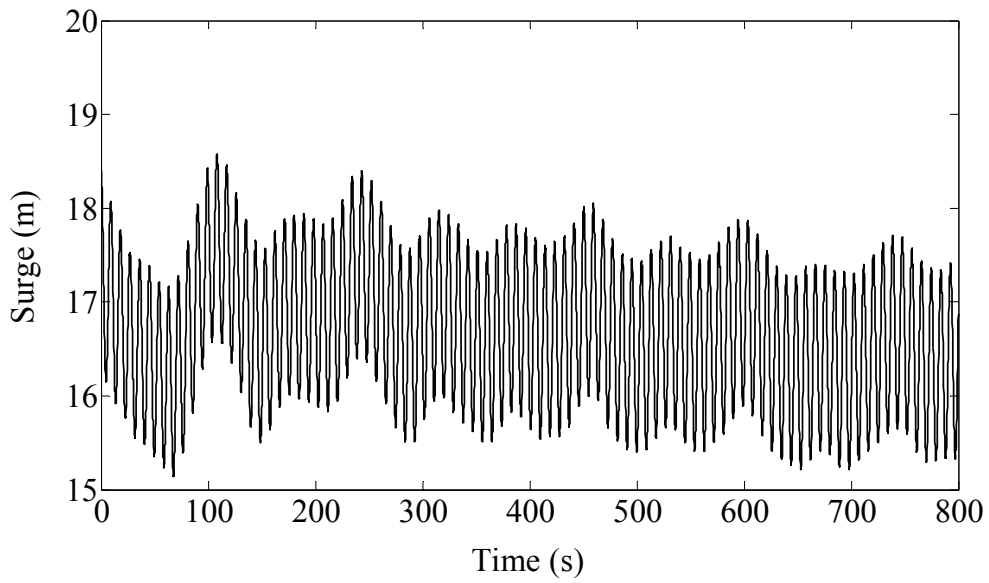


Figure 6.26: Surge time series for Case 2 (experiment measurements)

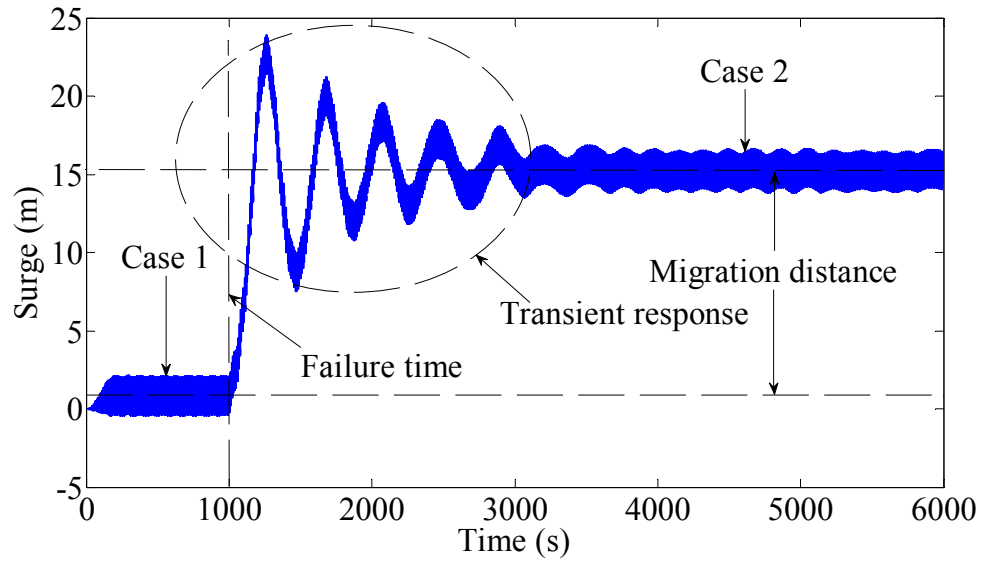


Figure 6.27: Surge time series for failure condition (numerical predictions)

6.4 Numerical and experimental studies on Marlin truss spar platform

In this section, numerical and experimental studies on a typical truss spar platform named Marlin truss spar are presented. The structure was positioned by nine taut mooring lines in 988 m water depth. As shown in Figure 6.28, the truss spar is composed of a large volume hard tank in the upper part and slender truss members in the lower section supported by heave plates. In addition, there is a soft tank in the lower part of the structure. The main particulars of the spar are summarized in Table 6.8. Mooring line arrangements and characteristics are shown in Figure 6.29 and Table 6.9 respectively.

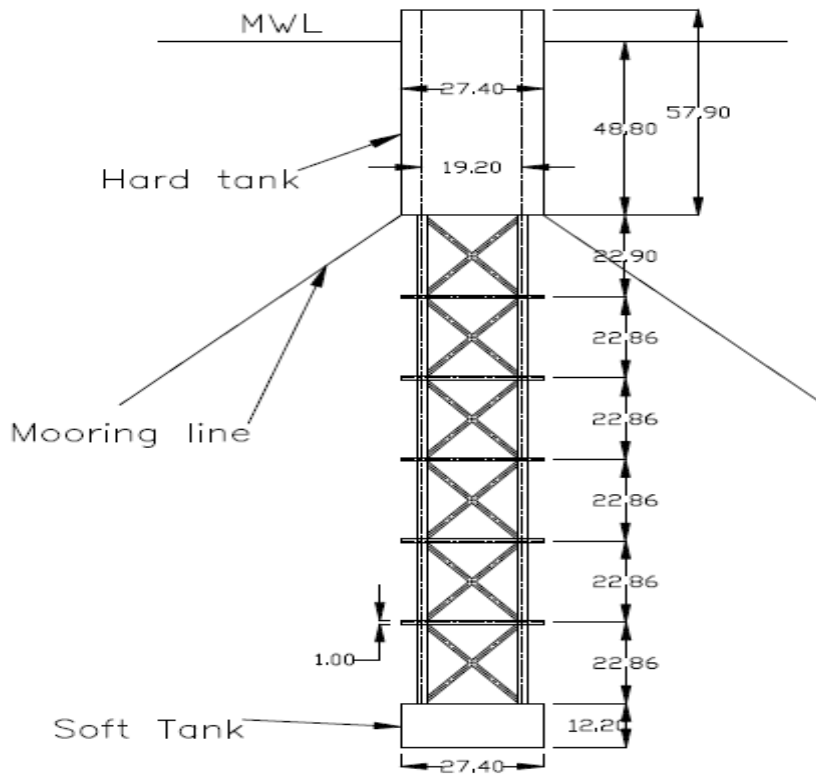


Figure 6.28: Overall configuration

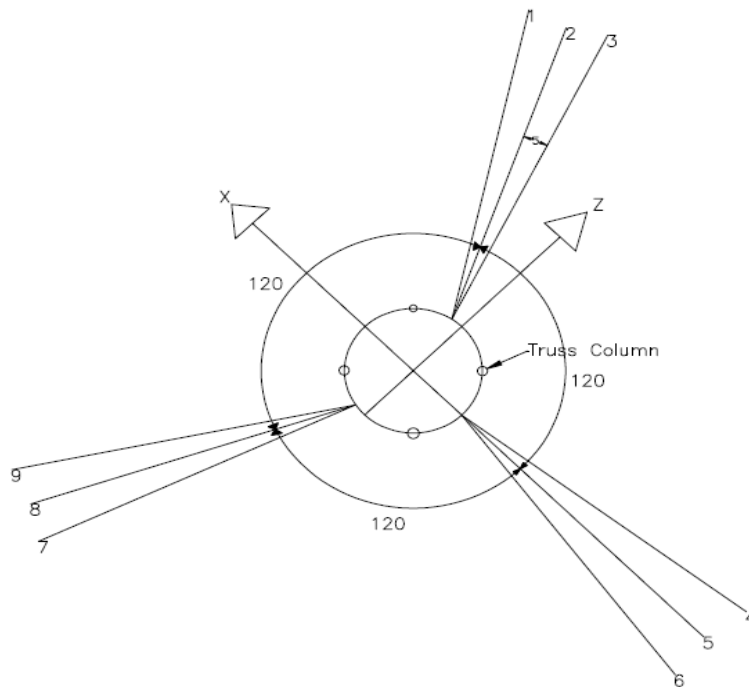


Figure 6.29: Truss spar mooring arrangement

Table 6.8: Physical characteristics of the truss spar

Hull diameter	27.4 m
Total draft	198.1 m
Draft of hard tank	48.8 m
Water depth	988 m
Fairlead depth	45.7 m
Weight	38980 ton
Vertical center of gravity from hard tank bottom	23 m
Vertical center of buoyancy from hard tank bottom	3 m
Pitch radius of gyration	86.2 m

Table 6.9: Characteristics of truss spar mooring lines

	Upper section	Middle section	Lower section
Type	Chain	Spiral strand	Chain
Size (cm)	12.4	12.4	12.4
Length (m)	76.2	1828.7	45.7
Wet weight (kn/m)	2.73	0.636	2.73
Eff. Modulus EA (kn)	665852	1338848	858882
Breaking strength (kn)	13188	12454	13188

6.4.1 Static offset test

To carry out the quasi-static simulation for mooring line system, a separate MATLAB code has been developed based on the method described in Section 4.3. As a result, mooring stiffness curve was obtained as shown in Figure 6.30. The calculated mooring stiffness shows a typical nonlinear hardening behavior and agrees well with the measured stiffness. For relatively large offset ($> 35\text{m}$), the numerical simulation gave higher results than the experiment. This is because of the different mooring line set-up between the prototype and the model test. For the prototype, there are nine mooring lines connected the structure with the seabed as shown in Figure 6.29 while five mooring lines, representing the prototype mooring, (2, 4, 5, 6 and 8) were used in the experiments.

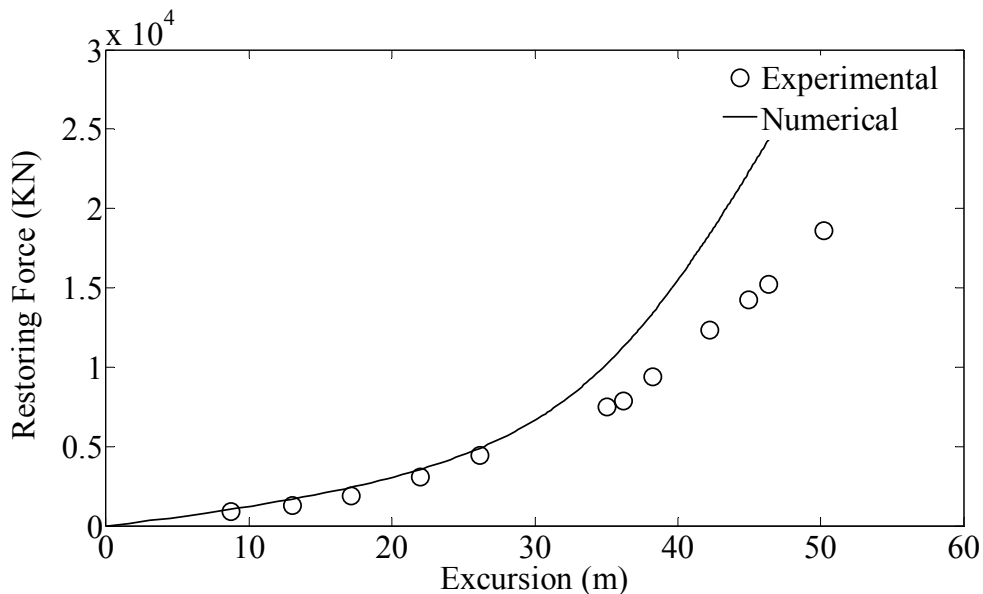


Figure 6.30: Static offset results comparisons (experiment vs. numerical)

6.4.2 Slow varying drift forces

In this section, the individual effects of the second order difference frequency forces, which were presented in Section 3.5, were studied numerically. Irregular wave was used for this purpose. The wave spectrum model considered here was the 100-year JONSWAP spectrum with a significant wave height of 12.7 m and a peak wave period of 13.9 s. The wave amplitudes were calculated directly from the spectrum,

while the initial phases were generated randomly. The frequency range, which was divided into 52 segments of regular spacing, was between 0.025 Hz and 0.19 Hz. This range covered the dominant range of ocean waves and it has no wave components near the natural frequency of the structure.

The surge response results of nine stages corresponding to the addition of the individual linear and nonlinear effects are shown in Figure 6.31 - Figure 6.39. These figures confirmed that there are no significant effects on the first order responses due to the second order nonlinear forces.

To start with, only the first order inertia and drag forces were considered as shown in Figure 6.31. These forces were calculated at the original position of the structure, and integrated only up to the MWL. In this case, no second order surge response was recognized.

Figure 6.32 represents the next step, which was the effect of calculation of the inertia forces at the displaced position of the structure, particularly in the surge direction. The second order surge response was dominant ($11.61 \times 10^4 \text{ m}^2.\text{s}$), which implied that the effect of inertia force calculation in the surge displaced geometry has a great effect on the second order surge response.

As shown in Figure 6.33, the calculation of the inertia force in the displaced position with respect to pitch boosted the second order surge response to ($17.1 \times 10^4 \text{ m}^2.\text{s}$). However, this effect was less than the previous one because the pitch angle was small compared to the surge magnitude. Figure 6.34 confirms that the truss spar platform is an inertia dominated structure since the increase in the second order surge due to addition of the difference frequency drag forces was insignificant compared to the other effects.

Figure 6.35 shows a significant reduction in the second order surge due to the addition of the Morison equation drag force damping. The second ordered surge decreased from $17.5 \times 10^4 \text{ m}^2.\text{s}$ to $2.6 \times 10^4 \text{ m}^2.\text{s}$. This is consistent with the findings in the literature, which consider the viscous damping as one of the major damping sources of the floating structures.

As shown in Figure 6.36, the addition of axial divergence caused an increase in the results. The second order surge spectrum increased to $5.7 \times 10^4 \text{ m}^2\cdot\text{s}$. In Figure 6.37, the free surface fluctuation (i.e., integration of the forces up to the free surface instead of MWL) magnified the second order surge spectrum to reach $17.3 \times 10^4 \text{ m}^2\cdot\text{s}$.

The convective acceleration in Figure 6.38 recovered the huge increase in the response due to the free surface fluctuation. The second order difference frequency surge became $6.14 \times 10^4 \text{ m}^2\cdot\text{s}$. The total response became slightly more than that before free surface fluctuation and convective acceleration was considered. This further verified and consistent with the observation of Section 3.5.1.4 where it was shown that the forces due to convective acceleration are slightly less than that due to free surface fluctuation and they are working opposite to each other.

Finally, the second order temporal acceleration was added in Figure 6.39. As the second order surge reach $8.31 \times 10^4 \text{ m}^2\cdot\text{s}$, the nonlinear temporal acceleration is considered as one of the important slowly varying drift forces.

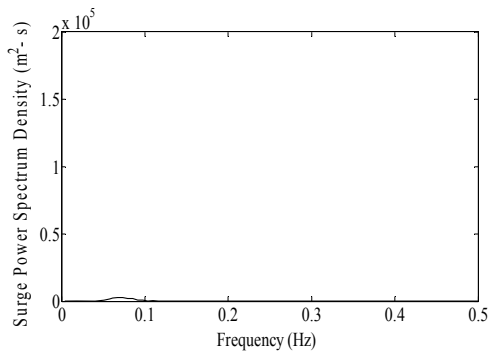


Figure 6.31: Surge: linear solution (LS)

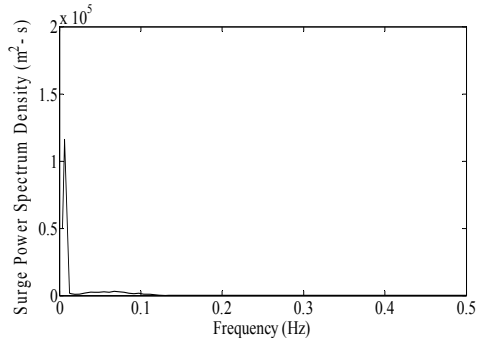


Figure 6.32: Surge: LS+ surge effect (SD1)

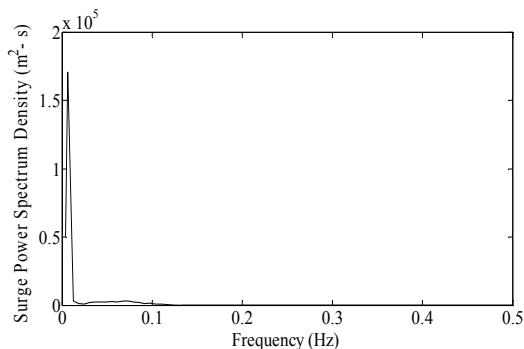


Figure 6.33: Surge: LS + SD1 + pitch effect (SD2)

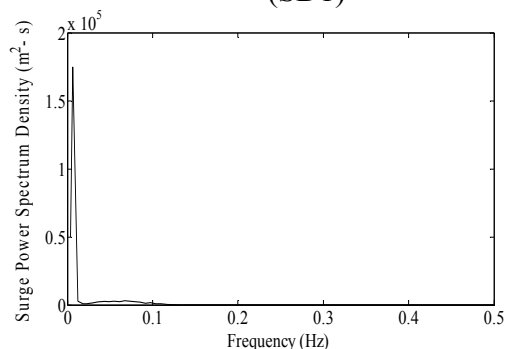


Figure 6.34: Surge: LS + SD1 + SD2 + Drag force without damping (DF1)

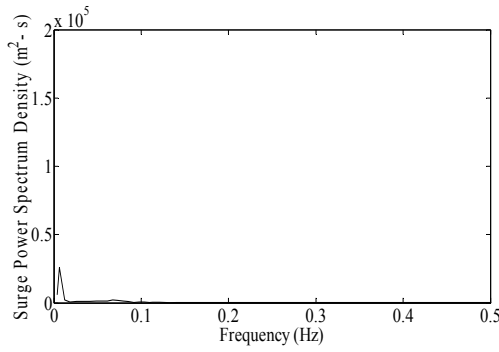


Figure 6.35: Surge: LS + SD1 + SD2 + DF1 + Drag damping effect (DF2)

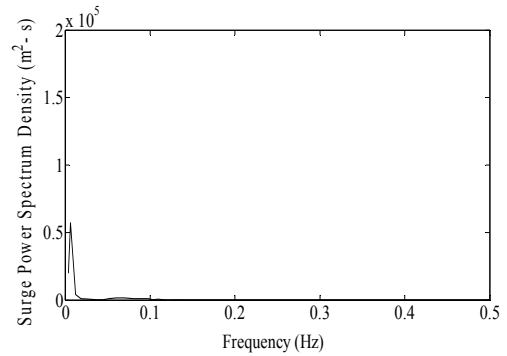


Figure 6.36: Surge: LS + SD1 + SD2 + DF1 + DF2 + Axial divergence (AD)

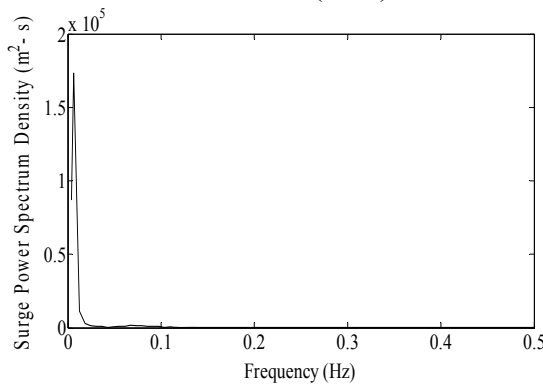


Figure 6.37: Surge: LS + SD1 + SD2 + DF1 + DF2 + AD+ Free surface (FS)

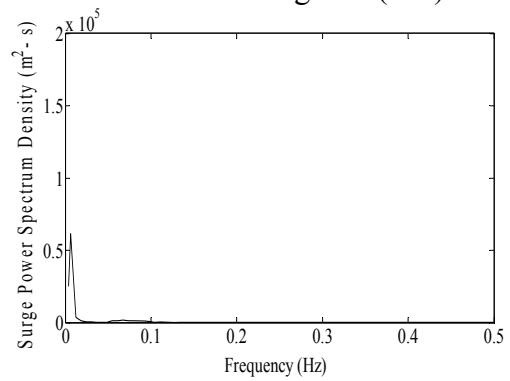


Figure 6.38: Surge: LS + SD1 + SD2 + DF1 + DF2 + AD+FS+ Convective acceleration (CA)

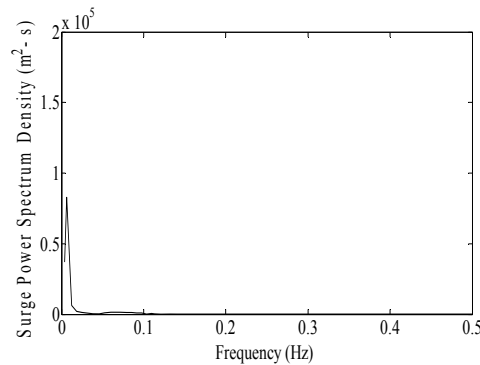


Figure 6.39: Surge: LS + SD1 + SD2 + DF1 + DF2 + AD+FS+ CA + Temporal acceleration (TA)

The same process of studying the second order effects on surge response was followed to study these effects on pitch response, as shown in Figure 6.40 - Figure 6.48. Most of the observations noticed for surge results were observed in pitch results also.

The first model for pitch response account for inertia and drag forces and both are calculated at the mean position of the structure. There are no second order forces in the wave frequency range and thus all the responses here are linear.

Consistent with the surge results, the calculation of the inertia forces at the displaced surge position of the structure in Figure 6.41 had significant effect on the second order pitch response, which reached 1134 deg².s, and its effects were slightly more than the pitch effect in Figure 6.42 where the second order pitch response became 2186 deg².s.

Figure 6.43 show the insignificant effect of the second order drag forces on the pitch response. However, including the drag damping caused significant reduction in the resonant pitch (811.5 deg².s) as shown in Figure 6.44.

Axial divergence contributed to the second order pitch motion as shown in Figure 6.45. The resonant pitch reached 1784.7 deg².s. The relation between the free surface effect (8976.3 deg².s) and the convective acceleration (4379.2 deg².s) is shown in Figure 6.46 and Figure 6.47 respectively. These results confirmed that, the convective acceleration is in opposite direction to the free surface fluctuation as indicated in 3.5.1.4 where the comparisons have been made between Eqs. 3.67 to 3.72. However, the contribution of the free surface to pitch response is larger than the reduction caused by the convective acceleration. This is because the moments' lever arm of the free surface force is greater than in convective acceleration force case. Finally, the second order temporal acceleration is added as shown in Figure 6.48. The addition to the previous step increases the second order pitch motions to 6319.6 deg².s.

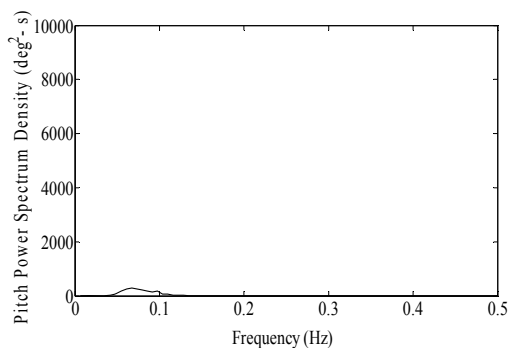


Figure 6.40: Pitch: LS

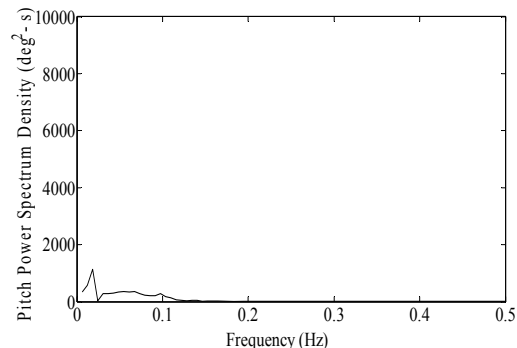


Figure 6.41: Pitch: LS+ SD1

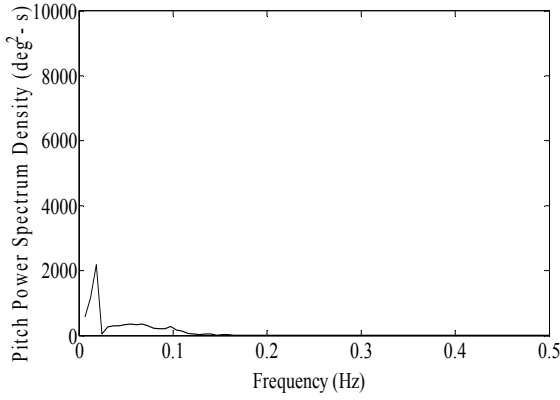


Figure 6.42: Pitch: LS + SD1 + SD2

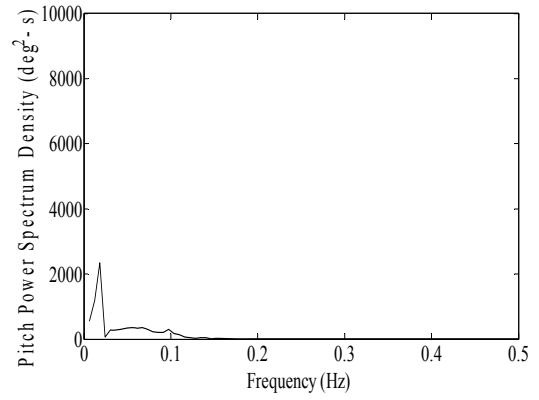


Figure 6.43: Pitch: LS + SD1 + SD2 + DF1

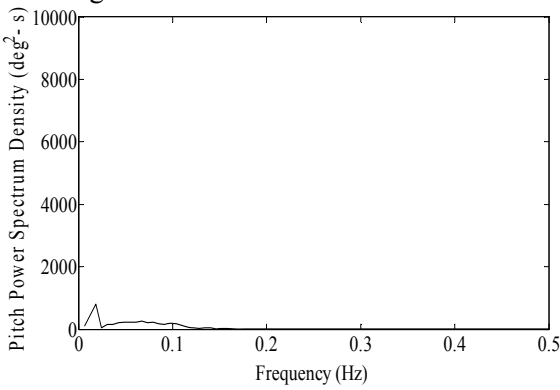


Figure 6.44: Pitch: LS + SD1 + SD2 + DF1 + DF2

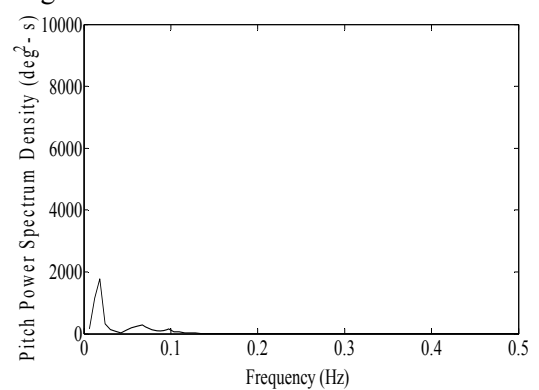


Figure 6.45: Pitch: LS + SD1 + SD2 + DF1 + DF2 + AD

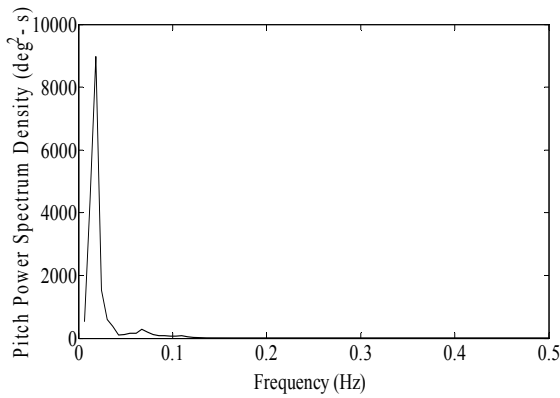


Figure 6.46: Pitch: LS + SD1 + SD2 + DF1 + DF2 + AD+ FS

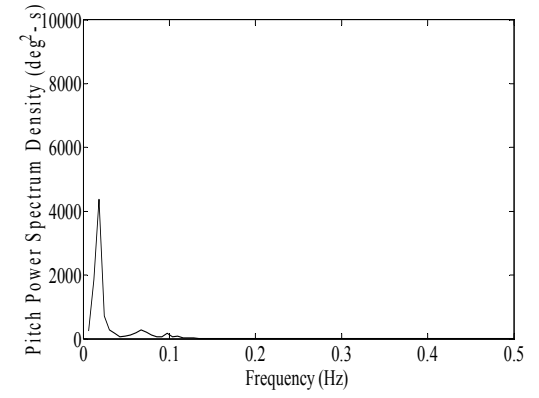


Figure 6.47: Pitch: LS + SD1 + SD2 + DF1 + DF2 + AD+FS+ CA

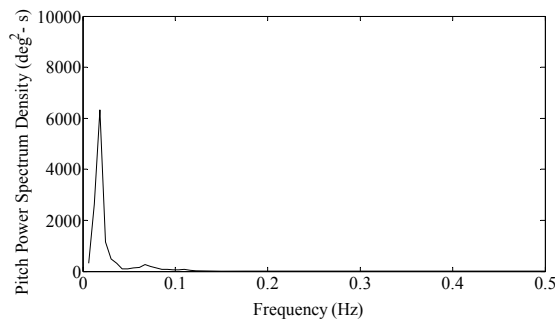


Figure 6.48: Pitch: LS + SD1 + SD2 + DF1 + DF2 + AD+FS+ CA + TA

6.4.3 Effect of current and wind

In this section, the responses of the Marlin truss spar in random waves, current and wind were simulated and compared with literature data. First, the responses due to the same random waves used in the previous section combined with collinear steady current are presented. This current was simulated by constant external string force of 1632 KN acting at 27.4 m below MWL. This force is equivalent to the static force in Eq. (4.33). Since the spar is inertia dominated structure, the first and second order dynamic drag forces, which were presented in Eq. (4.34), are not considered due to its insignificant effects.

The surge and pitch responses spectra due to combined random waves and current are shown in Figure 6.49 and Figure 6.50 respectively. It was noticed that the presence of current substantially decreased the surge and pitch resonant responses. The surge response decreased from $8.31 \times 10^4 \text{ m}^2 \cdot \text{s}$ (Figure 6.39) to $8684 \text{ m}^2 \cdot \text{s}$ (Figure 6.49) while the pitch response decreased from $6320 \text{ deg}^2 \cdot \text{s}$ (Figure 6.48) to $3300 \text{ deg}^2 \cdot \text{s}$ (Figure 6.50) when current was added. This is because adding current to the wave results in additional damping as illustrated in Eq. (4.35). In addition to increasing the structure viscous damping, current significantly increase the surge mean offset as compared between Figure 6.51 and Figure 6.52. Due to current, the mean surge offset increased from 3.7 m to 18 m because of the substantial current static force (Eq. (4.33)).

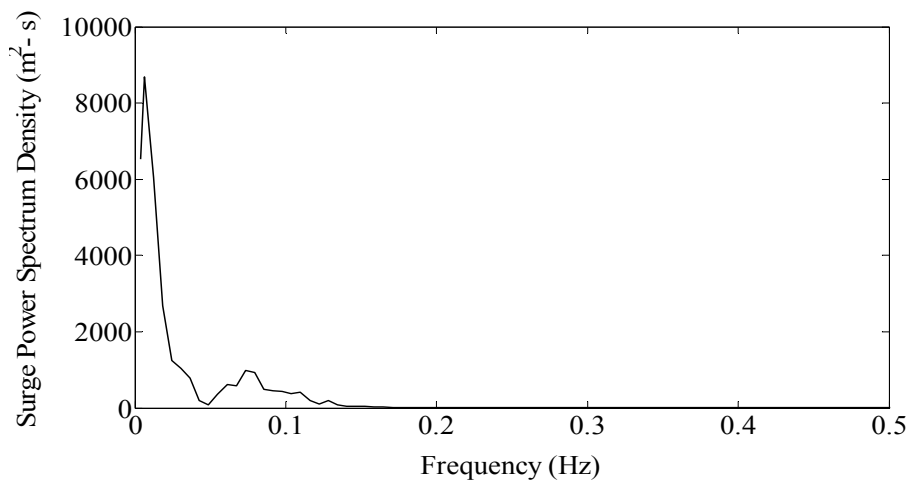


Figure 6.49: Surge spectrum due to combined random waves and current

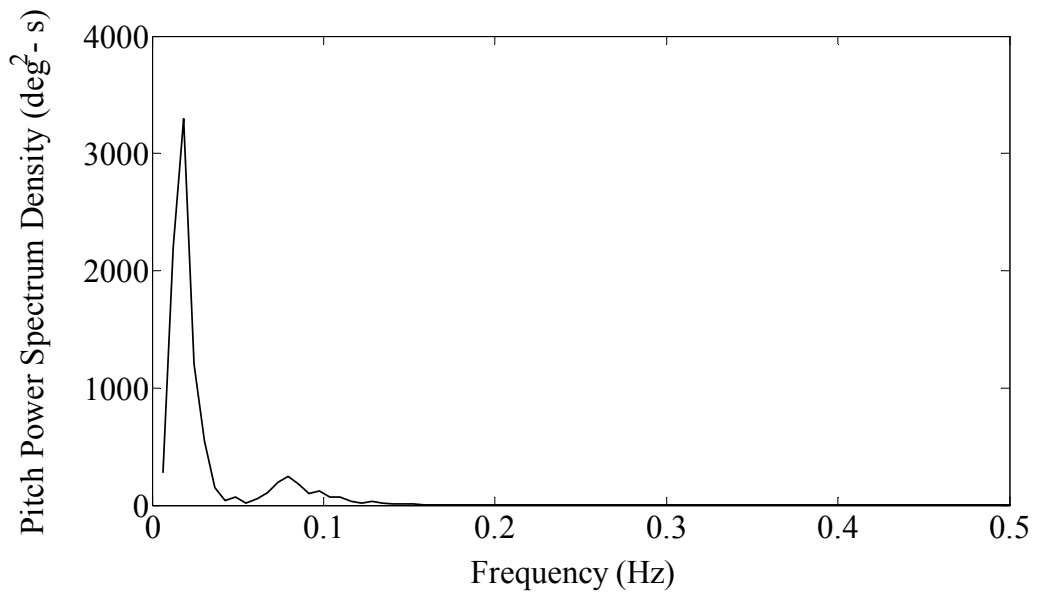


Figure 6.50: Pitch spectrum due to combined random waves and current

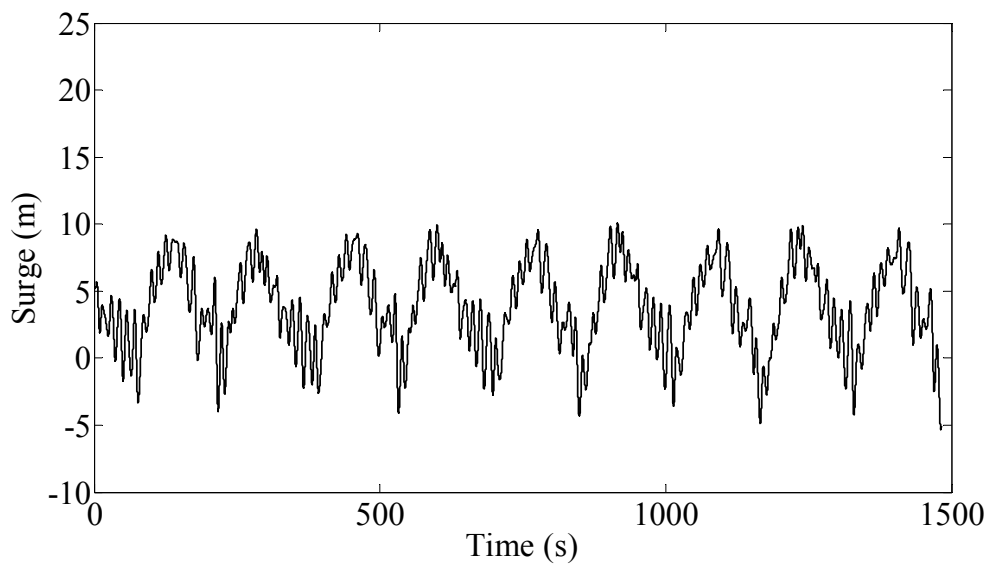


Figure 6.51: Surge time series due to random waves

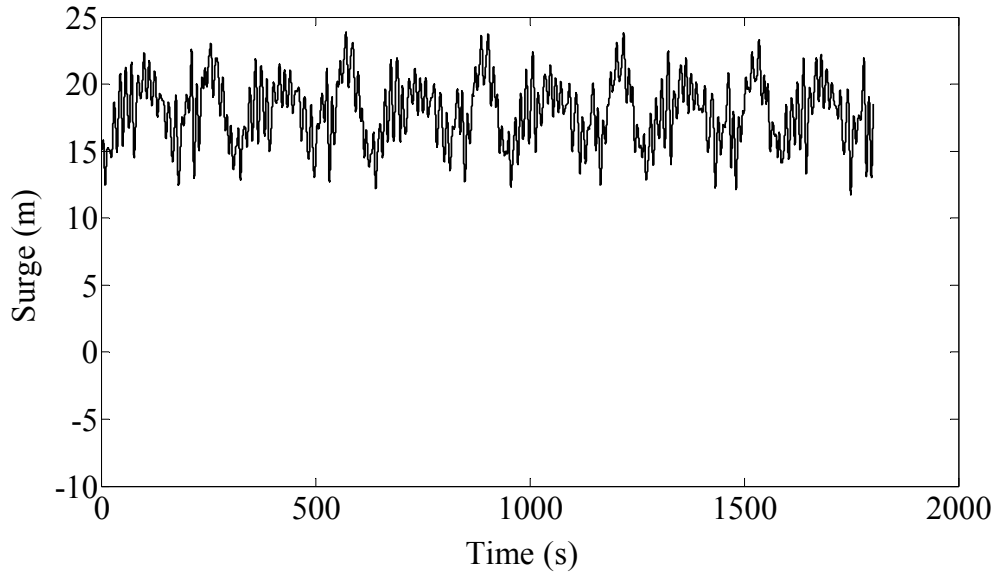


Figure 6.52: Surge time series due to random waves and current

The responses due to random waves combined with current and wind are presented and compared with the fully coupled dynamic analysis results [127] as shown in Figure 6.53 - Figure 6.54. Steady wind was taken for the analysis. It was simulated by constant force of 2251 KN acting at 27.5 m above MWL.

As compared between Figure 6.52 and Figure 6.55, wind static force resulted in an increased in surge mean offset. The mean offset is increased from 18 m in Figure 6.52 to 26 m in Figure 6.55. This increase in the surge mean offset increased the surge stiffness, which is obtained from the mooring line only, more than the pitch stiffness, which is obtained from both mooring line and hydrostatic stiffness. Therefore, resonant surge response is decreased significantly compare to pitch response. The surge response decreased from 8684 $\text{m}^2.\text{s}$ in Figure 6.49 to 4716 $\text{m}^2.\text{s}$ in Figure 6.53 while the pitch response decreased from 3300 $\text{deg}^2.\text{s}$ in Figure 6.50 to 3166 $\text{deg}^2.\text{s}$ in Figure 6.54.

To validate current and wind simulation results, a comparison has been made with fully coupled dynamic analysis results obtained by a numerical code named WINPOST. As could be seen from Figure 6.53 and Figure 6.54, TRSPAR results follow the same trend of WINPOST. However, TRSPAR resonant responses are higher compare to WINPOST. This is because of mooring line damping which is

considered in WINPOST and ignored in TRSPAR. Moreover, risers were modeled in WINPOST and not considered in TRSPAR.

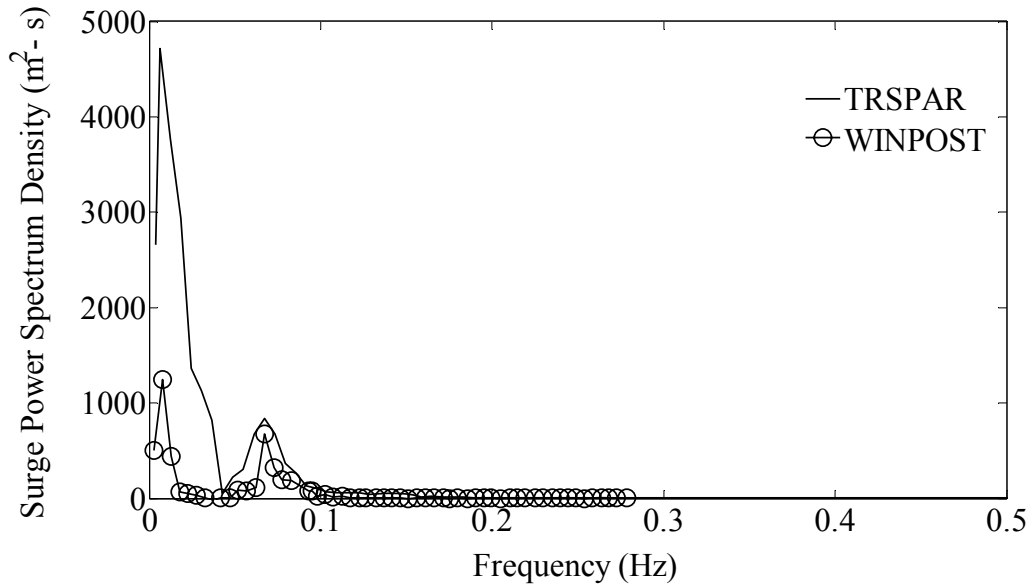


Figure 6.53: Surge spectra comparisons
(Source of numerical data: *International Journal of Offshore and Polar Engineering*; M. H. Kim, 2001)

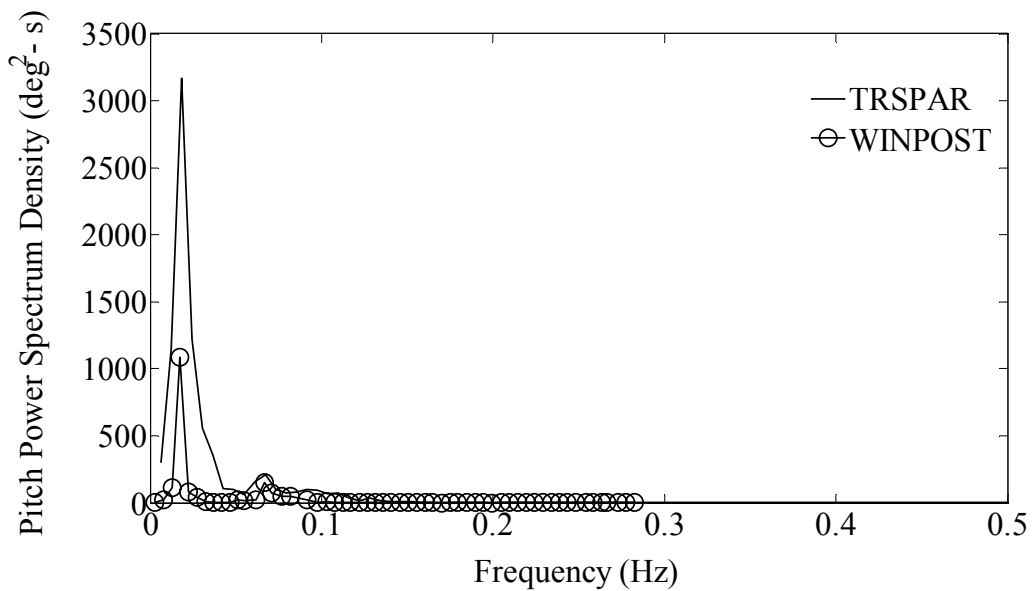


Figure 6.54: Pitch spectra comparisons
(Source of numerical data: *International Journal of Offshore and Polar Engineering*; M. H. Kim, 2001)

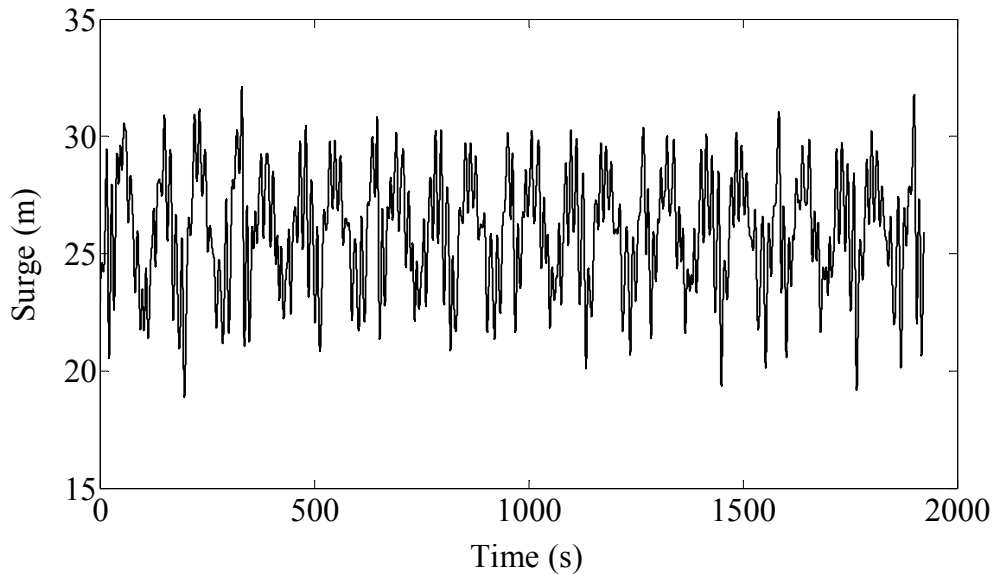


Figure 6.55: Surge time series due to random waves, current and wind

6.4.4 Numerical studies on strengthening of the station keeping systems

In this section, the simulation of Marlin truss spar was conducted assuming six additional mooring lines attached to the structure's keel as shown in Figure 6.56 - Figure 6.57. Mooring lines No. 1', 3', 4', 6', 7' and 9' were attached to the keel in the same orientation of lines No. 1, 3, 4, 6, 7 and 9 respectively. The effects of adding these mooring lines on the dynamic responses of the spar were studied numerically.

Quasi-static analysis was performed for the extra mooring lines. As a result, horizontal excursion vs. mooring lines restoring force relationship was obtained as shown in Figure 6.58. In the analysis, these restoring forces were added to the original mooring line restoring forces presented in Figure 6.30.

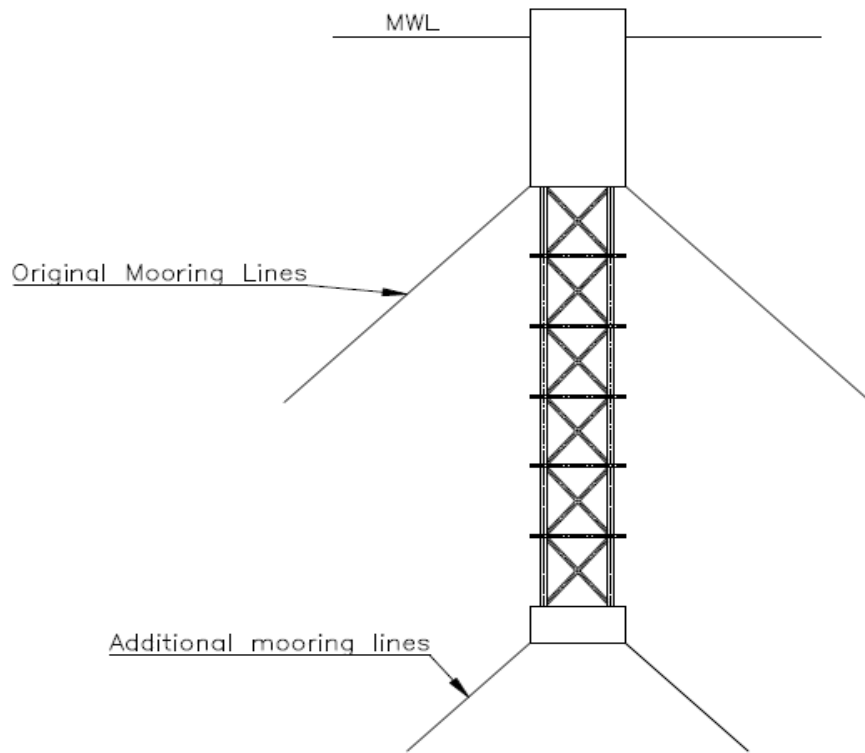


Figure 6.56: Marlin truss spar side view with additional mooring lines

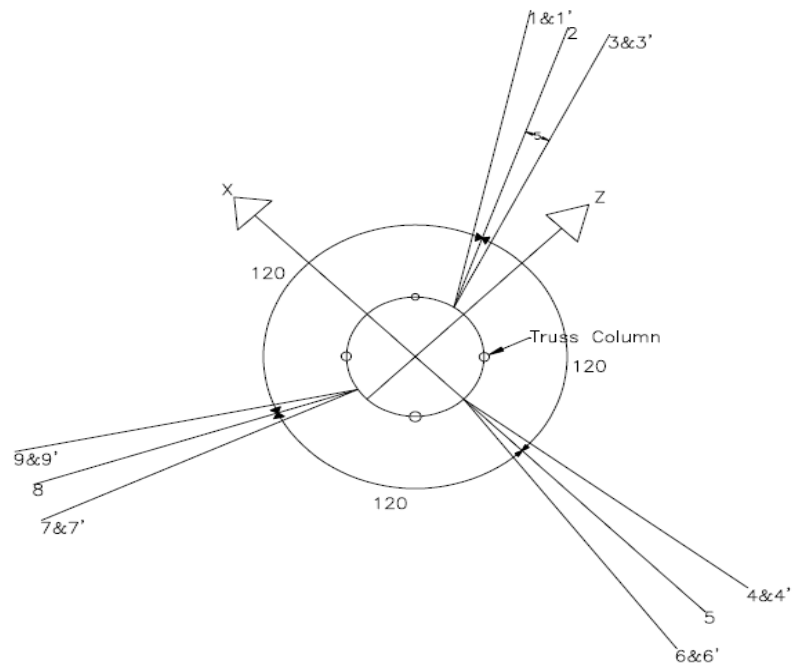


Figure 6.57: Marlin truss spar top view with additional mooring lines

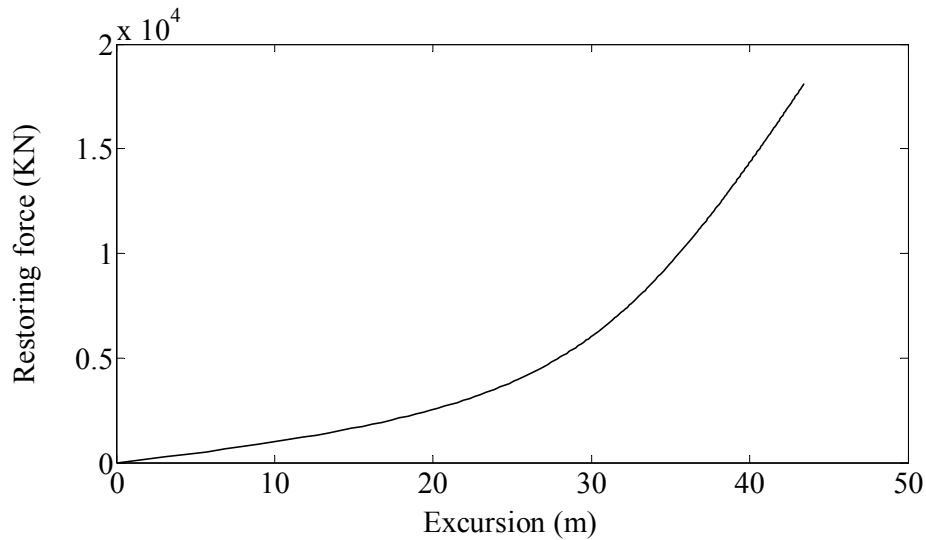


Figure 6.58: Additional mooring lines restoring force vs. horizontal excursion

As this study focuses on the nonlinear slow drift responses, only surge and pitch results are presented. For the purpose of comparisons, the same random wave used in the previous sections was adopted in this section. As shown in Figure 6.59 - Figure 6.60 and by comparing with Figure 6.39 and Figure 6.48, strengthening of the station keeping system by adding mooring lines affect surge response more than the pitch response. This is because the additional mooring lines increase the surge stiffness more than pitch stiffness. The surge resonant response decreased from $8.31 \times 10^4 \text{ m}^2 \cdot \text{s}$ (Figure 6.39) to $3.71 \times 10^4 \text{ m}^2 \cdot \text{s}$ (Figure 6.59) while the pitch response decreased from $6320 \text{ deg}^2 \cdot \text{s}$ (Figure 6.48) to $5654 \text{ deg}^2 \cdot \text{s}$ (Figure 6.60).

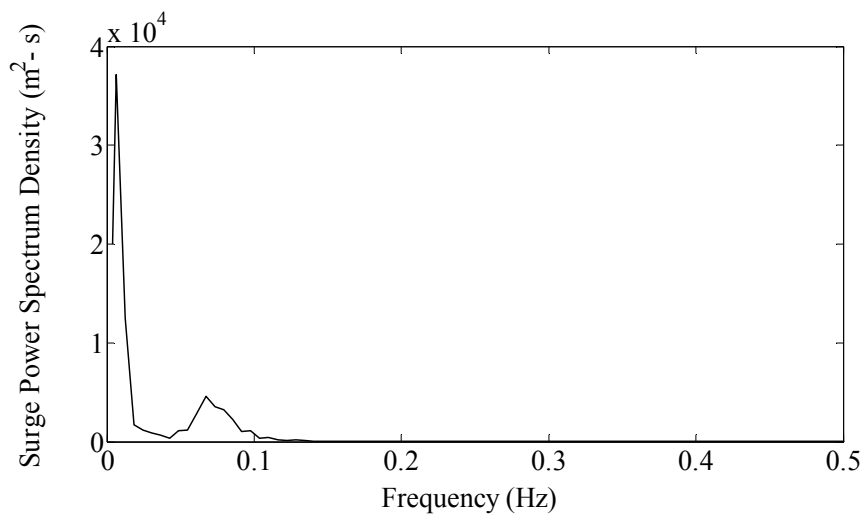


Figure 6.59: Surge spectrum

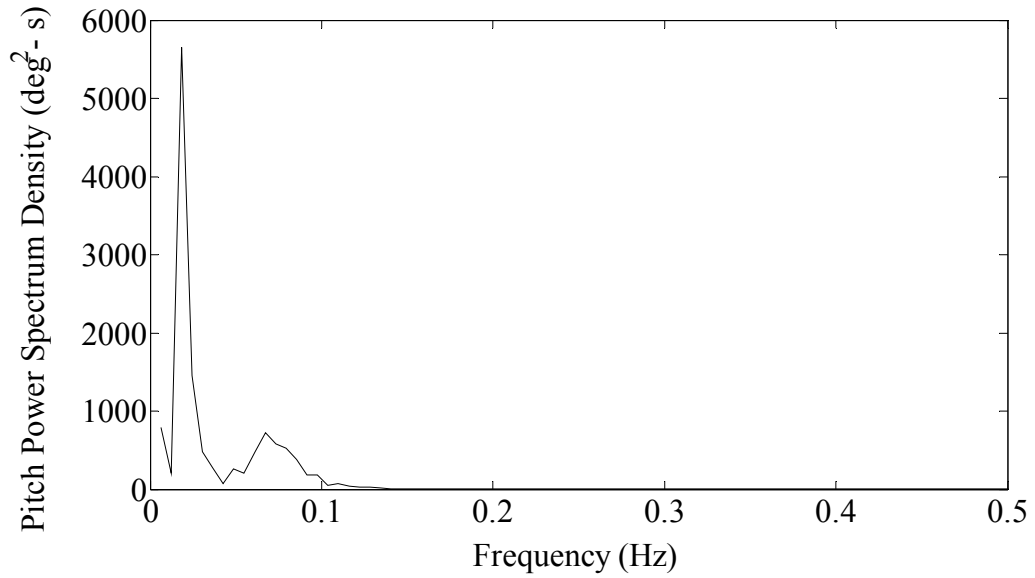


Figure 6.60: Pitch spectrum

6.4.5 Mooring line dynamic analysis in regular waves

Based on the mathematical formulation described in Section 4.4, a numerical code was developed in the MATLAB environment for deepwater mooring line dynamic analysis. The dynamic tension and configuration of mooring line No. 5 in Figure 6.29 were predicted numerically using the developed code and compared to literature experimental results [86] for the case of regular waves shown in Table 6.10. The general data used for the analysis were presented in Table 6.9 and the mooring line attached to the structure is shown in Figure 6.61. The mooring line was divided into 196 nodes, where mass, external forces and internal reactions were lumped.

Table 6.10: Regular waves used in the experiment and simulation

Regular wave type	H (m)	T (s)
Reg1	13.1	16
Reg2	7	12

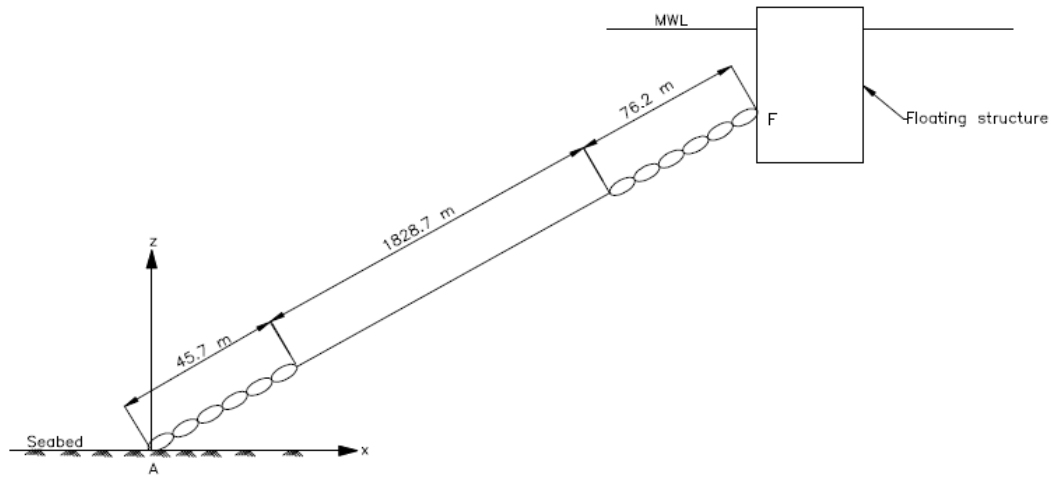


Figure 6.61: Mooring line No. 5 attached to the structure

The numerical tension time series results for Reg1 and Reg2 are presented in Figure 6.62 and Figure 6.64 respectively. The comparison between the numerical simulations and experimental results [86] is summarized in Table 6.11. The numerically predicted dynamic tension is greater (1.17 times for Reg1 and 1.33 times for Reg2) than the measured one. The difference was attributed to the different mooring line set-up between the prototype case and model test. In addition, the dynamic effects seemed to be underestimated as truncated mooring lines were used in the experiments. Figure 6.63 and Figure 6.65 show the motion time histories for the 196 nodes with its segments for the mooring line No. 5 due to Reg1 and Reg2 respectively.

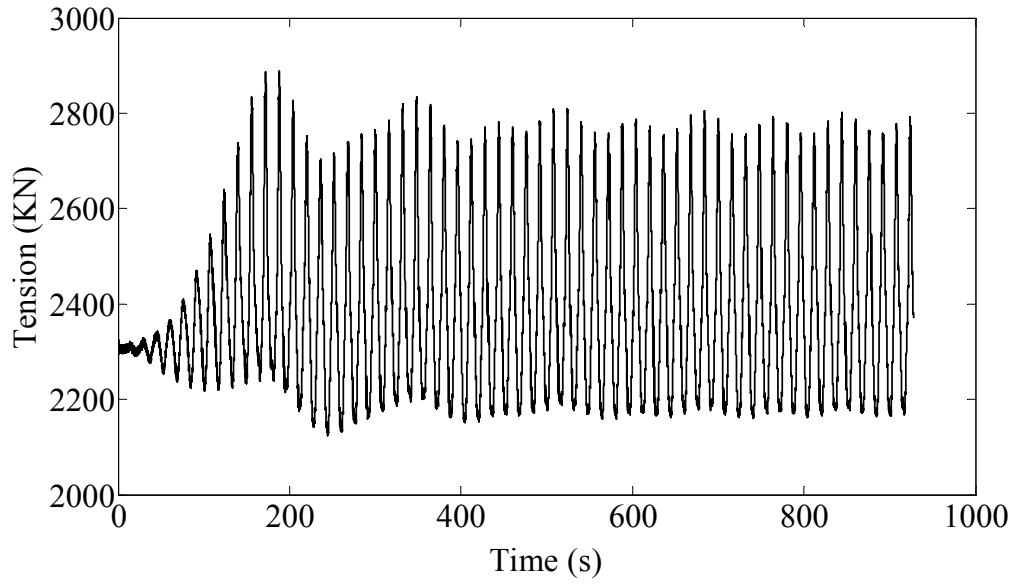


Figure 6.62: Mooring line No. 5 dynamic tension due to Reg1

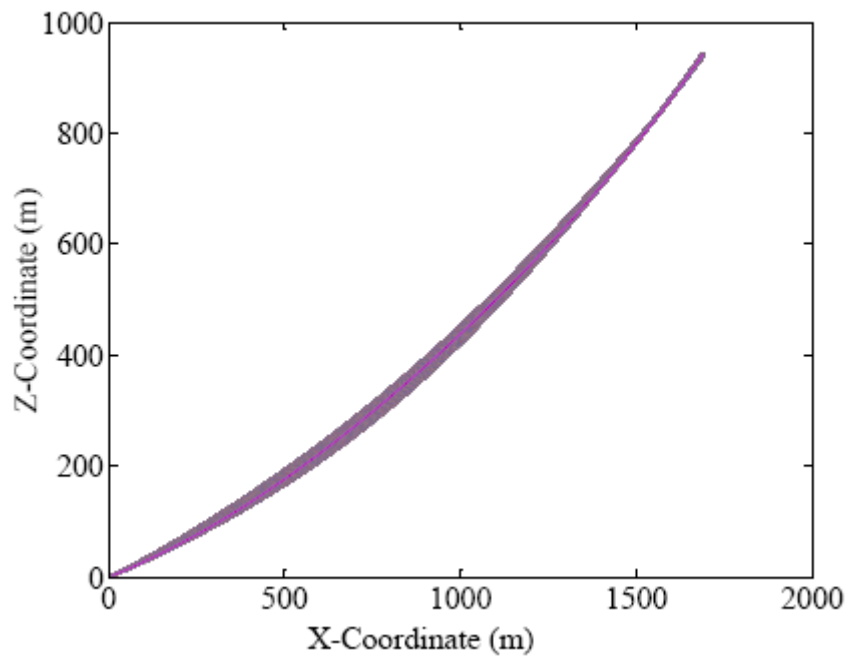


Figure 6.63: Mooring line No. 5 dynamic configuration due to Reg1

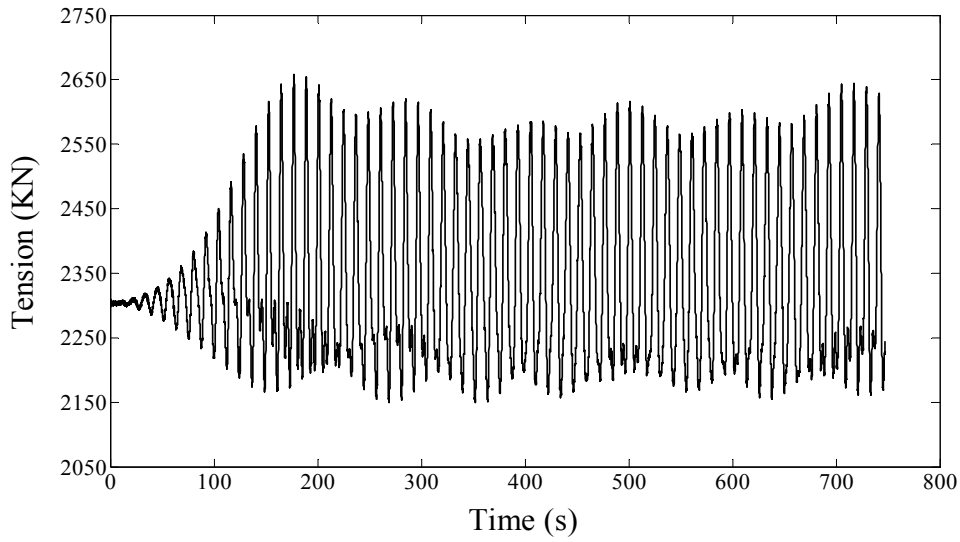


Figure 6.64: Mooring line No. 5 dynamic tension due to Reg2

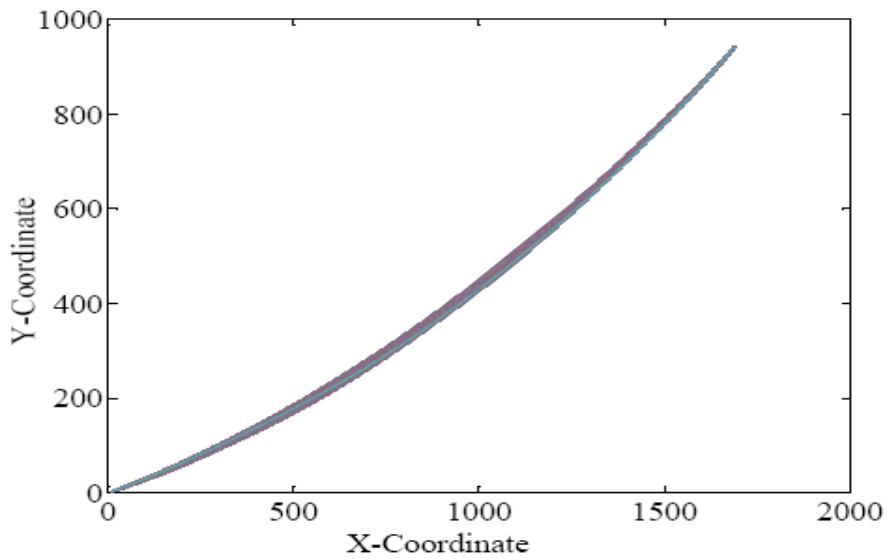


Figure 6.65: Mooring line No. 5 dynamic configuration due to Reg2

Table 6.11: Comparison between numerical and experimental results [86]

Regular wave	Amplitude (KN)		Mean (Kn)	
	Experiment	Simulation	Experiment	Simulation
Reg1	257.1	300	2273	2500
Reg2	150.8	200	2237	2350

6.5 Parametric studies on deepwater mooring line

The quasi-static analysis procedure explained in Section 4.3 for analyzing multi-component mooring lines was used to construct the nonlinear mooring line force-excursion relationship for a single multi-component taut line. Table 6.9 shows the basic data used for the purpose of these parametric studies. In this section, numerical studies on various parameters affecting the horizontal tension component at the

fairlead are presented. The effects of pretension, cable elongation and unit weight were investigated on the mooring line stiffness. The mooring line stiffness was evaluated as the first derivative of the tension with respect to the fairlead horizontal excursion.

Figure 6.66 shows the pretension effect on the mooring line fairlead tension for 1572 KN, 2209 KN, 2662 KN horizontal component pretension. It can be seen that the multi-component mooring line fairlead horizontal tension component was proportional to the pretension. The effect of the pretension is relatively high for relatively small pretension horizontal component ($H_o < 2000$ KN).

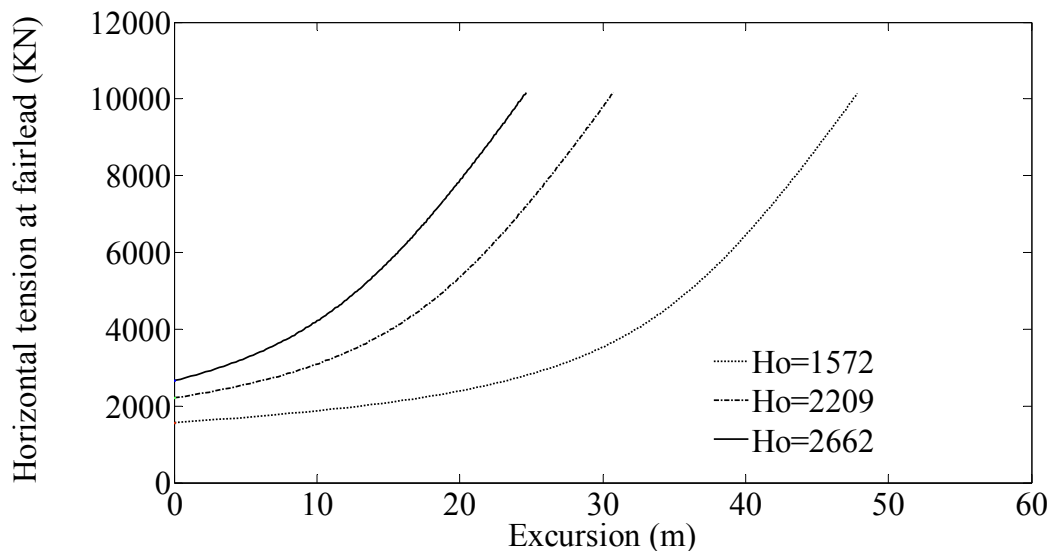


Figure 6.66: Effect of pretentions on the fairlead horizontal tension

Figure 6.67 shows the elongation effect for the cable. The elongation effect was studied using two different sets of axial stiffness; each set consists of three axial

stiffness corresponding to the three mooring line components. It was noted that for relatively small tension range of horizontal tension component ($H_o < 2100$ KN), there was insignificant effect of elongation, while in the large range of horizontal tension component ($H_o > 4000$ KN), the effect increased exponentially as shown in the same figure.

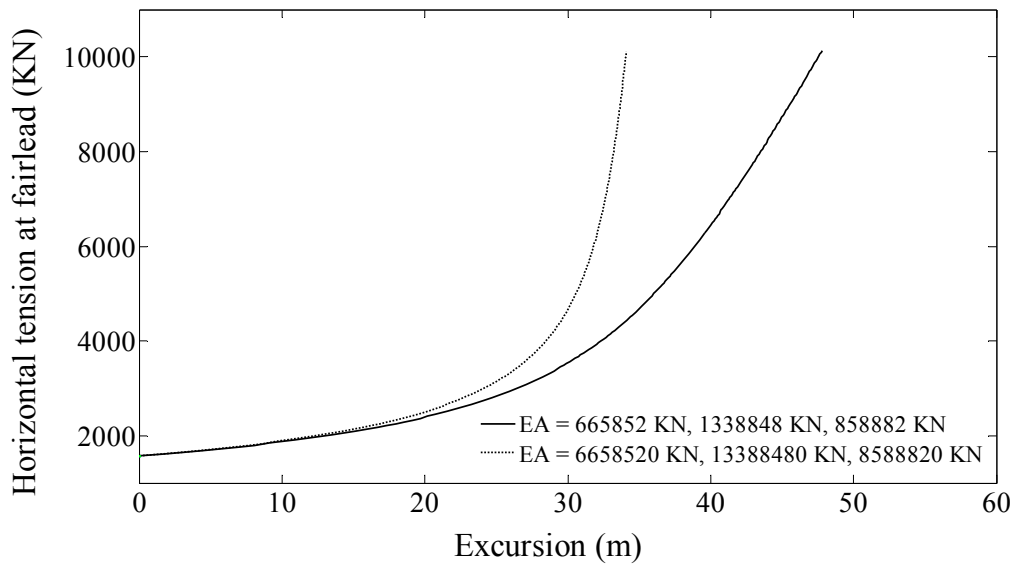


Figure 6.67: Effect of cable elongation on the fairlead horizontal tension

Figure 6.68 shows the nonlinear force-excursion relationship due to different mooring line unit weights. It was found that the cable restoring force was inversely proportional to the unit weight of the cable for horizontal excursion. Moreover, the force-excursion relationship was found linear for relatively light cable and nonlinear for the heavy one.

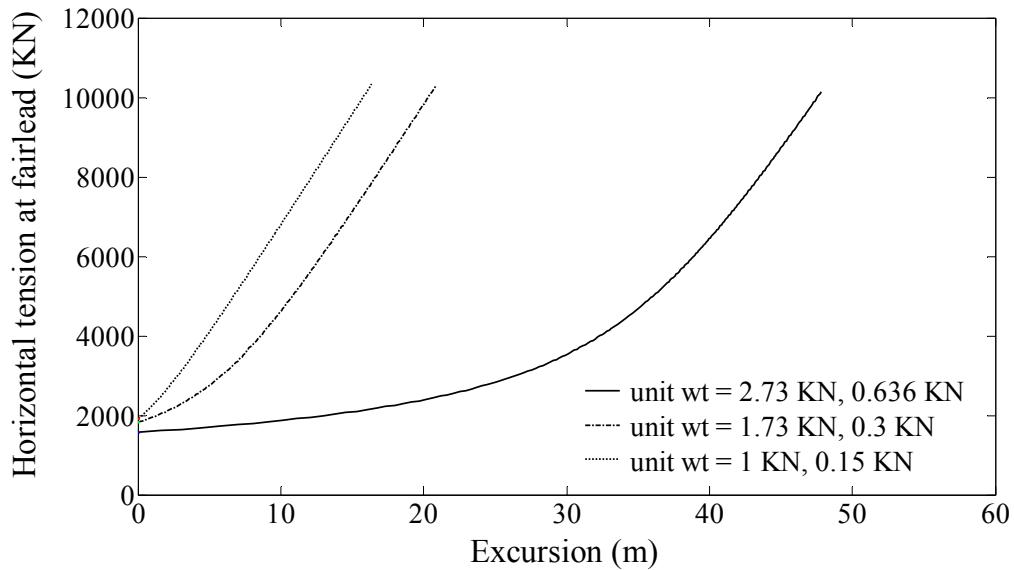


Figure 6.68: Effect of cable components unit weight on the fairlead horizontal tension

6.6 Chapter summary

In this chapter, comparisons between experimental and numerical motion RAOs were presented for investigating the truss spar motion characteristics. In order to validate TRSPAR predictions and examine the effect of mooring line failure, comprehensive and systematic comparisons between experimental and numerical results were presented in two cases. One was the intact mooring lines condition and the other was mooring lines failure condition. These comparisons cover both, wave frequency and low frequency responses. Moreover, experimental and numerical surge response results representing the transition process from intact to mooring lines failure condition were presented. Marlin truss spar was chosen as a case study to investigate the effect of slow varying drift forces on surge and pitch responses. The same structure was used to investigate the effect of current and wind forces on the slow drift surge and pitch responses. Comparisons between TRSPAR and the fully coupled analysis code WINPOST was presented to validate the numerical findings. For the purpose of examining the effect of strengthening mooring line system on the resonant responses, mooring lines have been added to the original Marlin truss spar lines and the resonant surge and pitch responses were compared with the corresponding motions in the original case. The effect of considering the dynamic effects on the mooring line analysis has been studied by comparing the numerical tension

predictions with the corresponding measurements. In addition, mooring line dynamic configuration during the simulation has been presented. Finally, the results and discussions for parametric studies based on nonlinear quasi-static analysis for multi-component taut mooring line were presented.

CHAPTER 7

CONCLUSIONS AND RECOMMENDATIONS

7.1 Summary

In this study, an attempt was made to develop an efficient numerical scheme used for dynamic analysis of floating structures. In this methodology, the equations used for calculating the second order difference frequency forces were derived. Based on the aforementioned methodology, a MATLAB code named TRSPAR was developed for the dynamic analysis of truss spar platform. The structure was analyzed in time domain for wave, current and wind forces. In this study, special attention was given to the slow drift motions. One of the requirements to solve the equations of motion is predicting of mooring line stiffness. For this purpose, a MATLAB code based on quasi-static analysis was developed. Based on the nonlinear mooring line wave interaction, a MATLAB code based on lumped mass method was developed for conducting dynamic analysis of multi component mooring line.

For the experimental studies, two phases of experiments were conducted for two main reasons. One was to verify the developed numerical scheme and the other was to examine the effect of mooring line failure on the motion characteristics of truss spar platforms. In the first phase, the motion characteristics of the truss spar were studied in the wave frequency range. In the second phase, the model was built to scale of 1:100 using Froude's law similitude. The sea keeping tests were conducted for regular and random waves. The second order slow drift motions for the structure with intact mooring and mooring line failure conditions were investigated.

Based on the validated numerical algorithms, numerical studies were conducted for investigating the contribution of the various second order difference frequency

forces on the resonant responses for surge and pitch motions. Moreover, the effects of strengthening the mooring line system on the slow drift motions were studied. Parametric studies on the mooring line restoring forces were conducted. The effects of pretension, cable elongation and cable unit weight on the nonlinear behavior of deepwater multi component mooring line were examined by using quasi-static analysis.

7.2 Conclusions

Based upon the studies described earlier, the following conclusions were derived:

7.2.1 Comparison with laboratory test results

The numerical simulations were compared to a number of laboratory tests for two experimental phases. Based on the results, the following conclusions were drawn:

1. The developed numerical model “TRSPAR” was able to predict the natural frequencies of the truss spar platforms in both intact mooring and mooring line failure conditions with acceptable accuracy. The surge, heave and pitch differences between the predictions and the measurements were ranged from 5.06% to 24.3% for the two conditions.
2. The numerical model “TRSPAR” developed for assessment of the truss spar wave frequency responses was able to predict the platform motions due to regular waves obtaining good agreement with experimental results. This was verified in the case of intact mooring (maximum RMSD was 0.061) and mooring lines failure (maximum RMSD was 0.08) conditions.
3. The numerical scheme developed for the evaluation of the floating offshore structure slow drift motions successfully estimated the low frequency responses of the truss spar platform when connected to its mooring and when mooring line failure occurred. For the two conditions, the RMSD values for the simulation and the experiment show that the predicted WFR trend was relatively agreed well with the measurements compared to the LFR. However,

WFR and LFR have been fairly well predicted by the developed numerical model (RMSD ranged from 107.4 to 1074). The peak responses were predicted with good accuracy as the maximum difference between the predictions and measurements for the two structure conditions was 17.3%.

4. Mooring line failure altered the system natural frequencies. The most significant effect was for the surge natural frequency.
5. In the wave frequency responses, mooring line damage has insignificant effect on the heave and pitch responses. However, the mooring line failure surge RAOs were almost same as in the intact mooring condition surge except for relatively low frequency wave components where mooring damage condition gave lower results. For random waves, mooring line failure affected resonant surge response (increased by 32.5%) more than the peak heave (increased by 19.8%) and pitch (increased by 14.4%) responses.
6. The major contribution of mooring line failure to the structure was causing the migration surge distance. This migration distance occurred due to the unbalanced upper and downstream mooring line forces. In addition, a noticeable transient surge response followed the failure.

7.2.2 Second order difference frequency forces

The total forces acting upon truss spar platform included nine linear and nonlinear forces. These nine sources of forces were analyzed and their equivalent effects were discussed. Some important conclusions are mentioned here:

1. Calculation of the wave forces (inertia and drag forces) in the mean position of the structure resulted in linear surge and pitch motions only.
2. The displaced geometry for the inertia forces significantly increased the surge and pitch resonant responses. With respect to surge response, the surge displaced geometry effect was greater than pitch effect while for pitch response, these two effects were almost equal.

3. Additional of the second order difference frequency drag forces had insignificant effect on surge and pitch motions, while inclusion of the viscous damping significantly decreased the resonant surge and pitch responses.
4. Axial divergence increased the resonant surge and pitch motions.
5. An interesting relationship between the free surface fluctuation and convective acceleration forces was observed that these forces were almost equal in magnitude and opposite to each other.
6. In addition to the earlier second order forces, temporal acceleration can be considered as one of the important second order difference frequency forces. Addition of this force increased the slow drift surge and pitch motions.

7.2.3 Current and wind forces

1. The main contribution of current and wind forces was a significant increase in the structure surge mean offset.
2. Presence of current substantially decreased the surge and pitch resonant responses as it increased the structure damping.
3. Wind force reduced the second order surge response more than pitch response as the mooring line stiffness increased.
4. The numerical model “TRSPAR” developed for the analysis of truss spar platform subjected to combined wave, current and wind forces gave same trend of results when compared to a fully coupled dynamic analysis code “WINPOST”. However, the resonant surge and pitch results were higher than the corresponding WINPOST results.

7.2.4 Strengthening of mooring line system

1. Strengthening the mooring line system of the structure by adding additional lines increased the mooring line restoring forces.
2. The major effect of adding mooring lines to the structure was the decrease in the second order surge and pitch responses. The surge response was affected more than the pitch response.

7.2.5 Quasi-static and dynamic mooring line analysis

1. The MATLAB code developed for quasi static analysis of deepwater mooring lines was able to predict the mooring line system restoring force obtaining good agreement with the experimental measurements.
2. The numerical results obtained from the MATLAB code, which was developed for dynamic analysis of deepwater mooring line, were compared to experimental results. These numerical model results demonstrated the importance of the mooring line dynamic effect in the design and analysis of deepwater mooring lines.

7.2.6 Investigations on the taut deepwater mooring line design parameters

1. For multi-component deepwater mooring line, the restoring force is directly proportional to the line pretension. The effect of pretension on the restoring forces is relatively high for small pretensions.
2. For relatively small horizontal tensions, the line elongation has insignificant effect on the mooring line restoring force. However, its effect became significant for relatively large mooring line tension.
3. The cable unit weight is inversely proportioned to the horizontal mooring line tension at fairlead. The force-excursion relationship becomes linear for relatively light cable and nonlinear for the heavy one.

7.3 Future studies

The main objective of this work was to study the nonlinear slow drift motions of truss spar platforms under various environmental loadings and mooring line conditions. The following studies should help in the ultimate endeavor for a better understanding of this topic:

1. Sea keeping performance of truss spar platforms for multi-directional random waves involving all six degrees of freedom.
2. More theoretical and accurate experimental work is needed on the modeling of current and wind loads in terms of the assumption of steady velocity and the independence of the current and wave velocities.
3. Assessment of the implementation of the third order difference frequency forces on the numerical solution.
4. Investigation of the riser effects on the dynamic responses of truss spar platforms subjected to different environmental loadings.
5. Fully coupled integrated dynamic analysis in time domain for the platform and its mooring lines is needed.

REFERENCES

- [1] J. A. van Santen, and K. de Werk, , "On the typical qualities of spar type structures for initial or permanent field development," in Proceedings of the 8th Offshore Technology Conference, Houston, TX, 3, OTC 2716, pp. 1105-1118, 1976.
- [2] R. S. Glanville, J. R. Paulling, J. E. Halkyard, and T. J. Lehtinen, "Analysis of the spar floating drilling production and storage structure," in Proceedings of the 23rd Offshore Technology Conference, Houston, TX, 4, OTC 6701, pp. 57-68, 1991.
- [3] E. E. Horton, and J. E. Halkyard, "A spar platform for developing deep water oil fields," *MTS 92*. Marine Technology Society, Washington, DC., pp. 998-1005, 1992.
- [4] C. Gunther, L. Eike, and O. Casten, *Offshore Structures vol. 1*. New York: Springer-Verlag, 1988.
- [5] A. Magee, A. Sablok, J. Maher, J. Halkyard, L. Finn, and I. Datta "Heave plate effectiveness in the performance of Truss Spars," in 19th Offshore Mechanics and Arctic Engineering (OMAE), pp. 469-479, 2000.
- [6] F. Zhang, J. M. Yang, R. P. Li, and Z. Q. Hu, "Effects of heave plate on the hydrodynamic behaviors of cell spar platform," in Proceedings of the 25th Offshore Mechanics and Arctic Engineering Conference, Hamburg, Germany, 2006.
- [7] L. D. Finn, J. V. Maher, and H. Gupta, "The cell spar and vortex induced vibration," in Offshore Technology Conference, Houston, Texas, 2003.
- [8] R. D. Blevins, J. E. Halkyard, and E. E. Horton, "Floating offshore drilling/producing structure," 2001.

- [9] J. D. Wheeler, "Method of calculating forces produced by irregular waves," in 1st Offshore Technology Conference, Huston, TX, 4, OTC 1007, pp. 89-93, 1969.
- [10] S. K. Chakrabarti, "Discussion of Dynamics of single point mooring in deep water " *Journal of Waterway, Port, and Ocean Engineering*, vol. 97(3), pp. 588-590, 1971.
- [11] D. Weggel, "Nonlinear dynamic response of large diameter offshore structures," Ph. D. Dissertation, The University of Texas, Austin, Texas, 1996.
- [12] J. D. Bax, and K. J. C. de Werk, "Afloating storage unit designed specially for the severest environmental conditions," presented at the Society of Petroleum Engineers, 1974.
- [13] B. Hunter, S. Menard, R. E. Ohman, and R. S. Glanville, "Spar drilling, production, storage platform design takes next step," *Offshore/Oilman*, PennWell Publishing Company, pp. 37-39, 1993.
- [14] J. E. Halkyard, "Status of spar platforms for deepwater production systems " in *Proceedings of the 6th International Offshore and Polar Engineering Conference*, Los Angeles, USA, pp. 262-272, 1996.
- [15] H. O. Berteaux, *Buoy Engineering*. New York: John Wiley & Sons, 1976.
- [16] F. H. Fisher, and F. N. Spiess "Flip-floating instrument platform," *Journal of the Acoustical Society of America*, vol. 35, pp. 1633-1644, 1963.
- [17] J. Korloo, "Design and installation of a cost-effective spar buoy flare system," in *Proceedings of the 25th Offshore Technology Conference*, Houston, Texas, pp. 479-485, 1993.
- [18] P. Johnson, "Spar model test Joint Industry Project final report: Project summary," Texas A&M University, College Station, TX 1995.

- [19] J. N. Newman, "Second order slowly varying forces on vessels in irregular waves," in International Symposium on the Dynamics of Marine Vehicles and Structures in Waves, London, 1974.
- [20] J. A. Pinkster, "Low frequency second-order wave exciting forces on floating structures," Ph. D. Dissertation, Technische Universiteit, Delft, 1980.
- [21] M. H. Kim, and D. K. P. Yue, "The complete second-order diffraction solution for an axisymmetric body. Part 1.," Journal of Fluid Mechanics, pp. 235-264, 1989.
- [22] M. H. Kim, and D. K. P. Yue, "The complete second-order diffraction solution for an axisymmetric body. Part 2. Bichromatic incident waves and body motions," Journal of Fluid Mechanics, pp. 557-593, 1990.
- [23] Z. Ran, M. H. Kim, J. M. Niedzwecki, and R. P. Johnson, "Responses of a spar platform in random waves and currents (Experimental vs. Theory)," International Journal of Offshore & Polar Engineering, vol. 6(1), pp. 27-34, 1996.
- [24] Y. H. Liu, C. H. Kim, and M. H. Kim, "The computation of mean drift forces and wave run-up by higher-order boundary element method " International Journal of Offshore & Polar Engineering, vol. 2, pp. 101-106, 1993.
- [25] M. H. Kim, and W. Chen "Slender-body approximation for slowly-varying wave loads in multi-directional waves," Applied Ocean Research, vol. 16, pp. 141-163, 1994.
- [26] J. R. Morison, M. P. O. Brien, J. W., Johnson, and S. A. Shaaf, "The force exerted by surface waves on piles," Petroleum Transaction, *AIME*, vol. 189, pp. 149-157, 1950.
- [27] P. M. Cao, and J. Zehang "Slow motion responses of compliant offshore structures," International Journal of Offshore and Polar Engineering, vol. 7, pp. 119-126, 1997.

- [28] J. Zhang, L. Chen, M. Ye, and R. E. Randall, "Hybrid wave model for unidirectional irregular waves, Part I: Theory and numerical scheme " *Applied Ocean Research*, vol. 18, pp. 77-92, 1995.
- [29] B.B. Mekha, C. P. Johnson, and J. M. Roesset, "Nonlinear response of spar in deep water: Different hydrodynamic and structural models," presented at the Fifth International Offshore and Polar Engineering Conference, The Hague, The Netherlands, 1995.
- [30] B. B. Mekha, D. C. Weggel, C. P. Johnson, and J. M. Roesset, "Effects of second order diffraction forces on the global response of spars," presented at the Sixth International Offshore and Polar Engineering Conference, Los Angeles, CA, 1996.
- [31] C. P. Johnson, B. B. Mekha, C. Matos, and J. M. Roesset, "Analysis in the time domain of a deepwater spar platform," in *Proceeding of Energy Week Conference & Exhibition , Drilling & Production Economic*, pp. 266-270, 1996.
- [32] J. M. Niedzwecki, B. B. Mekha, O. Rijken, and J. M. Roesset, "Deepwater spar platform response: Analysis and prediction," in *Proceedings of International Symposium of Offshore Energy*, Rio de Janeiro, Brazil, 1995.
- [33] D. C. Weggel, and J. M. Roesset, "The behavior of spar platforms," presented at the OTRC Spar related papers, Offshore Technology Research Center, Texas A&M University, College Station, TX, 1996.
- [34] D. C. Weggel, and J. M. Roesset, "Second order dynamic response of a large diameter spar platform: Numerical predictions versus experimental results," presented at the Offshore Mechanics and Arctic Engineering Conference, Florence, Italy, 1996.
- [35] C. H. Lee, "WAMIT theory manual," Department of Ocean Engineering, MIT, Cambridge, MA, 1995.

- [36] T. C. Ude, S. Kumar, and S. R. Winterstein, "TFPOP 2.1: Stochastic response analysis of floating structures under wind, current and second-order wave loads," Stanford University, 1996.
- [37] M. G. Donley, and P. D. Spanos, "Dynamic analysis of nonlinear structures by the method of quadratization," in Lecture Notes on Engineering, ed Berlin, Germany: Springer-Verlag, 1990.
- [38] A. S. Chitrapu, S. Saha, and V. Y. Salpekar, "Time domain simulation of spar platform response in random waves and current," in Proceedings of the 17th International Conference on Offshore Mechanics and Arctic Engineering (OMAE98-0380), pp. 1-8, 1998.
- [39] G. Xu, Q. W. Ma, and L. Sun, "Numerical investigations on truss spar motion in waves," in Proceedings of the 20th International Offshore Polar Engineering Conference, Beijing, China, 2010.
- [40] O. T. Gudmestad, "Engineering approximations to nonlinear deepwater waves," *Journal of Applied Ocean Research*, vol. 8, pp. 76-88, 1986.
- [41] C. Spell, J. Zehang, and R. E. Randall, "Hybrid wave model for unidirectional irregular waves-part II. Comparison with laboratory measurements," *Journal of Applied Ocean Research*, vol. 18, pp. 93-110, 1996.
- [42] A. Iftekhar, and J. M. Roesset, "Effect of nonlinear wave kinematics on dynamic response of spars " *Journal of Engineering Mechanics*, vol. 128, pp. 925-934, 2002.
- [43] I. Prislín, and A. K. Blom, "Significance of short crested and diffracted waves on full scale motion correlation of a truss spar," in Proceedings of the International Conference on Civil Engineering in the Oceans VI, pp. 281-294, 2006.

- [44] W. Ye, I. Anam, and J. Zhang, "Effect of wave directionality on wave loads and dynamic response of a spar," in Proceedings of the 17th International Conference on Offshore Mechanics and Arctic Engineering (OMAE98-0601), pp. 1-6, 1998.
- [45] A. S. Chitrapu, S. Saha, and V. Y. Salpekar, "Motion response of spar platform in directional waves and current," in Proceedings of the 18th International Conference on Offshore Mechanics and Arctic Engineering (OMAE99/OFT-4237), 1999.
- [46] L. J. Bernt, M. Dag, and V. Jarle, "Dynamic response analysis of a spar platform subjected to wind and wave forces," in Proceedings of the ASME 27th International Conference on Offshore Mechanics and Arctic Engineering Estoril, Portugal, 2008.
- [47] R. I. Harris, and D. M. Deaves, "The structure of strong winds," in Proceedings of CIRIA Conference on Wind Engineering in the Eighties, CIRIA, London, 1981.
- [48] M. K. Ochi, and Y. S. Shin, "Wind turbulent spectra for design considerations of offshore structures," in Proceedings of 20th Offshore Technology Conference, Houston, Texas, pp. 461-467, 1988.
- [49] A. Iftekhar, J. M. Roesset, and J. M. Niedzwecki, "Time domain and frequency domain analysis of spar platforms," in Proceedings of the Thirteenth International Offshore and Polar Engineering Conference, Honolulu, Hawaii, USA, pp. 240-247, 2003.
- [50] M. Le Boulluec, Ph. Le Buhan, X. B. Chen, G. Deleuil, L. Foulhoux, B. Molin, and F. Villeger "Recent advance on the slow-drift damping of offshore structures," in Proceedings of BOSS'94 Behaviour of Offshore Structures, Massachusetts Institute of Technology, Cambridge, Massachusetts, pp. 9-30, 1994.

- [51] J. E. W. Wichers, and M. F. van Sluijs, "The influence of waves on the low-frequency hydrodynamic coefficients of moored vessels " in Proceedings of the Offshore Technology Conference, Houston, pp. 2313-2322, 1979.
- [52] J. E. W. Wichers, "On the low-frequency surge motion of vessels moored in high sea," in Proceedings of the Offshore Technology Conference, Houston, pp. 711-723, 1982.
- [53] J. E. W. Wichers, and R. H. M. Huijismans, "On the low-frequency damping forces acting on offshore moored vessel," in Proceedings of the Offshore Technology Conference, Houston, pp. 315-324, 1984.
- [54] E. Huse, "Influence of mooring line damping upon rig motions," in Proceedings of the Offshore Technology Conference, Houston, pp. 433-438, 1986.
- [55] E. Huse, and K. Matsumoto, "Practical estimation of mooring line damping," in Proceedings of Offshore Technology Conference, Houston, pp. 543-552, 1988.
- [56] E. Huse, "New developments in prediction of mooring system damping," in Proceedings of the Offshore Technology Conference, Houston, pp. 291-298, 1991.
- [57] J. E. W. Wichers, and R. H. M. Huijismans, "The contribution of hydrodynamic damping induced by mooring chains on low-frequency vessel motions," in Proceedings of the Offshore Technology Conference, Houston, pp. 171-182, 1990.
- [58] T. Sarpkaya, "Force on a circular cylinder in viscous oscillatory flow at low Keulegan-Carpenter numbers," *Journal of Fluid Mechanics*, vol. 165, pp. 61-71, 1986.
- [59] S. K. Chakrabarti, "Motion analysis of articulate tower," *Journal of Waterway*, vol. 105, pp. 281-292, 1979.

- [60] G. Rodenbusch, D. L. Garret, and S. L. Anderson, "Statistical linearization of velocity squared drag forces," in Proceedings of the fifth OMAE Conference, Tokyo, pp. 123-129, 1986.
- [61] E. Huse, "Resonant heave damping of Tension Leg Platforms," presented at the Proceedings of the 22nd Offshore Technology Conference, Houston, Texas, 1990.
- [62] S. K. Chakrabarti, and S. Y. Hanna, "Added mass and damping of a TLP coulumn model," presented at the Proceedings of the 22nd Offshore Technology Conference, Houston, Texas, 1990.
- [63] E. Huse, T. Utnes, "Springing damping of Tension Leg Platforms," in Proceedings of the 26th Offshore Technology Conference, Houston, Texas, 1994.
- [64] K. P. Thiagarajan, and A. W. Troesch, "Hydrodynamic heave damping estimation and scaling for Tension Leg Platforms," Journal of Offshore Mechanics and Arctic Engineering, vol. 116, pp. 70-76, 1994.
- [65] N. Srinivasan, A. S. J. Swamidas, and J. S. Pawlowski, "Effect of induced drag damping on the near resonant responses of a deepwater tripod tower platform," in Proceedings of the 23rd Offshore Technology Conference, Houston, Texas, pp. 431-442, 1991.
- [66] K. P. Thiagarajan, and A. W. Troesch, "Effects of Appendages and small currents on the hydrodynamic heave damping of a TLP coulmnns," Journal of Offshore Mechanics and Arctic Engineering, vol. 120, pp. 37-42, 1998.
- [67] M. Lake, H. He, A. W. Troesch, M. Perlin, and K. P. Thiagarajan, "Hydrodynamic coefficient estimation for TLP and spar platforms " Journal of Offshore Mechanics and Arctic Engineering, vol. 122, pp. 118-124, 2000.
- [68] I. Prislín, R. D. Belvins, and J. E. Halkyard, "Viscous damping and added mass of solid square plates," in Proceedings of the 17th Offshore Mechanics and Arctic Engineering Conference, Lisbon, Portugal, 1998.

- [69] F. J. Fischer, and R. Gopalkrishnan, "Some observations on the heave behaviour of spar platforms," *Journal of Offshore Mechanics and Arctic Engineering*, vol. 120, pp. 221-225, 1998.
- [70] M. J. Downie, J. M. R. Graham, C. Hall, A. Incecik, and I. Nygaard, "An experimental investigation of motion control devices for truss spars," *Journal of Marine Structures*, vol. 13, pp. 75-90, 2000.
- [71] L. Tao, K. Y. Lim, and K. Thiagarajan, "Heave response of classic spar with variable geometry," *Journal of Offshore Mechanics and Arctic Engineering*, vol. 126, pp. 90-95, 2004.
- [72] H. A. Haslum, and Faltinsen, "Alternative shape of spar platforms for use in hostile areas," in *Proceedings of the Offshore Technology Conference*, Houston, Texas, 1999.
- [73] DNV, "SESAM user's manual-WADAM," Det Norske Veritas, 1993.
- [74] P. J. Clark, S. Malenica, and B. Molin, "An heuristic approach to wave drift damping," *Applied Ocean Research*, vol. 15, pp. 53-55, 1993.
- [75] O. J. Emmerhoff, and P. D. Sclavounos, "The slow-drift motion of arrays of vertical cylinders," *Journal of Fluid Mechanics*, vol. 242, pp. 31-50, 1992.
- [76] Department of Ocean Engineering, MIT, "SWIM: Slow wave-induced motions- Users' Manual," in *SWIM 2.0*, 1995.
- [77] A. K. Jha, P. R. de Jong, and S. R. Winterstein, "Motions of a spar buoy in random seas: Comparing predictions and model test results," in *Proceedings of the behaviour of offshore structures*, pp. 333-347, 1997.
- [78] K. A. Ansari, "Mooring with multicomponent cable systems," *Journal of Energy Resources Technology, Trans. ASME*, vol. 102, pp. 62-69, 1980.
- [79] A. K. Agarwal, and A. K. Jain, "Dynamic behavior of offshore spar platforms under regular sea waves," *Ocean Engineering Journal*, pp. 487-516, 2003.

- [80] A. K. Agarwal, and A. K. Jain, "Nonlinear coupled dynamic response of offshore spar platforms under regular sea waves," *Journal of Ocean Engineering*, vol. 30, pp. 517-551, 2003.
- [81] K. A. Ansari, and N. U. Khan, "The effect of cable dynamics on the station-keeping response of a moored offshore vessel " *Journal of Energy Resources Technology. ASME*, vol. 108, pp. 52-58, 1986.
- [82] N. U. Khan, and K. A. Ansari, "On the dynamics of a multicomponent mooring line," *Computers and Structures*, vol. 22, pp. 311-334, 1986.
- [83] J. R. Pauling, and W. C. Webster, "A consistent large-amplitude analysis of the coupled response of a TLP and tendon system " in *Proceedings of the 5th International Conference on Offshore Mechanics and Arctic Engineering*, Tokyo, Japan, pp. 126-133, 1986.
- [84] D. L. Garrett, "Dynamic analysis of slender rods," *Journal of Energy Resources Technology*, *Trans. ASME*, vol. 104, pp. 302-307, 1982.
- [85] C. H. Kim, M. H. Kim, Y. H. Liu, and C. T. Zhao, "Time domain simulation of nonlinear response of a coupled TLP system," *International Journal of Offshore & Polar Engineering*, vol. 4, pp. 284-291, 1994.
- [86] R. Zhihuang, "Coupled Dynamic analysis of floating structures in waves and currents," Ph. D Dissertation, Office of Graduate Studies, Texas A&M University, Texas, 2000.
- [87] M. S. Traintafyllou, A. Bliet, and H. Shin, "Dynamic analysis as a tool for open-sea mooring system design," *SNAME Transactions* 93, pp. 303-324, 1985.
- [88] H. J. J. Boom, "Dynamic behaviour of mooring lines," in *BOSS'85 Behavior of Offshore Structures*, Delft, The Netherlands, pp. 359–368, 1985.

- [89] Orcina, "Visual Orcaflex User Manual, Version 7.4c," in Orcina Limited, Daltongate, U.K., 2000.
- [90] D. T. Brown, and S. Mavrakos, "Comparative study on mooring line dynamic loading," *Journal of Marine Structures*, vol. 12, pp. 131-151, 1999.
- [91] Z. Ran, M. H. Kim, and W. Zheng "Coupled dynamic analysis of a moored spar in random waves and currents (Time-domain versus Frequency-domain analysis)," *Journal of Offshore Mechanics and Arctic Engineering* vol. 121, pp. 194-200, 1999.
- [92] S. X. Zhang, Y. G. Tang, and X. J. Liu "Analysis of nonlinear dynamic response of mooring lines in deepwater," in *Proceedings of the 29th International Conference on Ocean, Offshore and Arctic Engineering Shanghai, China*, pp. 489-494, 2010.
- [93] X. H. Chen, "Studies on dynamic interaction between deep-water floating structures and their mooring/tendon system," Doctor of Philosophy, Office of Graduate Studies of Texas A&M University, Texas A&M University, Houston, 2002.
- [94] H. Yin, "Nonlinear analysis of mooring lines and marine risers," in *Memorial University of Newfoundland, Canada*, 2007.
- [95] C. T. Stansberg, R. Yttervik, O. Oritsland, and G. Kleiven, "Hydrodynamic model test verification of a floating platform system in 3000 m water depth," in *Proceedings of the Offshore Mechanics and Arctic Engineering, New Orleans*, pp. 325-333, 2000.
- [96] B. Buchner, J. E. W. Wichers, and J. J. de Wilde, "Features of the state-of-the-art deepwater offshore basin," in *Proceedings of the Offshore Technology Conference, Houston*, pp. 363-373, 1999.
- [97] X. H. Chen, J. Zhang, P. Johnson, and M. Irani, "Studies on the dynamics of truncated mooring line," in *Proceedings of the International Offshore and Polar Engineering Conference, Seattle, USA*, pp. 94-101, 2000.

- [98] H. Ormberg, C. T. Stansberg, and R. Yttervik "Integrated vessel motion and mooring analysis applied in hybrid model testing," in Proceedings of the Offshore and Polar Engineering Conference, Brest, France, pp. 339-346, 1999.
- [99] R. S. Glanville, J. E. Halkyard, R. L. Davies, A. Steen, and F. Frimm, "Neptune project: Spar history and design considerations," in Proceedings of the Offshore Technology Conference, Houston, Texas, 1997.
- [100] R. D. Vardeman, S. Richardson, and C. R. McCandless, "Neptune project: Overview and project management," in Proceedings of the Offshore Technology Conference, Houston, Texas, 1997.
- [101] Anon, "Drilling the ultra-deepwater corridor," in Proceedings of the Offshore Technology Conference, Houston, Texas, 1996.
- [102] J. Wang, S. Berg, Y. H. Luo, A. Sablok, and L. Finn, "Structural design of the truss spar - an overview," in Proceedings of the 11th International Offshore and Polar Engineering Conference, Stavanger, Norway, pp. 354-361, 2001.
- [103] R. R. Lu, J. J. Wang, and E. Erdal, "Time domain strength and fatigue analysis of truss spar heave plate," in Proceedings of the 13th International Offshore and Polar Engineering Conference, Hawaii, USA, pp. 272-279, 2003.
- [104] I. Datta, I. Prislun, J. E. Halkyard, L. G. William, S. Bhat, S. Perryman, and P. A. Beynet, "Comparison of truss spar model test results with numerical predictions," in Proceedings of the 18th International Conference on Offshore Mechanics and Arctic Engineering, Newfoundland, Canada, pp. 1-14, 1999.
- [105] J. R. Paulling, "TDSIM6: Time domain platform motion simulation with six degrees of freedom. Theory and user guide," 1995.
- [106] "Inplace model test result correlation," Technip Doc. No. KIK-TMM-30-NA-RP-1206-B, 2005.
- [107] J. R. Paulling, "MLTSIM: Time domain platform motion simulation. Theory and user guide," 2000.

- [108] B.Theckumpurath, Y. Ding, and J. Zhang, "Numerical simulation of the truss spar "Horn Mountain"," in Proceedings of the 16th International Offshore and Polar Engineering Conference, San Francisco, California, USA, pp. 203-209, 2006.
- [109] J. L. Seung, B. R. Jun, and S. C. Hang, "An experimental study on motion characteristics of cell spar platform," in Proceedings of the 15th International Offshore and Polar Engineering Conference, Seoul, Korea, 2005.
- [110] F. Zhang, J. Yang, R. Li, and G. Chen, "Numerical investigation on the hydrodynamic performances of a new spar concept," Journal of Hydrodynamics, vol. 4, pp. 473-481, 2007.
- [111] Y. Su, J. Yang, L. Xiao, and G. Chen, "Model test verification of a cell truss spar using hybrid model testing technique," in Proceedings of the 26th International Conference on Offshore Mechanics and Arctic Engineering, San Diego, California, USA, pp. 1-8, 2007.
- [112] F. Zhang, J. Yang, R. Li, and G.Chen, "Coupling effects for cell-truss spar platform: Comparison of frequency - and domain - domain analysis with model tests," Journal of Hydrodynamics, vol. 4, pp. 424-432, 2008.
- [113] W. Yu, and W. Huang, "A new concept of spar and its hydrodynamic analysis," presented at the Proceedings of the 20th International Offshore and Polar Engineering Conference, Beijing, China, 2010.
- [114] L. B. P. Le Boulluec M., Chen X. B., Deleuil G., Foulhoux L., Molin B., Villeger F., "Recent advance on the slow-drift damping of offshore structures," in Proceedings of BOSS'94 Behaviour of Offshore Structures, Massachusetts Institute of Technology, Cambridge, Massachusetts, pp. 9-30, 1994.
- [115] J. J. Stoker, Water waves: The mathematical theory with applications. New York: Interscience, 1957.

- [116] S. K. Chakrabarti, *Hydrodynamics of Offshore Structures*. Southampton, England: Computational Mechanics Publications, 1987.
- [117] G. Rodenbusch, and G. Z. Forristall, "An empirical method for calculation of random directional wave kinematics near the free surface," in *Proceedings of Offshore Technology Conference*, Houston, TX, pp. 137-146, 1986.
- [118] K. Hasselman, "Measurement of wind-wave growth and swell decay during the Joint North Sea Wave Project (JONSWAP)," *Deutsches Hydrographisches Institut, Ergänzungsheft*, 1973.
- [119] M. S. Longuet-Higgins, and R. W. Steward, "Changes in the form of short gravity waves and tidal currents. ," *Journal of Fluid Mechanics*, vol. 8, pp. 575-583, 1960.
- [120] Y. Li, and A. Kareem, "Computation of wave-induced drift forces introduced by displaced position of compliant offshore platforms," *Journal of Offshore Mechanics and Arctic Engineering*, vol. 114, pp. 175-184, 1992.
- [121] R. C. T. Rainey, "A new equation for calculating wave loads on offshore structures," *Journal of Fluid Mechanics*, vol. 204, pp. 295-324, 1989.
- [122] R. W. Clough, *Dynamics of offshore structures*, 2nd ed.: McGraw-Hill, Inc, 1993.
- [123] T. Nakajima, S. Motora, and M. Fujino, "On the dynamic analysis of multi-component mooring lines," presented at the OTC Paper 4309, 1982.
- [124] L. E. Borgman, "Ocean wave simulation for engineering design," *Journal of the Waterways and Harbors Division, ASCE*, pp. 557-583, 1969.
- [125] HR Wallingford, "Multi-element wave generation system with AC drives and dynamic wave absorption for Universiti Teknologi PETRONAS: user manual," 2008.
- [126] S. K. Chakrabarti, *Offshore structure modeling*: World Scientific, 1994.

- [127] M. H. Kim, Z. Ran, W. Zheng, S. Bhat, and P. Beynet, "Hull/Mooring coupled dynamic analysis of a truss spar in time domain," *International Journal of Offshore & Polar Engineering*, vol. 2, pp. 42-54, 2001.

PUBLICATIONS LIST

Journal publications:

Published paper:

1. **O. A. Montasir**, V. J. Kurian, “Effect of slowly varying drift forces on the motion characteristics of truss spar platforms,” *Ocean Engineering Journal*, vol. 38, pp. 1417-1429, 2011.

Conference Proceedings:

1. **O. A. Montasir**, V. J. Kurian, “Effect of wave kinematics on the response of spar platform,” in the National Postgraduate Conference (NPC), UTP - Malaysia, 2008.
2. **O. A. Montasir**, V. J. Kurian, S. P. Narayanan, M. A. W. Mubarak, “Dynamic response of spar platforms subjected to waves and current,” in the International Conference on Construction and Building Technology (ICCBT), Malaysia, 2008.
3. V. J. Kurian, B. S. Wong, **O. A. Montasir**, “Frequency domain analysis of truss spar platform,” in the International Conference on Construction and Building Technology (ICCBT), Malaysia, 2008.
4. **O. A. Montasir**, V. J. Kurian, “Model tests on truss spar platform,” in the National Postgraduate Conference (NPC), UTP - Malaysia, 2009.
5. V. J. Kurian, **O. A. Montasir**, S. P. Narayanan, “Numerical and model test results for truss spar platform,” in the 19th of International Offshore (Ocean) and Polar Engineering Conference (ISOPE), Osaka – Japan, 2009.
6. **O. A. Montasir**, V. J. Kurian, N. Shafiq, “Numerical and model test results for truss spar platform subjected to random waves,” in the 2nd International Conference on Engineering Technology (ICET), Malaysia, 2009.

7. **O. A. Montasir**, V. J. Kurian, “Time domain and frequency domain analysis of truss spar platform,” in the Offshore Asia 2010 Conference and Exhibition, Malaysia, 2010.
8. **O. A. Montasir**, V. J. Kurian, M. A. W. Mubarak , “Effect of mooring line damage on the responses of truss spar platforms,” in the International Conference on Sustainable Building and Infrastructure (ICSBI), Malaysia, 2010.
9. C. Y. Ng, V. J. Kurian, **O. A. Montasir**, “An experimental and analytical investigation of classic spar response,” in the International Conference on Sustainable Building and Infrastructure (ICSBI), Malaysia, 2010.
10. **O. A. Montasir**, V. J. Kurian, “Effect of adding mooring lines to the truss spar platform,” in the Asia Pacific Offshore Conference “Challenges in Deepwater Oil & Gas Industry” (APOC), Malaysia, 2010.

Under preparation:

1. **O. A. Montasir**, V. J. Kurian, M. S. Liew, “Effect of Mooring Lines Failure on the Dynamic Responses of Truss Spar Platforms,” Ocean Engineering Journal, 2011.
2. **O. A. Montasir**, V. J. Kurian, M. S. Liew, “Effect of Mooring Lines Failure on the Wave frequency Responses of Truss Spar Platforms,” in the 22nd of International Offshore (Ocean) and Polar Engineering Conference (ISOPE), Rhodes – Greece, 2012.